Universidade Federal de Pernambuco

Centro de Ciências Exatas e da Natureza

Departamento de Física

Juan Nicolás Moreno Tarquino

Transition from integrable to chaotic domain in spectra of spin chains

Recife

2016

Juan Nicolás Moreno Tarquino

Transition from integrable to chaotic domain in spectra of spin chains

Dissertação apresentada ao Programa de Pós-Graduação em Física da Universidade Federal de Pernambuco, como requisito parcial para obtenção do título de Mestre em Física.

Supervisor: Prof. Dr. Antonio Murilo Santos Macêdo

Recife

2016

Catalogação na fonte
Bibliotecária Joana D'Arc Leão Salvador CRB 4-572

M843t Moreno Tarquino, Juan Nicolas.
Transition from integrable to chaotic domain in spectra of spin chains / Juan Nicolas Moreno Tarquino. – 2016.
108 f.: fig., tab.

Orientador: Antonio Murilo Santos Macêdo.
Dissertação (Mestrado) – Universidade Federal de Pernambuco. CCEN. Física. Recife, 2016.
Inclui referências.

1. Matéria condensada. 2. Transporte quântico . 3. Caos quântico I. Macêdo, Antonio Murilo Santos (Orientador). II. Titulo.

530.41 CDD (22. ed.) UFPE-FQ 2016-55

JUAN NICOLAS MORENO TARQUINO

TRANSITION FROM INTEGRABLE TO CHAOTIC DOMAIN IN SPECTRA OF SPIN CHAINS

Dissertação apresentada ao Programa de Pós-Graduação em Física da Universidade Federal de Pernambuco, como requisito parcial para a obtenção do título de Mestre em Física.

Aprovada em: 31/08/2016.

BANCA EXAMINADORA

_____

Prof. Dr. Antônio Murilo Santos Macêdo
Orientador
Universidade Federal de Pernambuco

_____

Prof. Dr. Flávio Menezes de Aguiar
Examinador Interno
Universidade Federal de Pernambuco

_____

Prof. Dr. Jorge Gabriel Gomes de Souza Ramos
Examinador Externo
Universidade Federal da Paraíba

Acknowledgements

Agradeço primeiramente aos meus pais que sem seus apoios, conselhos e amor, não teria chegado até aqui.

Quero agradecer ao professor Antonio Murilo pelo apoio que permitiu desenvolver este trabalho de pesquisa além de mostrar-se um modelo de cientista a seguir. Agradeço ao Ivan pelos conselhos e a disposição de discutir ideias da pesquisa.

Agradeço aos meus amigos de toda a vida por ter sempre confiança em mi. Também quero agradecer as agências CNPQ e CAPES pelo financiamento que permitiram poder finalizar este trabalho.

Abstract

In this thesis we present an approach, similar to random matrix ensembles, in order to study the integrable-chaotic transition in the Heisenberg spin model. We consider three ways to break the integrability: presence on an external field on a single spin, coupling of an external random field with each spin in the chain and next nearest neighbor interaction between spins. We propose a transition described by a power law in the spectral density, i.e. $S(k) \propto 1/k^{\alpha}$, where $\alpha = 2$ for the integrable case and $\alpha = 1$ for the chaotic case, with $1 < \alpha < 2$ for systems in the crossover regime. The transition is also described by the behavior of the "burstiness" B and the *Kullback–Leibler* divergence $D_{LK}(P_{W-D}(s)|P_{data}(s))$, where $P_{W-D}(s)$ and $P_{data}(s)$ are the Wigner-Dyson and the system's spacing distribution respectively. The B coefficient is associated to a sequence of events in the system. The Kullback–Leibler divergence provides information on how two distributions differ from each other. From analyzing the behavior of these three quantities, we obtain a universal description of integrable-chaotic transition in the spin chains.

Key words: Power spectral density. Burstiness. Kullback–Leibler. Transition to chaos. Crossover functions. Time series.

Resumo

Nesta dissertação apresentaremos uma descrição, similar a dos ensembles da teoria de matrizes aleatórias, com o objetivo de estudar transições entre os regimes integrável e caótico em uma cadeia de spins de Heisenberg. Consideramos três formas de quebrar a integrabilidade: interação de um campo externo com um único spin, interação com um campo aleatório em cada spin da cadeia e interação entre segundos vizinhos. Nós propomos uma transição integrável-caótica pode ser descrita por uma lei de potências na densidade espectral $S(k)$, ou seja os sistemas quânticos caóticos apresentam ruído $S(k) \propto 1/k^{\alpha}$, onde $\alpha = 2$ para o caso integrável e $\alpha = 1$ para o caso caótico, com $1 < \alpha < 2$ para sistemas que estão entre os dois regimes. A transição também é descrita pelo comportamento do "*burstiness*" B e da divergência de Kullback–Leibler $D_{LK}(P_{W-D}(s)|P_{dados}(s))$, onde $P_{W-D}(s)$ é a distribuição de Wigner-Dyson e $P_{dados}(s)$ é a distribuição de espaçamentos obtida do sistema. O primeiro é associado a séries de eventos de caráter regular e o segundo mede o grau com que diferem as duas distribuições estatísticas. Analisando o comportamenteo desses indicadores, obtivemos uma rota universal para a transição integrável-caótico na cadeia de spins.

Palavras-chave: Teoria de matrizes aleatórias. Densidade espectral de potencias. Burstiness. Divergencia Kullback–Leibler. Transição ao caos. Funções de crossover. Series de tempo.

List of Figures

Contents

1 Introduction

1.1 Classical Chaos

There are systems described by equations of motion which may have different qualitative properties. One of them is integrability. Suppose we have a system with N degrees of freedom, so that its phase space has $2N$ dimensions. Such system will be integrable if there are N independent integrals of motion I_i, such that (REICHEL, 1992)

$$I_i(p_1, p_2, ..., p_N; q_1, q_2, ..., q_N) = C_i, \tag{1.1}$$

where $i = 1, ..., N$, C_i is a constant, p_i and q_i are the canonical momentum and position associated with the i-th degree of freedom. Integrals of motion can be classified as non-isolated or isolated. Non-isolated integrals do not give much information, whereas the isolated integrals are related to the symmetries of the system and define phase space surfaces. Another way to describe the integrability condition is via the observation that the Poisson brackets between all integrals of motion vanish, i.e.

$$\{I_i, I_j\}_{Poisson} = 0 \tag{1.2}$$

for all i and j. In the case of non integrable systems, internal nonlinear resonances may exist that drive the system into a chaotic dynamic.

Establishing if a system is integrable or not is usually a hard task. In the case of systems with two degrees of freedom, we may proceed by using a Poincaré surface section. Suppose we have a conservative system with two degrees of freedom. Time translation symmetry implies that the system has the energy as a constant of motion

$$H(p_1, p_2; q_1, q_2) = E. \tag{1.3}$$

Therefore, the Hamiltonian is an isolated integral of motion. So if the system has another

isolated integral $I_2 = C_2$ and the initial conditions are given, the trajectories will be constrained to the intersection of I_2 and E. However, we usually do not know if the additional isolated integral I_2 exists. One way to proceed is to numerically solve the equations of motion $\frac{dp_i}{dt} = -\frac{\partial H}{\partial q_i}$ and $\frac{dq_i}{dt} = \frac{\partial H}{\partial p_i}$, for $i = 1,2$. Next, we plot p_2 and q_2 each time the condition $q_1 = 0$ is satisfied. If the system is integrable, its trajectory appears as series of points on a curve. If the system is non integrable the trajectory may appear as points spread all over the phase space and limited to a finite area due to energy conservation.

Chaotic systems form a subclass of non-integrable systems. A measure of the chaotic property is given by a positive *Kolmogorov-Sinai* metric entropy or *KS* metric entropy. This is a measure of hyperbolic instability flow of trajectories in phase space and it is related to fixed points of the Hamiltonian. The description of the fixed points can be made in terms of action-angle variables. As a concrete example, consider the single Hamiltonian resonances

$$H = J_1 - J_1^2 - J_1 J_2 + 3J_2^2 + \alpha J_2 (J_1 - J_2)\cos(2\Theta_2). \tag{1.4}$$

The fixed points are given by $\frac{dJ_2}{dt} = 0$ and $\frac{d\Theta_2}{dt} = 0$. The neighborhood of these points allows us to describe the behavior and nature of the flux by linearizing the equations of motion in their vicinity. It is important to mention that the nature of the flux in the neighborhood of fixed points can also be studied by moving a point in phase space. To be specific, consider a system with N degrees of freedom and define two vectors: $X_t^N = X^N(p_1(t),...,p_N(t);q_1(t),...,q_N(t))$ and $Y_t^N = X_t^N + \Delta X_t^N$. These vectors evolve according to Hamilton's equations of motion. The magnitude of the displacement ΔX_t^N is defined as

$$d_t(X_0^N, Y_0^N) = \sqrt{(\Delta X_t^N \cdot \Delta X_t^N)}, \tag{1.5}$$

where ΔX_0^N and ΔY_0^N are the initial values of ΔX_t^N and ΔY_t^N respectively. Then, the rate of exponential growth of $d_t(X_0^N, Y_0^N)$ is given by

$$\lambda(X_0^N, Y_0^N) = \lim_{t \longrightarrow \infty} \frac{1}{t} \ln\left(\frac{d_t(X_0^N, Y_0^N)}{d_0(X_0^N, Y_0^N)}\right), \tag{1.6}$$

where $\lambda(X_0^N, Y_0^N)$ is called the Lyapounov exponent. It is related with the separability of the trajectories in phase space. From Eq.(1.6), we may write $d_t(X_0^N, Y_0^N)$ in terms of the Lyapunov exponent

$$d_t \sim d_0 e^{\lambda t}. \tag{1.7}$$

The exponent λ quantifies the growth of the deviation between two orbits in phase space due to a perturbation. It also sets a specific time scale $\tau \sim \frac{1}{\lambda}$ that helps to classify the dynamical regimes. Chaos, for instance, is appreciable only for $t >> \tau$, if λ is positive. If $\lambda < 0$ the system approaches a regular attractor.

In summary, we saw that chaos can be measured with the KS entropy, and precisely defined with Lyapounov exponents. Therefore, there is a relation between these two concepts, which was established by (YA.G, 1976). To see it, let:

$$P(X^N) = \sum_{i=1}^{N-1} \lambda_i(X^N), \tag{1.8}$$

where $\lambda_i(X^N)$ denotes the Lyapounov exponent on the interval $X^N \longrightarrow X^N + dX^N$, then the KS entropy is given by (BENETTIN; GALGANI; STRELCYN, 1976)

$$h(E) = \int_{\Gamma_E} P(X^N) d\mu_E, \tag{1.9}$$

where $d\mu_E$ is the invariant volume element of the energy surface. Therefore the KS entropy has a qualitative behavior similar to the Lyapunov exponents.

Some systems have phase-spaces containing a mixture of regular and chaotic trajectories. One of the most famous is the $Henon - Heiles$ system. It is useful to describe the non-linear movement of a star around a galactic center. Such movement takes place in a plane, and the KS entropy has an intrinsic dependence on the energy. The fraction of phase spaces occupied by regular and chaotic trajectories can be varied by changing the system's parameters.

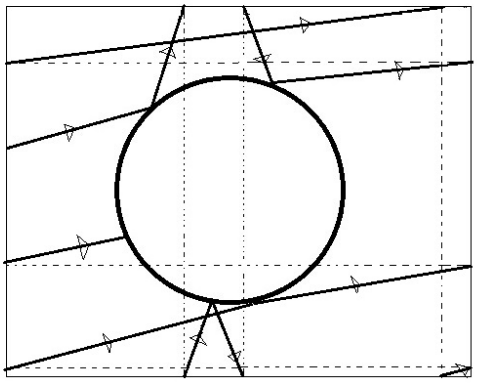

Figure 1 – Sinai billiard

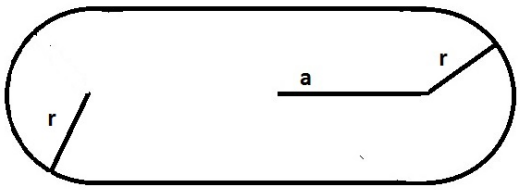

Figure 2 – Bunimovich billiard

Another type of behavior is the K-flow, usually found in strongly chaotic systems. The *Sinai billiard* is a typical example. It consists of a particle inside of a box which has a hard circular barrier, as shown in figure 1. The system has periodic boundary conditions and the convex surface of the barrier causes the neighboring trajectories to change abruptly generating a divergence among them in phase space. A particle in a planar concave cavity (stadium) is another example of K-flow. The stadium consists of two half circle of radius r connected to parallel lines of size $2a$, as we see in figure 2. When $a = 0$ the stadium has a circular form but if a increases the system becomes chaotic, as was proved by Bunimovich (BUNIMOVICH, 1974). Another interesting characteristic of this billiard is the possible existence of transition between regular and chaotic flow for $a << r$.

1.2 Quantum Chaos

1.2.1 Symmetries and Universality Classes

To understand how quantum chaos arises we must begin with basic concepts which will be the physical pillars to build a theory of quantum chaos. As we saw, the emergence of classical chaos depends on the absence of integrals of motion, which can be related to the breakdown of symmetries in the system. In the case of quantum mechanics, every symmetry is associated with a quantum number and, if the system is invariant under a specific symmetry then there will be an associated operator $\hat{R}$ which commutes with the Hamiltonian $\hat{H}$. This fact can be expressed as follows

$$[\hat{R},\hat{H}] = 0. \tag{1.10}$$

As we saw, if $\hat{R}$ commutes with $\hat{H}$, we may assume that $\hat{R}$ is self-adjoint and we can choose a base set of functions $\{\phi_{n,\alpha}\}$ that are eigenfunctions of $\hat{R}$. It is represented by the eigenvalues equation $\hat{R}\phi_{n,\alpha} = r_n\phi_{n,\alpha}$, where α labels all eigenfunctions $\phi_{n,\alpha}$ with the same eigenvalue r_n. The Hamiltonian elements in this new basis can be obtained from the following equation

$$\langle \phi_{n,\alpha} | \hat{H} | \phi_{m,\beta} \rangle = \delta_{nm} H^m_{\alpha\beta}, \tag{1.11}$$

which implies a block-diagonal matrix representation of $\hat{H}$

$$\hat{H} = \begin{bmatrix} H^1 & 0 & \cdots \\ 0 & H^2 & \cdots \\ \cdots & \cdots & \ddots \end{bmatrix}.$$

The first symmetry that we are going to consider is the time reversal symmetry, which can be represented by an operator $\hat{T}$ that changes the sign of time, $\hat{T}f(t) = f(-t)$. Taking this $\hat{T}$ operator into account, we can construct a new operator $\hat{C}\hat{T}$ that commutes with the temporal part of the Schrödinger equation $i\hbar\frac{\partial}{\partial t}$, thus

$$\left[\hat{C}\hat{T}, i\hbar\frac{\partial}{\partial t}\right] = 0, \tag{1.12}$$

where $\hat{C}$ is a complex-conjugation operator, which when applied either to another operator or function returns its complex conjugate. Next, we need to know under what conditions the operators $\hat{C}\hat{T}$ and $\hat{H}$ commute. For conservative systems, we only have to consider the commutation between $\hat{C}$ and $\hat{H}$. We consider three different situations. First, consider the Hamiltonian of a particle in an electromagnetic field

$$\hat{H} = \frac{1}{2m}\left(\hat{p} - \frac{e}{c}\hat{A}\right)^2 + \hat{V}(x). \tag{1.13}$$

Due to the $\hat{p}$ operator, $\hat{H}$ does not commute with $\hat{C}$. Therefore, time-reversal symmetry is broken for such systems (STÖCKMANN, 2000) and the Hamiltonian is not usually represented by a real matrix. However, the hermitian property of the Hamiltonian is preserved under unitary transformations like transformed using unitary matrices

$$\hat{H}' = \hat{U}\hat{H}\hat{U}^{\dagger}. \tag{1.14}$$

In the case of systems which have time reversal symmetry, we have two possibilities: if the system does not have spin interactions the Hamiltonian is invariant under orthogonal transformations

$$\hat{H}' = \hat{O}^T\hat{H}\hat{O}. \tag{1.15}$$

However, if there are spin interactions the Hamiltonian will be invariant under symplectic transformations

$$\hat{H}' = \hat{S}\hat{H}\hat{S}^R. \tag{1.16}$$

In the formulas above, $\hat{U}$ is a unitary matrix, $\hat{O}$ is an orthogonal matrix and $\hat{S}$ is a symplectic matrix.

1.2.2 Random Matrix Theory

With the intent to explain the spectra of complex nuclear systems (heavy nuclei), E.P.Wigner in 1950-1960 proposed a theoretical model in which the spacings between the spectral lines of a heavy nuclei could be described as spacings between eigenvalues of a random

matrix. This model marks the beginning of random matrix theory (RMT). In its early days, RMT consisted of three different kinds of random matrix ensembles according to the presence or absence of certain physical symmetries. Seven additional ensembles were found later, but since they are irrelevant for the present work we shall not address them. The three main ensembles are the Gaussian orthogonal ensemble (GOE), the Gaussian unitary ensemble (GUE) and the Gaussian symplectic ensemble (GSE).

1.2.3 Gaussian Orthogonal Ensemble

The first ensemble that we are going to consider is related to orthogonal transformations and its elements can be represented by real symmetric matrices, leading to $N(N+1)/2$ independent matrix elements. A Hamiltonian matrix that belongs to this class satisfies the property

$$H_{nm} = H_{mn} = H_{nm}^{*}, \tag{1.17}$$

where H_{nm}^{*} is the complex conjugate element. Also, since the Hamiltonian elements are real numbers, we may associate them to only one degree of freedom. The Gaussian orthogonal ensemble is thus appropriate for systems that are invariant under time reversal and spin rotation symmetries. The matrices of GOE have elements that are independent random numbers that obey a Gaussian distribution with zero mean and variance $< H_{i,i}^{2} >= 4\sigma^{2}$ for the diagonal elements, and variance $< H_{i,j}^{2} >= 2\sigma^{2}$ for the off-diagonal elements.

With the assumption that the GOE eigenvalues are a good description of a given complex spectrum, then the distribution of spacings between adjacent eigenvalues $s_i = \varepsilon_{i+1} - \varepsilon_i$ is given by

$$P_{GOE}(s) = \frac{\pi}{2} s e^{-\frac{\pi}{4}s^{2}}, \tag{1.18}$$

which is known as the GOE Wigner-Dyson distribution.

1.2.4 GUE: Gaussian Unitary Ensemble

Systems with preserved spin rotation symmetry but not invariant under time reversal, e.g an atom in the presence of an external magnetic field, cannot be described by the GOE. We assume that the external field perturbs the energy levels' positions in an amount at least as large as the average spacing in absence of the field. It is important to stress that the random hypothesis must be ensured if we want to model the system through an ensemble of random matrices, thus the magnetic field has to be strong enough (MEHTA, 2004). Bearing this in mind, this system allow us to introduce the Gaussian unitary ensemble which is appropriate to systems with broken time reversal symmetry. A member of the GUE is a hermitian matrix with the property

$$H_{nm} = H_{mn}^{*} \tag{1.19}$$

where H_{nm} are the matrix elements and H_{mn}^{*} denotes the complex conjugate. The matrix elements being complex numbers can be associated with two degrees of freedom. The GUE is appropriate in the description of systems such as billiards having the reflection properties in the walls changed for ensuring the breaking of the time reversal symmetry(MEHTA, 2004). The level spacing distribution of the GUE is given by

$$P_{GUE}(s) = \frac{32s^2}{\pi^2} e^{-\frac{4s^2}{\pi}}, \tag{1.20}$$

which is known as the GUE Wigner-Dyson distribution.

1.2.5 GSE: Gaussian Symplectic Ensemble

The previous ensembles were characterized by the presence or absence of time reversal symmetry, with spin rotation invariance being present in GOE and irrelevant in GUE. Now we consider systems with time reversal symmetry, but in the absence of spin-rotation symmetry. In this case, the RMT ensemble is known as Gaussian symplectic ensemble (GSE). The GSE is invariant under symplectic transformations and its members are given by the next equation

$$H_{nm} = H_{nm}^{0} 1 - i \sum_{j=1}^{3} H_{nm}^{j} \sigma_j, \tag{1.21}$$

	DF	TRS	SRS	$H_{n,m}$	TT
GOE	1	yes	yes	Real	Orthogonal
GUE	2	no	yes/no	Complex	Unitary
GSE	4	yes	no	Quaternionic	Simplectic

Table 1 – Table contains information about the three main ensembles: GOE, GUE and GSE. The acronyms DF, TRS, SRS and TT stand for degrees of freedom, time reversal symmetry, spin rotation symmetry and type of transformation respectively.

where 1 is the 2x2 identity matrix, H_{nm}^{j} are complex coefficients and σ_j are the Pauli matrices. The fact that the elements of a GSE matrix have a quaternionic spin representation implies that they can be associated with four degrees of freedom. The level spacing distribution of the GSE is given by

$$P_{GSE}(s) = \frac{2^{18}s^4}{3^6\pi^3}e^{-\frac{64s^2}{9\pi}}, \tag{1.22}$$

which is known as the GSE Wigner-Dyson distribution.

Finally, we summarize the fundamental properties and symmetries of these three ensembles in table 1.

1.2.6 Quantum Billiards

As we mentioned before the Sinai and Bunimovich billiards are examples of classical chaotic systems (K-flows). The chaotic behavior is essentially caused by the shape of the boundary. For example, in the case of a Bunimovich billiard the deformation from the circle to the stadium breaks integrability and gives rise to chaos. In the case of a Sinai billiard, chaos is due to a defocussing effect of reflection at the inner circle (GUHR; MÜLLER-GROELING; WEIDENMÜLLER, 1998a). The quantum analog of this kind of classical chaotic systems is defined by the stationary Schrödinger equation with Dirichlet boundary conditions, i.e. the wave function is zero at the boundary. Thus, the problem is similar to the study of membrane vibrations since the Schrödinger equation of free particle is just a Helmholtz equation, which makes the problems mathematically equivalent. For this reason, many mathematicians were motivated to study this kind of model independent of the quantum physics connections. Hence, the smoothed part of the cumulative density of the levels that they found is related to the geometry of the

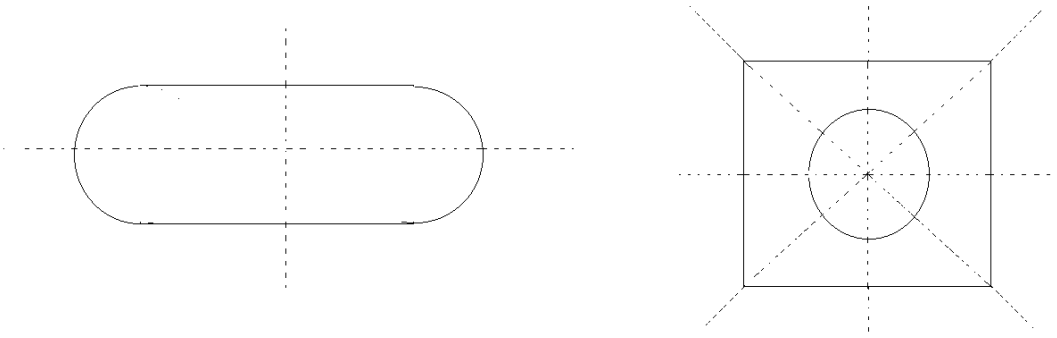

Figure 3 – Bunimovich (left) and Sinai(right) billiards. The dashed lines divide them on their symmetry axes (GUHR; MÜLLER-GROELING; WEIDENMÜLLER, 1998a).

system and can be expressed as follows(GUHR; MÜLLER-GROELING; WEIDENMÜLLER, 1998a)

$$\zeta(k) = \frac{A}{4\pi}k^2 \mp \frac{L}{4\pi}k + C, \tag{1.23}$$

where A is the area and L is the length of the perimeter of the billiard, k is the wave number and C gives information of curvature corrections and topological properties too. This formula is valid for arbitrary geometries. The area and the perimeter terms were found by Weyl (WEYL, 1912) and Kac (KAC, 1966) respectively.

We focus our attention on the spectral fluctuations of the systems. These fluctuations depend on the boundary's shape in a sensitive way. Thus, for a suitable spectral analysis we must unfold the spectrum using equation (1.23) and separate the energy levels in sets according to the proper quantum numbers of the system. For that purpose, we remove spatial symmetries by dividing the billiards as shown in figure 3.

A number of interesting facts came from billiard's research. One of the most important works was that by McDonald and Kaufman (MCDONALD; KAUFMAN, 1979) in 1979. They calculated the eigenstates of the Bunimovich and circle billiard, obtaining the spacing distribution of the Wigner type for the Bunimovich billiard and Poisson distribution for the circular billiard. They concluded that the differences between spacing statistics were due to the integral or non-

integral properties of the billiard's dynamics. The Sinai billiard was studied by Berry(BERRY, 1981) in 1981. He demonstrated the relation between RTM and the spacing distribution using numerical methods. Later, Bohigas *et al.*(BOHIGAS; GIANNONI; SCHMIT, 1984a) found results for the spacing distribution of the Sinai billiard, which were in very good agreement with the Wigner-Dyson distribution, by computing more than 700 eigenvalues. Albeit quite modest on today's computational standards, it was seen as a relevant statistical evidence of the validity of the Wigner-Dyson distribution in chaotic billiards.

The quantum analog description of these systems can also be obtained through the assumption that the billiards are microwave cavities. Thus, we have two ways to study the system: simulations and experiments. Both ways allow us to modify parameters of the billiard, such as perimeter and curvature. Experimental studies of chaotic microwave cavities showed a number of interesting results. Stöckmann and Stein, e.g., studied the Bunimovich and Sinai billiards obtaining around 1000 eigenmodes using microwave cavities about half a meter in size and 8mm thick. The experimental result for the spacing distribution was very close to the RMT prediction, i.e. the Wigner-Dyson distribution. In the case of a rectangle cavity the same authors found a Poisson distribution, as expected for an integrable system. Other important microwave experiments were made by Sridhar(SRIDHAR, 1991), Sridhar and Heller(SRIDHAR; HELLER, 1992). Their results showed that there is a connection between wave functions and classical periodic orbits.

Measurements of spectral observables in a crossover between universality classes also gave interesting results. For instance, Stoffregen *et al* (STOFFREGEN et al., 1995) constructed a microwave cavity inside which a wave guide was inserted. Such a setup allowed the study of the eigenvalues spectrum and the nearest neighbor distribution as a function of the cavity length.

1.3 Quantum Chaos in spin Systems

1.3.1 Integrability in spin systems

The study of quantum chaos in spin systems was developed within the same framework of concepts that have defined this theory in billiards and Hamiltonian systems. We may summarize these concepts in two ideas about what is quantum chaos before focusing in the spin case:

1. Quantum chaos is a spectral manifestation which arises in systems that have few degrees of freedom and the classical counterpart is characterized by non-integrability and a positive Lyapunov exponent.

2. Quantum chaos is observed in systems that have an energy spectrum which behaves statistically similar to the time evolution of a dynamical variable close to the equilibrium value predicted by statistical mechanics.

Although, these two quantum chaos characteristics give a general idea about what this theory means, it is important to highlight how the integrability concept arises in spin systems. So, there are two classical integrability concepts in those systems: dynamical integrability and thermodynamic integrability.

1.3.2 Dynamical Integrability

Consider a system with N localized classical spin components $\hat{S_n}$ with $n = 1,2,...,N$ associated with the interaction Hamiltonian $\hat{H}(\hat{S_1},\hat{S_2},...,\hat{S_N})$. The time evolution is given by the Hamilton equation of motion,

$$\frac{d}{dt}\hat{S_n} = i\{\hat{H},\hat{S_n}\}, \tag{1.24}$$

where $\{\hat{H},\hat{S_n}\}$ is the Poisson bracket. The above equation is consistent with the Heisenberg equation of motion

$$\frac{d}{dt}\hat{S_n} = i[\hat{H},\hat{S_n}]. \tag{1.25}$$

Thus, a system with N classical spins is *dynamical integrable* if there exist N distinct integrals of motion (MÜLLER, 1986)

$$J_k[\hat{S_1},\hat{S_2},...,\hat{S_N}] = constant, \tag{1.26}$$

where $k' = 1,2,...,N$, $k = 1,2...,N$ and J_k is the J_k-th action variable, which are in involution, i.e. the following Poisson commutation relations hold: $\{\hat{H},J_k\} = 0$ and $\{J_k,J_k\} = 0$. These

N integrals of motion are confined in a $2N$ phase space and are intersected with $N(2N-1)$ dimensional hyper-surfaces $J_k = constant$. This description based on integrals define a invariant tori due to periodic motion obtained from action-angle variables since these coordinates, for an integrable Hamiltonian, define a toroidal hyper-surface. On the other hand, if the foliation (union of small manifolds obtained by decomposition of the initial manifold) of the entire phase produced by an invariant tori is destroyed by broken symmetries, the trajectories leave the tori and become chaotic.

A popular example of a dynamical spin system is a Heisenberg chain. The integrals of motion are: the total energy, the z-component of the total spin and the total spin. When the system has an anisotropic interaction in one direction the total spin invariance is broken, albeit the dynamical integrability remains. On the other hand, we have spin systems where dynamical chaos arises, such as the XY model with single-ion anisotropy(MÜLLER, 1986), the XY model with external field applied in a single spin and the Ising model in a transverse field.

1.3.3 Thermodynamic Integrability

For a classical spin system with N spins, the partition function can be expressed as an N-fold integral(MÜLLER, 1986)

$$Z_N = \int dS_1 \int dS_2 \cdots \int dS_N e^{-\beta H(S_1,S_2,\ldots,S_N)}. \tag{1.27}$$

This function has to be analytic if N is finite, although the *thermodynamic integrability* is reached in the limit $N \to \infty$ and the analytical properties of the partition function experiment some qualitative changes. Hence, the thermodynamic integrability can be present in 1D spin system with nearest neighbor interaction. Nevertheless, the thermodynamic integrability is studied by the transfer operator technique(MÜLLER, 1986). Then, the partition function defined by the equation (1.27) has an integral operator which has a kernel. That kernel, in turn has one integral equation with n eigenvalues that allow us to describe the partition function as a sum of them. In the case of higher dimensions the transfer operator works as an infinite set of integrals or matrices without knowing properties However, models like the Ising guarantee the existences of the integrability property.

The infinite classical spin systems have associated infinite conservation laws, which

support the method of diagonalizing the transfer operator (MÜLLER, 1986; BAXTER, 1982). The spectrum related to these transfer operators are associated, in a critical point, to quasi-particle excitations close to the largest eigenvalue, which determines the free energy form.

Consequently, the integrability properties related to a spins system show two important facts: the dynamical integrability is due to the foliation of the phase space by invariant tori is preserved whereas the thermodynamic integrability is associated with the existence of the limit $N \to \infty$.

1.3.4 Chaos in Quantum Spin Systems

The foliation is partially broken the non-integrability occurs providing chaotic trajectories in the dynamical systems; whereas in thermodynamical systems the non-integrability could be related to the level repulsion in the spectrum of the transfer operator. In the case of quantum spin systems there are different properties that are related to the Hamiltonian. Thus, in the case of dynamical and thermodynamical integrability the structure of the Hamiltonian determines the time evolution of dynamical variables and the functional energy form alters the thermodynamic property.

On the other hand, the non-integrability effects in the quantum spin systems are associated with Classical and thermodynamic limits. The first takes into account N finite, but $s \to \infty$ and the opposite for the thermodynamical case (s finite, $N \to \infty$). It is important to say that the chaos can arise by other facts that will be discussed later. We have already seen that the quantum spectrum is discrete for spin systems. The parts of the spectrum that are regulars tend to be separated in a equidistant way. Moreover, level repulsion is presented where the spectrum is regular with narrow gaps. The energy level distribution of integrable systems is an intrinsic characteristic of the system, although this lacks of universality. Thus, this can be different for many quantum integrable systems. Nevertheless, the distribution of the differences between neighbor energies (spacing) into the total spectrum after making a statistical treatment called $unfolding$ is a property well known that characterizes the quantum integrable systems. Actually, this spacing distribution is Poisson type i.e if s is an spacing after making unfolding the equation of the spacing distribution will be

$$P_p(s) = e^{-s}. \tag{1.28}$$

We will discuss with more detail the unfolding procedure and the distribution behavior later.

The Poisson spacing distribution is an universal property which identifies any quantum integrable system, although, we must say that in systems like 1D Heisenberg chain, the quantum integrability depends also on the existence of a good number of conservations laws. Hence, the set of quantum numbers plays analogous role of the action-angle variables in the integrable classical Hamiltonian systems.

A fundamental proposal of the quantum integrability is framed in the existence of set of properties whose results preserve the conservation laws. Nevertheless, the quantum chaos is obtained with a set of statistical features that are related to the behavior of a specific dynamical variable when it evolves in time until approaches to its equilibrium value that is predicted by the statistical mechanics. Taking into account that these kinds of systems satisfy $N \to \infty$. However, the statistical test associated to these systems for checking its quantum integrability represent a hard task, even so a good quantity that allows us to obtain information about the statistical behavior is the time-dependent correlation function. Hence, this quantity can be understood as a long-time asymptotic property in quantum spin models when they are analyzed in a thermodynamic limit. It is important to say that the asymptotic correlation function property, in the case of quantum spins models is more probable at the time of formulating conclusions about the integrability or non-integrability of the system.

1.4 Transition from integrable to chaotic in spin chains

The quantum systems explained before can be differentiated according to their properties, whose result allows us to infer whether the system is integrable or chaotic. Therefore, if the level spacing distribution of such system is Poisson type, the system will be defined integrable which means that the quantum numbers is equal to the degrees of freedom. On the other hand, systems whose spacing distributions satisfies the Wigner-Dyson distribution are called chaotic.

The Poisson distribution as a condition of integrability implies that the spacing energies are uncorrelated. However, this condition can be broken by diverse ways obtaining as final result one system whose spacing distribution is either an intermediate distribution between Poisson and Wigner- Dyson or completely Wigner-Dyson. In other words, the integrability can be broken

generating one system which may be in one intermediate or chaotic state.

In the case of many body interactions, the spin chain systems reveal interesting chaotic and integrable properties. Thus, The Heisenberg spin model allows us to understand this properties. The Hamiltonian that describes this model, without considering external interactions is defined as follows

$$\hat{H} = \frac{1}{2}\sum_{i=1}^{L}(J_x\hat{\sigma}_i^x\hat{\sigma}_{i+1}^x + J_y\hat{\sigma}_i^y\hat{\sigma}_{i+1}^y + J_z\hat{\sigma}_i^z\hat{\sigma}_{i+1}^z). \tag{1.29}$$

where $\hat{\sigma}_i^j\hat{\sigma}_{i+1}^j$ with $j = x,y,z$ are the interaction terms between nearest neighbor in any direction defined by the Pauli matrices. J_i are strength coupling constants respectively. This model is understood as a chain which can be open with $L = N-1$ or closet with $L = N$. The last one implies that the last spin interacts with the first one in all directions.

The integrability is usually broken in this model due to specific parameter which affects the system. Such parameter can increase until certain value where the system is chaotic. Thus, if this parameter goes from zero to the associated chaotic value the system will experiment one $transition$ from integrable to chaotic state. Such transition is observed in diverse Heisenberg model variations. For instance two coupled chains, next nearest neighbor interaction introduced in the chain and external magnetic field (HSU; D'AURIAC, 1993) interaction are most of the common models whose transition are studied as a function of coupling parameter. Some of these models must separate the eigenvalues in sets according to symmetries. The transition is usually observed in the behavior of the spacing distribution. It goes from Poisson to Wigner-Dyson when the transition finishes.

The spin chain models which describes transition to chaos are related to external parameters as a magnetic fields. Such fields produce $defects$ in the chain, that is one spin which is affect by the external field. This transition is observed if the defect takes place in the middle of the chain and the amplitude field increases. Defects in the edges of the chain break some symmetries but not to allow the transition to occur. It is important to say that external interaction with a random magnetic field, whose mean square amplitude increases, is a cause of chaos transition if the interaction takes places in each spin of the chain. In other words, there is a transition to chaos when each site in the chain is interacting with a random magnetic field. However, in both cases when the amplitude is larger than a specific value the system becomes localized and the

integrability is recovered. The randomness is not the causes of integrability breaking but the existence of the defect is(SANTOS, 2004). The transition is also dependent on parameter given through the distance of the Wigner-Dyson distribution and the distribution obtained from the data. It has a maximum value equal to one for the integrable case and zero for the chaotic domain.

The Heisenberg model with next nearest neighbor interaction describes integrability breaking. Furthermore, the transition is observed through crossover functions, whose independent parameters are strength coupling terms, are fitted by hyperbolic functions of peak position (RABSON; NAROZHNY; MILLIS, 2004). There are crossover functions which relate the strength couping with the distance between the Wigner-Dyson distribution and data distributions that decrease following a power law.

On the other hand, the Bosonic and Fermionic systems also present integrable-chaotic transition, more precisely hard core bosons and spinless fermions in 1D dimensional lattice (SANTOS; RIGOL, 2010) where the next nearest neighbor hopping interaction is taken into account. This interaction depends on two parameters which represent the hopping strength, when this strength increases the integrability is broken and the system undergoes a transition to chaotic domain. It can be observed in the peak position of the spacing distribution which can be also associated with *Brody distribution*(BRODY et al., 1981). This is defined as follows

$$P_\beta(s) = (\beta+1)bs^\beta e^{-\beta s^{\beta+1}}, \qquad b = \left[\Gamma\left(\frac{\beta+2}{\beta+1}\right)\right]^{\beta+1} \tag{1.30}$$

where $\beta = 0$ in the integrable case and $\beta = 1$ in the chaotic case. If $0 < \beta < 1$ we obtain intermediate distributions between Poisson and Wigner-Dyson. There are other quantities which describes the transition in this model as the Shannon entropy and the level number variance. The first of these two quantities changes its form depending on the hopping parameter. That is, the Shannon entropy changes with the temperature but its functional form in the graphics is different depending on the hopping strength. The GOE value corresponding to the Shannon entropy turns out in one asymptote, thus in the chaotic domain the entropy graphics displays this behavior. In the case of the level number variance(GUHR; MÜLLER-GROELING; WEIDENMÜLLER, 1998b), it provides information of long-range correlation in the energy spectrum making a fit

over staircase function in a level window. It is defined as follows

$$\Sigma(l)^2 = \left\langle [N(l,\varepsilon)]^2 \right\rangle - \left\langle N(l,\varepsilon) \right\rangle^2. \tag{1.31}$$

where $N(\varepsilon, l)$ gives the number of the states in the interval $[\varepsilon, \varepsilon + l]$ If the distribution is Poisson type this quantity has a linear form which implies that long correlation grow as l increases, whereas if the system obeys the Wigner-Dyson, distribution the functional form is logarithmic. Thus, the correlations are less significant than the regular systems.

Other systems which describe transition integrable-chaotic are the quantum billiards(ROBNIK, 1983). For example, the Rubnick Billiard is a cavity whose shape is defined in the complex plane by the equation $w = z + \lambda z$. Where $|z| = 1$ and the λ parameter produces a deformation over this cavity. Depending on λ the billiard experiments a smooth transition. Hence it is observed in the interval $[0, 1/2)$. Furthermore, small values of λ make this billiard obey the rules of Kolmogorov-Arnold-Moser systems, whereas larger λ values generate only one chaotic region in the phase space.

The energies of these billiards are obtained from stationary Schrödinger equation of a free particle and are divided in two sets according to the parity of wave functions (GÓMEZ et al., 2005). It is important to say that the transition is observed in the power spectral density exponent related to the Metha-Dyson statistic obtained from the unfolded energies. This kind of transition will be explained in detail later.

On the other hand, the transitions explained before have been studied in quantum systems, although it can be present in other systems. For instance, points uniformly distributed over self-similarity Koch fractals, whose dimension is K, experiment Integrable-chaotic transitions (SAKHR; NIEMINEN, 2005).

The intermediate states distribution of those fractals is represented by the Brody distribution. In the case of fractals their dimension is equal to the Brody parameter. Therefore, as the dimension fractal increases these point sets begin to describe a transition to chaotic domain.

2 Gaussian Ensembles Analysis

The random matrix theory is based on the ensemble construction in order to explain the behavior of heavy atoms. The theory predicts specific distributions for energy spacing according to the system symmetries. There are three common ensembles in this theory: Gaussian orthogonal ensemble, Gaussian unitary and Gaussian symplectic ensemble. However in this chapter we will study the properties of the GOE ensemble and subsequent results since its spacing distribution is directly related to the quantum chaos after making a statistical procedure which allows us to eliminate the non-universal part of the energy spectrum.

On the other hand, the spacing statistics are related to the time series analysis and, therefore with the power spectral density which characterizes the noise system. In this sense, the noise characterization reveals a power law with exponents well defined for the chaotic and integrable case. Thus, in this chapter we will discuss, through computational results made in Matlab, related concepts to the noise and time series associated to Gaussian orthogonal ensemble in order to find out other universal property which relates the chaos and the time series analysis.

2.0.1 GDE Eigenvalue Distribution

As we saw, the random matrix theory is intrinsically related to the chaotic properties of a system; it can describe correctly the statistical behavior of systems with broken integrability features. It is done by the ensemble constructions which are based on conservation laws. As we have seen, the invariance of the Hamiltonian by a specific transformation determines one ensemble construction. In this sense, we have studied three different ensembles: GOE, GUE and GSE.

However, there is another ensemble which reproduces the statistical properties associated with integrable spectrum, which is called *Gaussian diagonal ensemble* (NO et al., 2002; CHATTERJEE; CHAKRABARTI, 2007). It consists in a set of n diagonal matrices of size $N \times N$ whose eigenvalues are the diagonal elements. Hence, we generate 100 matrices ($n = 100$) of dimension $N = 2000$, The eigenvalues distribution (level density) will be given in the figure 4

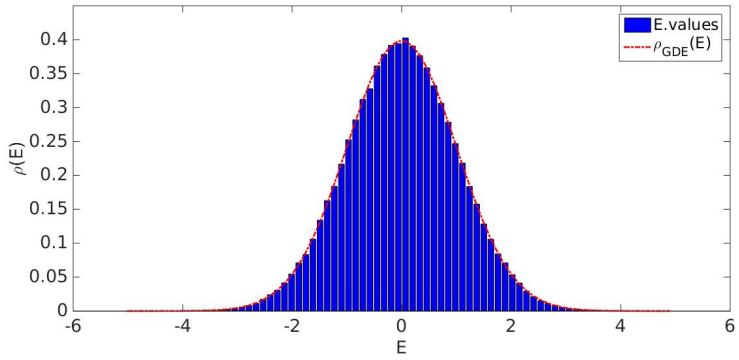

Figure 4 – Eigenvalue density for an ensemble GDE of $n = 100$ and dimension matrix $N = 2000$. The dashed line represents the theoretical fit

.

Due to matrix form, the distribution density $\rho_{GDE}(E)$ has a Gaussian behavior, whose statistical parameters are the mean $\mu = 0$ and standard deviation $\sigma = 0.99$, given by the equation

$$\rho_{GDE}(E) = A(\sigma)e^{-\frac{(x-\mu)^2}{2\sigma^2}}, \tag{2.1}$$

where $A(\sigma) = \frac{1}{\sigma\sqrt{2\pi}}$ is a normalization constant. The last equation gives information of the eigenvalues distribution and the probability to obtain one of them. In our case, the fit made has good approximation to the histogram obtained due to large data quantity.

2.0.2 GOE Eigenvalue Distributions

The heavy nuclei analysis involves behaviors associated with resonances obtained through scattering methods. Neutrons colliding a target heavy nucleus show narrow resonances which compound a coexistent state between neutron and nucleus. For a better understanding, of these kinds of collision we can treat the description made by N.Bohr (BOHR, 1936). The strong interaction produced by a neutron-induced nuclear reaction was understood like an equal distribution between all nucleons. Therefore, Bohr constructed one analogous model (figure 5) which is related to the classical context of chaos and very close to the random Matrix Theory.

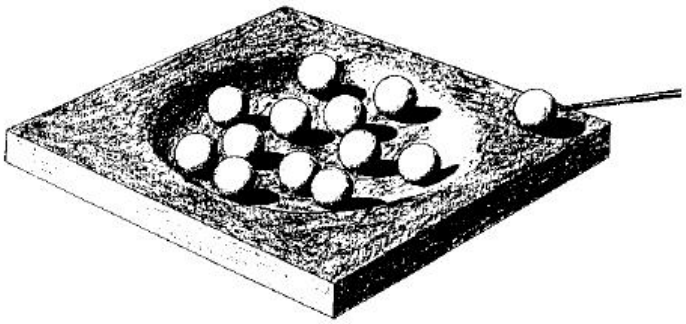

Figure 5 – Wooden model for compound-nucleon scattering. Taken from (BOHR, 1936)

.

The nucleons are represented in figure 5 as a small spheres and the trough simulates the potential which binds the individual nucleons. The collision is represented by an external sphere that enters in the recipient and produces successive collisions between nucleons.

Therefore, the nuclear phenomena described were tried to explain by P.Wigner in 1951. The model developed by Wigner is a statistical description which is different in its procedure to the standard statistical mechanics since we have ensembles of $different$ states governed by the *same* Hamiltonian. Wigner purposes ensemble with $different$ Hamiltonians but governed by the *same* symmetries. These ensembles give a good statistical energy description of the nuclear phenomena. As we could see briefly before, one of the most common ensembles preserves time reversal and rotational symmetries: The Gaussian orthogonal ensemble. We can define this ensemble as follows(MEHTA, 2004):

2.0.2.1 Definition of GOE

The Gaussian orthogonal ensemble E_{1G} is defined in a tangent space T_{1G} of the real symmetric matrices with two conditions

1. The ensemble is invariant under transformations

$$\hat{H} \longrightarrow \hat{O}^T \hat{H} \hat{O} \tag{2.2}$$

where $\hat{O}$ is an orthogonal matrix. This equation implies that the probability $P(\hat{H})d\hat{H}$ that a system of E_{1G} belongs to a volume element $dH = \prod_{i \leq j} dH_{ij}$ is invariant under a real

orthogonal transformation:

$$P(\hat{H}')d\hat{H}' = P(\hat{H})d\hat{H} \tag{2.3}$$

where $\hat{H}'$ is

$$\hat{H}' = \hat{O}^T \hat{H} \hat{O}, \tag{2.4}$$

and it satisfies the condition

$$\hat{O}^T \hat{O} = \hat{O}\hat{O}^T = 1 \tag{2.5}$$

2. The various elements H_{ij},$i \leq j$, are statistically independent. Then we may say that $P(\hat{H})$ is a product of functions, where every function deepens on a single variable:

This ensemble predicts the statistical results in the context of RMT for diverse systems (billiards, hydrogen atom in strong magnetic field, nuclear data etc). The GOE matrices are characterized by the fact that their independent matrix elements are $N(N+1)/2$ and the diagonal elements and the off diagonal elements have variance

$$< H_{i,i}^2 >= 4\sigma^2, \tag{2.6}$$

$$< H_{i,j}^2 >= 2\sigma^2, \tag{2.7}$$

respectively. We can construct the GOE ensemble in the following way

1. Generate a matrix M_N with dimensions $N \times N$ with mean equal to zero and standard deviation $\sigma = 1$.

2. Add to M_N its transpose for obtaining a symmetric matrix $S_N = M_N + M_N^T$.

3. Diagonalize the matrix S_N storing its eigenvalues E.

4. Repeat 1-3 n times storing every matrix. At the end we will have a GOE ensemble $\Gamma_{GOE}(N)^n$ with n matrices and energy ensemble $\Sigma_{GOE}(N)^n$ with N eigenvalues per matrix.

2.0.3 Wigner Semicircle Law

As we have seen, the Random Matrix Theory associates random matrix construction with a Hamiltonian of a physical system. In this sense, the GOE ensemble must be diagonalized for every matrix in $\Gamma_{GOE}(N)^n$, the result will be a set of energies (eigenvalues) which establishing a specific density $\rho_{GOE}(E)$ with a semicircular form, this is called *Wigner semicirle*. This law is based on the statistical independence hypothesis associated with the matrices, where the Equation of the level density is given by(REICHEL, 1992; STÖCKMANN, 2000; HAAKE, 2013; PORTER, 1965)

$$\rho_{GOE}(E,N) = \frac{1}{2\pi\sigma^2}\sqrt{4\sigma^2 N - E^2} \tag{2.8}$$

E are the energy values of a GOE matrix and σ is the standard deviation. The density $\rho_{GOE}(E,N)$ is defined over values less than $4\sigma^2 N$, if $E > 4\sigma^2 N$ we will have $\rho_{GOE}(E,N) = 0$.

Therefore, we generate a GOE ensemble of $n = 100$ realizations of random matrices with dimension $N = 2000$ following the GOE construction procedure. The semicircle law is obtained in figure 6

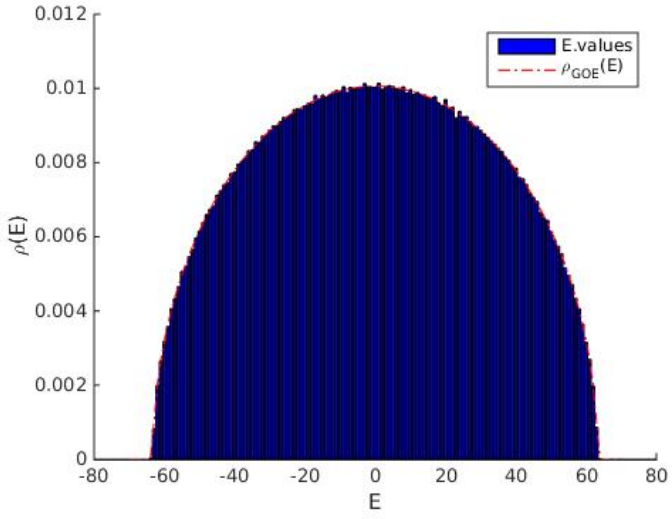

Figure 6 – Eigenvalue density for a GOE ensemble of $n = 100$ realizations and matrix dimension $N = 2000$. The dashed line represents the theoretical equation of $\rho_{GOE,N}(E)$.

.

The density obtained in figure 6 was normalized by its area $A = \frac{4\pi\sigma^2 N}{2}$.

The density values of two other ensembles (GUE and GSE) is also described by the semicircle law. The accuracy ensemble is higher when the matrix size $N \to \infty$.In our case, the result obtained in figure 6 is too close to the theoretical value obtained in Eq.(2.37) since we are working with an ensemble which implies a decrease of the statistical fluctuations due to the ensemble size. Note that the figure 6 does not reveal a semicircular form, rigorously speaking, due to the computational normalization. In general, the computational results of Wigner semicircle are usually obtained in this way(REICHEL, 1992; STÖCKMANN, 2000; HAAKE, 2013; EDELMAN; SUTTON; WANG, 2014).

2.1 Nearest Neighbor Spacing Distribution for GOE and GDE

The set of eigenvalues obtained from the Hamiltonian matrices belonging to GOE ensemble is the mainstay for understanding the integral and more precisely chaotic properties of the system which can be described by RTM. Therefore, the analysis will be developed taking into account not directly the energy ensemble but an alternating ensemble composed by the differences of the successive energy levels (eigenvalues sequence of a GOE matrix). The statistical set of these spacing levels produce a distribution which is known as *nearest neighbor distribution*. This was derived by Wigner to analyze nuclear resonances. He derived the nearest neighbor distribution for an ensemble of random real matrices 2×2 since it provides a very good approximation to the nearest neighbor distribution for $N \times N$ ensemble. One of the most interesting features is that the Wigner distribution is very robust and describing very well the spacing distribution for a sequence of N eigenvalues of a symmetric random matrix, although it lacks accuracy.

$$P(\hat{H}) = \left(\frac{1}{2\pi\delta^2}\right)^{N(\beta N+2-\beta)/4} \times exp\left(-\frac{1}{2\delta^2} Tr[\hat{H}\cdot\hat{H}^{\dagger}]\right) \tag{2.9}$$

Where $\beta = 1,2,4$, N is the matrix dimension and δ is a free parameter. Due to features of ensemble 2×2 we will construct the $P(\hat{H})$ for the case of complex Hermitian matrices. Then, if we define the product between complex Hermitian matrix $\hat{H}$ and its adjoint matrix $\hat{H}^{\dagger}$ as follows

$$\hat{H}_R \cdot \hat{H}_R^{\dagger} = \begin{bmatrix} h_{11}^2 + h_{12}^* h_{12} & h_{11}h_{12} + h_{12}h_{22} \\ h_{11}h_{12}^* + h_{22}h_{12}^* & h_{22}^2 + h_{12}^* h_{12} \end{bmatrix}$$

ensemble	β	$\eta_{N,\beta}$	$\delta\Omega_{V,\beta}$
GOE	1	1	$\delta\Omega_O$
GUE	2	1	$\delta\Omega_V$
GSE	4	2^N	$\delta\Omega_S$

Table 2 – Terms of invariant measure.β is the number of degrees of freedom of ensemble, N is the size matrix, $\delta\Omega_{V,\beta}$ is the differential volume defined as $\delta\Omega_{V,\beta} = \Omega_{V,\beta}^T d\Omega_{V,\beta}$,$V$: unitary,$O$ orthogonal and S simplectic transformations.

The invariant measure for a complex Hermitian matrix will be written

$$d\Omega_{H_c} = (2)^{N(N-1)/2} \cdot dh_{1,1} \times \cdots \times dh_{N,N} dh_{1,2}^R \times \cdots \times dh_{N-1,N}^R \times dh_{1,2}^I \times \cdots \times dh_{N-1,N}^I. \quad (2.10)$$

The normalizing condition allows to integrate the probability $P(\hat{H})$ using the invariant measure

$$\begin{aligned} \int P(\hat{H}) d\Omega_{H_c} = \frac{1}{\delta^4 \pi^2} \int_{-\infty}^{\infty} e^{-\frac{h_{11}^2}{2\delta^2}} dh_{1,1} \int_{-\infty}^{\infty} e^{-\frac{h_{11}^2}{2\delta^2}} dh_{2,2} \\ \int_{-\infty}^{\infty} e^{-\frac{h_{11}^2}{2\delta^2}} dh_{1,2}^R \int_{-\infty}^{\infty} e^{-\frac{h_{12}^2}{2\delta^2}} dh_{1,2}^I = 1. \end{aligned} \quad (2.11)$$

In this part, it is convenient to make a change of coordinates. Such change is supported by the trace invariance under unitary transformation of $\hat{H}$ and the suitable choice is the use of polar coordinates. Hence, we can introduce another general expression of the invariant measure useful for different kinds of matrices (symmetric, complex Hermitian and quaternionic matrices). It is defined by

$$d\Omega_H(\beta) = \eta_{N,\beta} \left[\prod_{i<j=1}^{N} |e_j - e_i|^\beta \right] de_1 \cdots de_N \delta\Omega_{V,\beta} \quad (2.12)$$

when every term is defined in the table 2

Therefore, we can write the probability density in its polar form using the last result Eq.2.12, the change variable $\beta x_j^2 = \frac{a_\beta e_j^2}{2\delta^2}$ integrating over $\delta\Omega_{V,\beta}$ we get

$$\begin{aligned} P_{N_\beta}(x_1, \cdots, x_N) dx_1 \cdots dx_N = \int P(\hat{H}) d\Omega_H = \\ C_{N,\beta} \left[\prod_{1 \le i \le j \le N}^{N} |x_j - x_i|^\beta \right] \times e^{-\beta \sum_{j=1}^N x_j^2} dx_1 \cdots dx_N. \end{aligned} \quad (2.13)$$

The constant $C_{N,\beta}$ is normalization constant. Obtaining such constant is a hard task, the definition is given in(MEHTA, 2004), whose result is

$$C_{N,\beta} = \frac{\beta^{\frac{N}{2}+\frac{\beta N(N-1)}{4}}\left[\Gamma(1+\frac{\beta}{2})\right]^N}{(2\pi)^{\frac{N}{2}}\left[\prod_{j=1}^{N}\Gamma(1+\frac{\beta j}{2})\right]}. \tag{2.14}$$

Using the last two equations we are able to define the nearest neighbor distribution for an ensemble of 2×2 matrices directly of the joint probability $P_{2\beta}(x_1,x_2)dx_1dx_2$ to find eigenvalues x_1 and x_2 in the intervals x_1+dx_1 and x_2+dx_2, Hence we can establish that $P_{2\beta}(x_1,x_2)dx_1dx_2$ is written as follows

$$P_{2,\beta}(x_1,x_2)dx_1dx_2 = \frac{\Gamma(1+\beta/2)\beta^{1+\frac{\beta}{2}}}{2\pi\Gamma(1+\beta)}|x_2-x_1|^{\beta}\times e^{-\beta x_1^2-\beta x_2^2}dx_1dx_2, \tag{2.15}$$

making substitutions $\chi = x_2-x_1$ $X=\frac{x_1+x_2}{2}$ and taking into account that $P_\beta(s)ds = 2P_\beta(\chi)d\chi$ we obtain

$$P_{2\beta}(\chi)d\chi = \frac{\Gamma(1+\beta/2)\beta^{\frac{\beta+1}{2}}\chi^\beta}{\Gamma(1+\beta)}\times e^{-\beta\frac{\chi^2}{4}}d\chi. \tag{2.16}$$

We assume that χ is the spacing between successive levels s. Thus, s will have absolute value $s=|\chi|$ in a range $0\leq s\leq\infty$ hence $P_\beta(s)ds = 2P_\beta(\chi)d\chi$. Therefore the spacing distribution is

$$P_\beta(s)ds = \frac{1}{\sqrt{\pi}}\beta^{\frac{1+\beta}{2}}\frac{\Gamma(1+\beta/2)}{\Gamma(1+\beta)}s^\beta e^{-\frac{\beta s^2}{4}}, \tag{2.17}$$

and its mean level spacing is obtained from

$$\int_0^\infty sP(s)ds = \frac{1}{\sqrt{\pi}}\beta^{\frac{1+\beta}{2}}\frac{\Gamma(1+\beta/2)}{\Gamma(1+\beta)}\int_0^\infty s^{\beta+1}e^{-\frac{\beta s^2}{4}}ds. \tag{2.18}$$

making the substitutions $t=\frac{\beta s^2}{4}$,$s=2\sqrt{\frac{t}{\beta}}$, $dt=\sqrt{\frac{t}{\beta}}$ and $ds=\sqrt{\beta t}$ it can be obtained solving the integral

$$<s>=\frac{1}{\sqrt{\pi}}\frac{\sqrt{\beta}\Gamma\left(\frac{2+\beta}{2}\right)}{\Gamma(1+\beta)}2^\beta\Gamma\left(\frac{\beta}{2}\right) \tag{2.19}$$

In the case of GOE ensemble ($\beta=1$) we have $<s>_{GOE}=\sqrt{\pi}$ and the nearest neighbor spacing is given by

$$P_{\beta=1}(s) = \frac{1}{2}se^{-\frac{s^2}{4}}. \tag{2.20}$$

The importance of this equation is based on that the RMT predicts the results for chaotic systems since the spacing distribution obtained in the systems mentioned before i.e heavy nucleus, billiards, spin systems, etc, is predicted by the random matrix theory renormalizing the spacing in $P_{\beta=1}(s)$ that is $x = \frac{s}{<s>_{GOE}} = \frac{s}{\pi}$. Then we have that

$$P_{GOE}(x) = \frac{\pi}{2} x e^{-\frac{\pi x^2}{4}}. \tag{2.21}$$

The last equation is known as *Wigner distribution*. Such distribution is a universal property of chaotic systems. Hence, this fact implies that every chaotic system satisfies the mentioned distribution. In practice, obtaining $P_{GOE}(x)$ is not an easy task since the mean level density of the system is not universal, therefore we need a method which allows us to take away the non-universal part in order to obtain correct results.

2.2 Unfolding Procedure

To establish the chaotic properties of a specific physical system (nucleus, billiards, spin systems, etc) we must guarantee that these properties are preserved for every chaotic systems. Hence, a signature of chaos must be determined by a universal feature. In the case, of level spacing distribution it describes very well a system in chaotic domain(BOHIGAS; GIANNONI; SCHMIT, 1984a) from the analysis of energy spectrum. However, the initial spectrum is related to a density level distribution which has associated a mean level density that changes for every system. Therefore we must remove this contribution to obtain a universal property which gives us information whether the system is chaotic or not. Hence, we must $unfold$ the spectrum removing the non universal part in order to obtain an universal feature of the system. The unfolding procedure is not a easy task, although there are some techniques whose results produce the desired features. These techniques have been treated in the literature(HAAKE, 2013; GUHR; MÜLLER-GROELING; WEIDENMÜLLER, 1998a; BRUUS; D'AURIAC, 1997; LUUKKO, 2015; DYSON, 1962; FRENCH; WONG, 1971; PAAR et al., 1991; BAE et al., 1992; GÓMEZ et al., 2005).

Before beginning to describe this method, we have to know two important facts:

1. A Hamiltonian eigenvalues must be separate according to the specific symmetry class.

2. The initial and final eigenvalues (ground state) are not universal, thus they could give us misleading information about possible chaotic proprieties.

With (1) and (2) in mind, there is still non-universal information in the system since the level density may be larger for some systems when the energy increases or when this decreases. Therefore, we are not interested in the smooth part of the density of energy levels but in the $fluctuations$ around its mean value(LUUKKO, 2015). Consequently, we have a sequence of eigenvalues $\{E_1, E_2, ..., E_N\}$ and the spectral function of energy is given as follows

$$S(E) = \sum_{i=1}^{N} \delta(E - E_i). \tag{2.22}$$

Thus, to analyze the local fluctuations, our spectrum has to be $unfolded$ to remove the non-universal part: the mean level density (smooth part of the total level density). Hence, we define the accumulative level function

$$N(E) = \int_{-\infty}^{E} S(E')dE' = \int_{-\infty}^{E} \sum_{i=1}^{N} \delta(E - E_i)dE. \tag{2.23}$$

Due to relation between Dirac delta and Heaviside function, we obtain the following result

$$\int_{-\infty}^{E} \delta(E - E_1)dE' + \int_{-\infty}^{E} \delta(E - E_2)dE' + ... + \int_{-\infty}^{E} \delta(E - E_N)dE' = \tag{2.24}$$

$$\Theta(E - E_1) + \Theta(E - E_2) + ... + \Theta(E - E_N). \tag{2.25}$$

Hence, the Eq.(2.23) will be

$$N(E) = \sum_{i=1}^{N} \Theta(E - E_i), \tag{2.26}$$

this function counts a number of level less than or equal to E and it also be separated in two parts

$$N(E) = \eta(E) + \eta_{fl}(E), \tag{2.27}$$

where $\eta(E)$ is the smooth part and η_{fl} is the fluctuations part of the accumulative level density. The first of them is related with the k-correlation function definition. Therefore, if we have a

energy set $\{E_1, E_2, ..., E_N\}$ the k-correlation function given by Dyson(DYSON, 1962; GUNSON, 1962)

$$R_k(E_1, \cdots, E_N) = \frac{N!}{(N-k)!} \int_{-\infty}^{\infty} dE_{k+1} \cdots \int_{\infty}^{\infty} dE_N P_N^{ensemble}(E_1, \cdots, E_N). \tag{2.28}$$

It measures the probability density of finding a level around of each position $E_1, E_2, \cdots E_k$(GUHR; MÜLLER-GROELING; WEIDENMÜLLER, 1998a). Taking into account, the k-correlation function and the smooth part of the accumulative density can be described as follows

$$\eta(E) = \int_{-\infty}^{E} R_1(E')dE'. \tag{2.29}$$

It also allows us to define a new set of unfolded energies

$$\varepsilon_i = \eta(E_i), \tag{2.30}$$

and the spacing between two energy unfolded levels is one $< s >= 1$. Thus, the new mean density of energies is constant.

The unfolding procedure is not an easy task. In fact, there are many ways to make a separation between the smooth and the fluctuating part e.g polynomial fit, moving averages, etc. These unfolding methods have in common the introduction of arbitrary parameter which makes the unfolding procedure an arbitrary technique. Therefore, when we study the billiard spectrum the chaos signature is entirely related to the geometry shape of the cavity. Hence, as we saw before Weyl(WEYL, 1912) found an equation that relates the accumulative density to the cavity parameters

$$\eta(E) = \frac{AE}{4\pi} \mp \frac{L\sqrt{E}}{4\pi} + c \tag{2.31}$$

E is the energy level, A is the area of cavity and L is the perimeter. c is related to the curvature and topological features of the billiard. The Weyl's law allows unfolding the spectrum in the case of the billiards, although it can not be applied in other systems whose symmetries are not geometric. For this reason, there are other methods to make unfold that are associated with the mean level density since there are many systems whose specific densities are unknown. Hence, it is possible to estimate the mean level density from a set of neighboring levels. This method is called $local\ unfolding$ and has been widely used in(FRENCH; WONG, 1971; PAAR et al.,

1991; BAE et al., 1992; GÓMEZ et al., 2005). The mean density is estimated assuming that it is approximately linear in a region of ν levels $W_\nu = E_{i+\nu} - E_{i-\nu}$, thus the equation for this density is given by

$$\langle \rho_L(E_i) \rangle = \frac{2\nu}{W_\nu}. \tag{2.32}$$

W_ν plays the role of "window" and weight over the mean level density, L stands for local unfolding. With $< \rho_L(E_i) >$ and using the equation Eq.(2.29) can be expressed as follows

$$\eta(E) = \int_{-\infty}^{E} < \rho_L(E') > dE'. \tag{2.33}$$

Another method more sophisticated is the *Gaussian broadening*(HAAKE, 2013; BRUUS; D'AURIAC, 1997; GÓMEZ et al., 2005). It consists in substituting a Gaussian function for $< \rho(E) >$ in the Eq.(2.33)

$$\langle \rho_G(E) \rangle = \frac{1}{\sigma\sqrt{2\pi}} \sum_i e^{-\frac{(E-E_i)^2}{2\sigma^2}}. \tag{2.34}$$

Where G stands for Gaussian. In this method the sum runs over all energy levels where the relevant contribution is given by the levels that satisfy the condition $|E - E_i| \leq \sigma$. Although, in the case of the Hubbard model (BRUUS; D'AURIAC, 1997) σ is not taken as a constant parameter since the appearance of mini bands in the spectrum for small values of the parameter interaction produce different densities for every parameter.

Another method introduced in(HAAKE, 2013) consists in defining the unfolded energy set as follows

$$\frac{d}{d_i} = \varepsilon_{i+1} - \varepsilon_i. \tag{2.35}$$

Where d_k is the smallest spacing for E_i. Here d_n becomes a free parameter. The importance of this method is because it allows us to unfold eigenvalues of a non-Hermitian matrix.

Everyone of these methods has an intrinsic dependence on an arbitrary parameter that increases the uncertainty if we study subsequent chaotic properties through other physical and statistical quantities. In fact, depending on the unfolded method the choosing of arbitrary parameter could generate levels in $\eta(E)$ containing parts of $\eta_{fl}(E)$ and vice versa producing spurious long range correlations leading us to misleading conclusions(GÓMEZ et al., 2005) .e.g a polynomial degree which is either too high or too small for our later analysis. Therefore, the

useful parameter has to be determined by trial and error. However in (MORALES et al., 2011) it is suggested methods used in time series analysis that are based on decomposition of a time series in IMF functions until obtaining the $detrend$ of a series as we shall see in later sections. On the other hand, there are other quantities that capture information about the statistical behavior of the energy levels but do not require to be unfolded, indeed the ratios distribution defined in (ATAS et al., 2013; OGANESYAN; HUSE, 2007) corresponds to a distribution defined as follows

$$r_n = \frac{min(s_n, s_{n-1})}{min(s_n, s_{n-1})}. \tag{2.36}$$

The reason why we must not unfold the spectrum is the independence of the local density states.

2.3 Nearest Neighbor Spacing Distribution for GOE and GDE Ensembles

As we have seen, the RMT predicts the results found in chaotic systems. In this part, we will analyze the universal properties associated with the spacing distributions of the ensembles GOE and GDE. The main motivation is that the GDE and GOE distributions characterize the integrability or chaoticity of specific systems. It is important to note that the unfolding procedure can be used for the GDE ensemble. Therefore we have two ensembles $\Gamma_{GOE}(N)^n$ and $\Gamma_{GDE}(N)^n$ with 100 matrices every one ($n = 100$) of dimensions $N = 2000$. The GOE ensemble is constructed from the algorithm explained in the section 2.0.2 implementing in Matlab using the command randn(N,N) whose elements are random numbers withing a Gaussian distribution with mean $\mu = 0$ and variance $\sigma^2 = 1$, hence in a qualitatively way we can say that a matrix M_N in our algorithm is $M_N = randn(N,N)$. In the case of GDE ensemble construction the Matlab command changes to randn(1,N). Hence, computationally we get a vector with dimensions $1 \times N$. Hence, after using some computational steps we finally obtain a diagonal $M_N^{diagonal}$ matrix with random numbers within a Gaussian distribution with mean $\mu = 0$ and variance $\sigma^2 = 1$. We can find a optional GOE algorithm in (EDELMAN; SUTTON; WANG, 2014)

Due to non-universality in the energy density we must unfold every set of energies (eigenvalues of a matrix M_N or $M_N^{diagonal}$). Hence, one of the unfolding procedure that we can use is the polynomial unfolding. It consists in fitting the accumulative mean density with

a polynomial degree η. It is important to say that high degrees do not guarantee a better fit. Indeed, in(FLORES et al., 2001) they show that when the polynomial degree increases the nearest neighbor distribution and number variance is more closely to the GOE predictions when the polynomial degree is small.

In our case, the result of the polynomial unfold for the ensembles are given in figure 7. We can see that the behavior of N_{GOE} and N_{GDE} is slow at the beginning of the graphics since the the first eigenvalues corresponds to the edges of the function ρ_{GDE} and ρ_{GOE}. In fact, the agreement in the center of the graphics between the accumulative density and the fit obtained from the polynomial method is linear in a good approximation for both cases. Therefore, the importance of α in the long and short range fluctuations is associated with quality of the fit, where it is related to the η value. Hence, we must remove some data values (close to 3%) in the edges of the spectrum for obtaining better results.

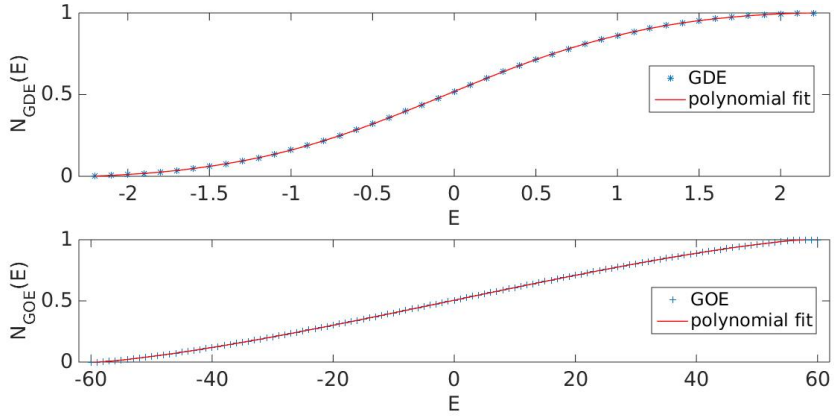

Figure 7 – Polynomial fit for GOE and GDE ensembles of $n = 100$ matrices with dimensions $N = 2000$, the dashed lines correspond to the polynomial fit of the accumulative level density of GOE and GDE with degree $\eta = 15$.

On the other hand, the fit functions N_{GOE} and N_{GDE} are the first step to obtain the spacing ensembles. Hence, we define an energy unfolded value ε_i as follows

$$\varepsilon_i = \frac{N(E_i)}{\frac{1}{N}\sum_{i=1}^{N}(N(E_{i+1}) - N(E_i))}. \tag{2.37}$$

This equation is defined in order to obtain the nearest neighbor spacing distribution, where the

mean spacing value is $< s >= 1$, where its elements are given by

$$s_i = \varepsilon_{i+1} - \varepsilon_i \tag{2.38}$$

and the distributions are showed in figure 8 and figure 9 for GDE and GOE. The figure 8 reveals a good behavior of the GDE ensemble, where the realization number and dimension matrix are $n = 100$ and $N = 2000$, due to a reasonable matrix quantity. It also shows that the level energies are repelling each other giving information about short range correlations. One of the most important features of the level spacing for a regular systems is that it is not sensitive to the unfolding procedure.

Generally the Poisson distribution for level spacing in regular systems usually reveals an uncorrelated behavior of the energy levels. Hence, the fluctuations of quantum systems whose classical counterparts are integrable can be associated with an infinite Poisson random process. It is important to note that if a system satisfies the Poisson distribution after making unfolding it will be integrable, although not all integrable systems satisfy the Poisson distribution. Actually the Berry and Tabor(BERRY; TABOR, 1977) proved that in the case of one harmonic oscillator with incommensurable frequencies the spacing distribution P(s) is peaked but if the frequencies are commensurable P(s) will not exist. Another example is given in (CASATI; CHIRIKOV; GUARNERI, 1985), they showed that the spacing distribution of a rectangular incommensurable billiard, which is integrable, has irregularities in the last intervals when the spacing distribution is obtained. Indeed, the χ^2 test showed very large values for 21 intervals proving that there are too large fluctuations in the random sequence.

On the other hand, the distribution obtained in figure 9 is in agreement with the Wigner distribution given in the Eq.(2.21). The ensemble parameter are the same: number of realizations $n = 100$ and dimensions $N = 2000$. The Wigner distribution is a universal parameters which describes chaotic quantum systems, moreover it was defined taking into account that levels have to be separated according to their parity and level mixture with different parity show an uncorrelated behavior. It allows us to conclude that the energy levels show correlations in the sense that the levels tend to avoid each other. For example, a big quantity of nuclear data were analyzed in 1980 by (BOHIGAS; GIANNONI; SCHMIT, 1984b) finding relations between the time reversal invariance of the forces and the Hamiltonian matrix structure; if the nuclear force is time reversal invariant the Hamiltonian will have eigenvalues similar to random real symmetric

matrices.

Due to the universality of the Wigner distribution we can find some many systems that are described by this spacing distribution. Indeed, O. Bohigas, M. J. Giannoni, and C. Schmit (BOHIGAS; GIANNONI; SCHMIT, 1984b) solved the Schrödinger equation for Sinai billiard since this has some advantages. For example, the Sinai billiard has the lowest degrees of freedom number, moreover the local and global properties can be separated using the Weyl's law. They found that these systems behave obeying the Wigner distribution.

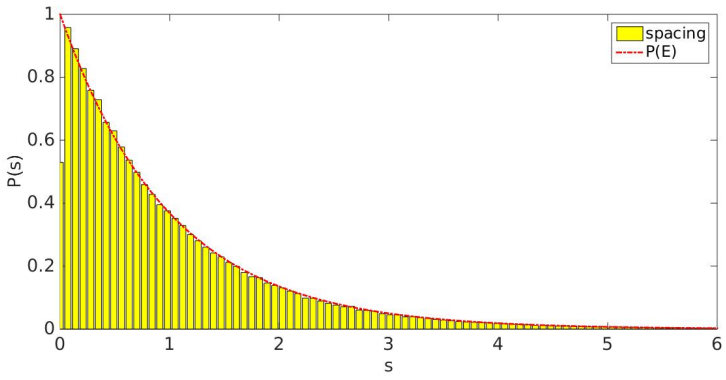

Figure 8 – Nearest neighbor distribution for GDE ensemble. $n = 100$ realizations of matrices with dimension $N = 2000$ using polynomial unfolding with $\eta = 15$. The dashed line is the theoretical Poisson distribution given by Eq.(1.29).

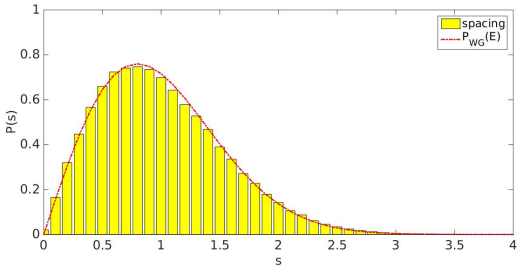

Figure 9 – Nearest neighbor distribution for GOE ensemble. $n = 100$ realizations of matrices with dimension $N = 2000$ using polynomial unfolding with $\eta = 15$.

2.4 Time Series Analysis and Spectral Density for GOE and GDE Ensembles

The description of chaotic behavior is not only constructed from the nearest neighbor spacing distribution. In fact there are other methods that give us information about the chaotic characteristics of quantum systems. Hence, if we analyze the accumulative density $N(E)$ through a specific fit we could obtain information about fluctuations between $N(E)$ and fit function. It can be done using a suitable choice like $N(E) = AE + B$ and the last square criterion is the key for getting accuracy results, thus, the equation could be

$$\Delta = \min_{A,B} \left(\frac{1}{2L} \int_{-L}^{L} [N(E) - AE - B]^2 dE \right) \tag{2.39}$$

Which $E \in [-L, L]$ and the negative energy levels change $N(E)$ by $-N(E)$ with $E \in [-L, 0]$.

On the other hand, there is another statistics which allows to obtain interesting information about the chaotic properties of a quantum system. If we consider the differences between spacings s_i respect its mean value $< s >= 1$ we could define a statistics called $\delta(n)$(MEHTA, 2004) as follows

$$\delta(n) = \sum_{i=1}^{n} (s_i - < s >). \tag{2.40}$$

We also infer

$$\delta(n) = s_1 + s_2 + s_3 + \cdots s_n - n < s >= (\varepsilon_2 - \varepsilon_1) + (\varepsilon_3 - \varepsilon_2) + (\varepsilon_4 - \varepsilon_3) + \cdots + (\varepsilon_{n+1} - \varepsilon_n) \cdots n < s >, \tag{2.41}$$

where ε_n is the nth unfolded energy value, then $\delta(n)$ can be written as follows

$$\delta(n) = \sum_{i=1}^{n} (s_i - < s >) = \varepsilon_{n+1} - \varepsilon_1 - n. \tag{2.42}$$

Consequently, we have that Eq.(2.40) represents an accumulative sum that reveals fluctuations of the spacing distribution. These Fluctuations are understood as differences between the elements s_i of nearest neighbor distribution and their mean value $< s >= 1$. The importance of these figures is due to the function $\delta(n)$ that describes a signal similar to a time series, where the value i plays the role of discrete time. From other point of view, the $\delta(n)$ description allows

to understand the behavior of fluctuations as a time series that can be understood as diffusion process of a particle. Thus, if we compare the spacing fluctuations $f_i = s_i - < s >$ with the displacement d_i of a particle from a collision to the next in the interval i the analogy will be clear. We have to note that there are differences, for example the displacement can be any real value, however $f_i > -1$ because there is no possibility to have spacing values less than zero. We also note that the amplitude and value of sign in f_i depends on a probability complex function in a sense that this function could be very hard to work. The dependence, in the case of $\delta(n)$ is also associated with high energy levels. Consequently, the $\delta(n)$ function represents the analogue of a particle moving itself with total displacement given at time n.

Therefore, we calculated the function $\delta(n)$ for two matrices of size $N = 2000$ belonging to GOE and GDE ensembles for three different values of polynomial degree. The result is obtained in figure 10 and figure 11. We can also infer from these figures that: (i) As the polynomial degree increases the signals tend to move around the zero value. (ii) The fluctuating behavior of GDE is different for GOE ensemble since it is smoother than the signals obtained in figure 11.

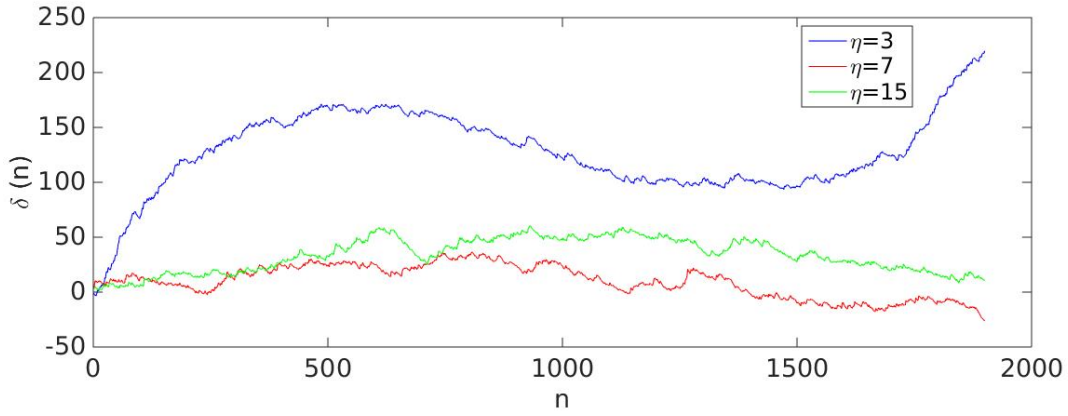

Figure 10 – $\delta(n)$ function for three different values of polynomial degree $\eta = 3$,$\eta = 7$ and $\eta = 15$ of a spacing distribution for a GDE matrix with size $N = 2000$.

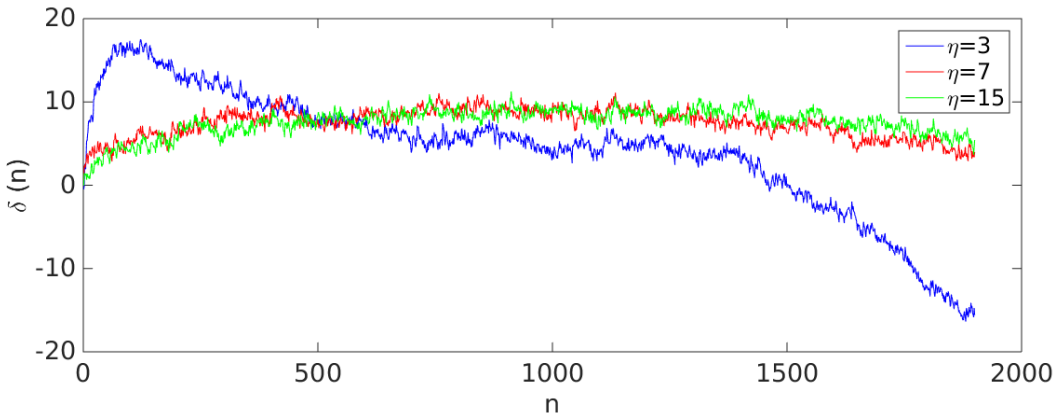

Figure 11 – $\delta(n)$ function for three different values of polynomial degree $\eta = 3$,$\eta = 7$ and $\eta = 15$ of a spacing distribution for a GOE matrix with size $N = 2000$.

On the other hand, the aim to study the $\delta(n)$ statistics is based on the idea of capturing other universal characteristics that describes chaotic systems. For this reason, we will use one of the complex system techniques that capture emergent properties: The spectral density.
Before defining this quantity we can consider a random continuous process $g(t)$, its Fourier transform is given by

$$\hat{g}(\omega) = \int_{-\infty}^{\infty} g(t) e^{-i\omega t} dt. \tag{2.43}$$

Then we also take into account the correlation function $< g(t)g(t') >$. If the process is stationary the Fourier transform of the correlation function will be

$$< \hat{g}(\omega)\hat{g}^*(\omega') >= \int_{-\infty}^{\infty}\int_{-\infty}^{\infty} < g(t)g^*(t') > e^{-i\omega t + i\omega' t'} dt dt'. \tag{2.44}$$

Due to stationary condition the correlation function only depends on the differences of times t and t'. Hence, it can be written as follows

$$< g(t)g^*(t') >=< g(t-t')g^*(0) > . \tag{2.45}$$

Considering the changes of variable $\tau = t - t'$ and $t_0 = (t' + t)/2$ or, in terms of t and t' we get

$t = t_0 + \frac{\tau}{2}$ and $t' = t_0 - \frac{\tau}{2}$

$$< \hat{g}(\omega)\hat{g}^*(\omega') >= \int_{-\infty}^{\infty}\int_{-\infty}^{\infty} < g(t)g^*(t') > e^{-i\omega t + i\omega' t'} dt dt' \tag{2.46}$$

$$< \hat{g}(\omega)\hat{g}^*(\omega') >= \int_{-\infty}^{\infty}\int_{-\infty}^{\infty} < g(\tau)g^*(0) > e^{-i\omega(t_0+\frac{\tau}{2}) + i\omega'(t_0-\frac{\tau}{2})} dt_0 d\tau. \tag{2.47}$$

Note that we assume the random variable $g(t)$ may take complex values. Then we have reorganizing the terms obtaining

$$< \hat{g}(\omega)\hat{g}^*(\omega') >= \int_{-\infty}^{\infty} e^{-i(\omega-\omega')t_0} dt_0 \int_{-\infty}^{\infty} < g(\tau)g^*(0) > e^{-\frac{\tau i}{2}(\omega+\omega')} d\tau. \tag{2.48}$$

The first integral is the Fourier transform of 1. Thus, we get

$$< \hat{g}(\omega)\hat{g}^*(\omega') >= 2\pi\delta(\omega-\omega') \int_{-\infty}^{\infty} < g(\tau)g^*(0) > e^{-\frac{\tau i}{2}(\omega+\omega')} d\tau. \tag{2.49}$$

With $\omega = \omega'$ we get

$$< \hat{g}(\omega)\hat{g}^*(\omega') >= \pi\delta(\omega-\omega') \int_{-\infty}^{\infty} 2 < g(\tau)g^*(0) > e^{-\tau i\omega} d\tau = \pi\delta(\omega-\omega')S(\omega). \tag{2.50}$$

The details of the last prof can be found in (RISKEN; EBERLY, 1985). Here $S(\omega)$ is the *spectral density* function. The last result is known as the *Wiener Khintchine* theorem. It shows that the relation between the correlation function for a stationary process and spectral density is given by a Fourier transform. Then, the spectral density function is the Fourier transform of the correlation function. It has some interesting properties

- S(ω)=S(-ω)
- $S(\omega) \geq 0$
- S(ω) is real
- S(ω) and S(K) have different units: $[S(\omega)] = power/radian$ and $[S(k)] = power/Hertz$

If the random process is real, the first property shows that $S(\omega)$ is real. Besides of this property, the process must satisfy the ergodic condition, that is during a long period of time the average over this quantity in a sequence of events will be the same as the total average over the ensemble.

On the other hand, the spectral density function reveals how the power of a signal is distributed in the frequency domain. It is also possible to describe $S(\omega)$ in terms of the signal, then we have

$$S(\omega) = \lim_{T\to\infty} \frac{1}{T}|g(\omega)|^2, \tag{2.51}$$

where $g(\omega)$ is the Fourier transform of the random process, which plays a role of the signal. Thus, we infer that the power spectral density can be described by the signal. Moreover, with the signal we can obtain the spectral density and, vice versa. Therefore, there are systems characterized by a power spectral behavior in some sense. For example, in(GREIS; GREENSIDE, 1991) it is examined time series that are associated with self-affinity process, whose properties are imposed over the power spectral density in the form $S(\omega) = C\omega^{-\alpha}$ for different exponents of α and different phases.

The self-affinity property consists in the absence of characteristic time scale assuming this structure in all time scales. That is, the total system is similar to a part itself. That implies another property called scale invariance. If we suppose that the increments of a time series are given in the form

$$\Delta x(\tau) = x(t+\tau) - x(t), \tag{2.52}$$

then

$$\Delta x(\lambda\tau) = \lambda^H \Delta x(\tau). \tag{2.53}$$

The equality implies that the distribution function of both process are the same. H is called the *Hurts exponent*. It is an scale exponent, lies between 0 and 1. With this information in mind, we can construct the time series, whose spectral density is imposed, from the time relations $t_i = i\Delta t$, $T = M\Delta t$ fixing the constant value C and spectral density exponent α. Then, the equation will be

$$x_i = \sum_{k=1}^{M/2} \sqrt{S(\omega_k)\Delta\omega} cos(\omega_k t_i + \phi_k), \tag{2.54}$$

where $1 \leq i \leq M$ and ϕ_k represents a random phases. The frequencies $\omega_k = k\Delta\omega$ are multipliers of smallest discrete frequency give by $\Delta\omega = 2\pi/T$.

The model described by Eq.(2.54) is not the unique that has a spectral density relation. For instance in(MOURA; LYRA, 1998) they investigate the nature of states for 1D Anderson model for electrons whose energies show a long-range correlated disorder that are characterized by an spectral density function. More precisely, the model consists in considering one electron inside of 1D chain whose interactions are given between nearest neighbors, where the Hamiltonian used is written as follows

$$H = \sum_n \varepsilon_n |n><n| + t \sum_n [|n><n+1| + |n><n-1|]. \tag{2.55}$$

ε_n is the energy at site n, t is known as first-neighbor hopping amplitude. The standard Anderson model takes into account the energies as random values that are uncorrelated site to site whose spectral density satisfies $S(k) \propto k^0$. This model also considers the introduction of trace of Brownian motion to describe long-range correlations in the form of disorder distributions by the use of spectral density and Hurts exponent $H = 2\alpha + 1$. Such trace construction is made through imposing a power spectral density in the energy form whose equation is expressed as a Fourier transform:

$$\varepsilon_i = \sum_{k=1}^{N/2} \left[K^{-\alpha} |\frac{2\pi}{N}|^{1-\alpha} \right]^{1/2} \times cos\left[\frac{2\pi ik}{N} + \phi_k \right], \tag{2.56}$$

where N is the number of the sites and ϕ_k represents the phases which are $N/2$ independent random number uniformly distributed over the interval $[0, 2\pi]$. It is necessary to impose the normalization sequence to have $< \varepsilon_n >= 0$ and $\Delta\varepsilon = \sqrt{< \varepsilon_n^2 > - < \varepsilon_n >^2} = 1$.

The Eq.(2.54) and Eq.(2.56) generate two kinds of time series where the spectral density plays a fundamental role since x_i and ε_i are obtained as a Fourier transform of this quantity. For this reason, from Eq.2.56 we generate two time series showed in the figure 12. Furthermore we construct a time series $\delta(n)$ for the ensembles GOE and GDE of a matrix with dimensions $N = 2000$. The results are exposed in the figure 13

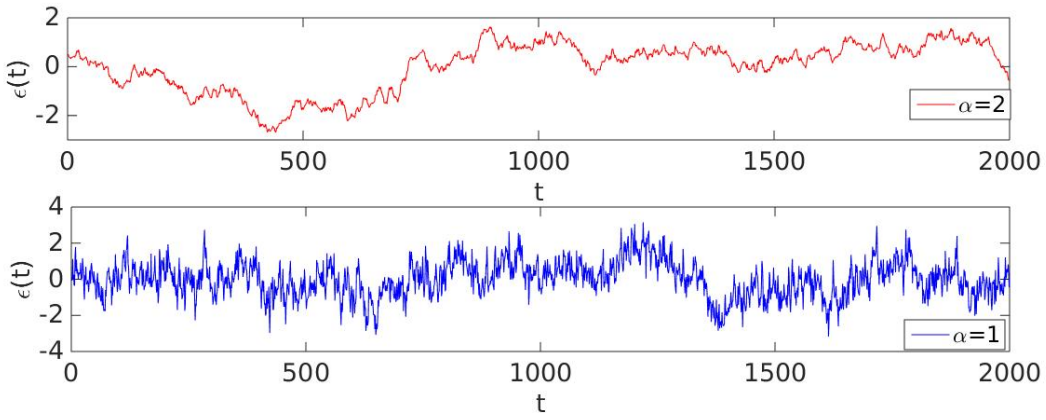

Figure 12 – One site energy behavior as a time series for two different spectral density exponents $\alpha = 1$ and $\alpha = 2$. Note that if α increases the signal becomes more smoothly.

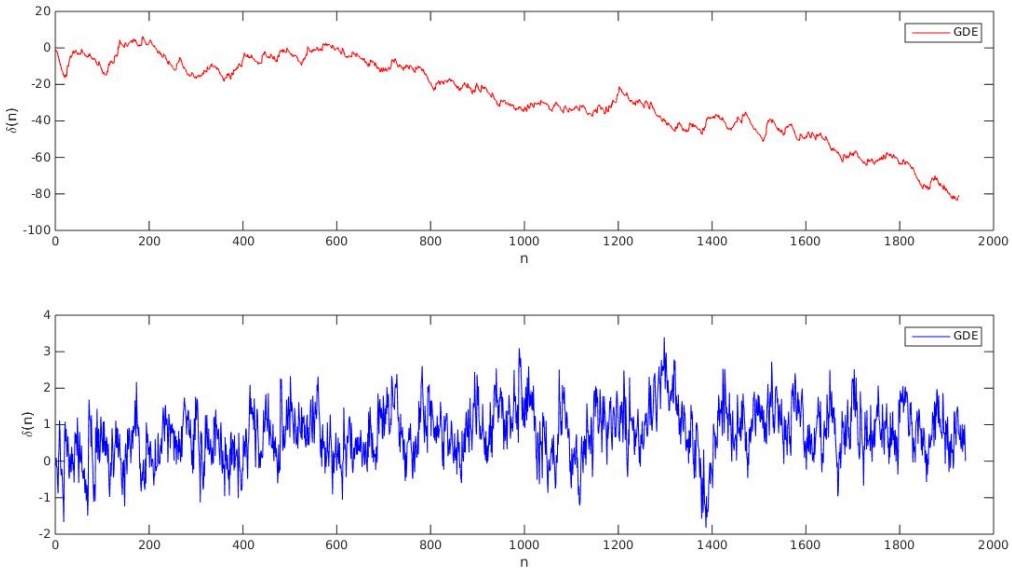

Figure 13 – Time series $\delta(n)$ for two kinds of ensembles GOE (red line) GDE (blue line). The matrix size is $N = 2000$ for every ensemble.

The signals are very different in figure 12 due to spectral density exponent. Hence, the main characteristic of this figure is the well defined behavior of $S(k)$. In the case of figure.2.10 the

behavior for both ensembles is analogous to the figure 12 since the GDE reveals more smoothness than GOE time series and we can infer two important facts:

- The GOE and GDE ensembles are characterized by the spectral density.
- The behavior of $S(k)$ is $< S(k) > \propto \frac{1}{k^{\alpha}}$ Exponents might be $\alpha = 2$ for GDE and $\alpha = 1$ for GOE ensemble.

In order to prove that these results obtained by Relaño *et al*(NO et al., 2002), we find out the mean power spectral density for both Ensembles. Then we take the last second fact

$$< S(k) > \propto \frac{1}{k^{\alpha}}. \tag{2.57}$$

In this sense, we construct 100 random Gaussian matrices of size $N = 2000$. For every matrix we obtain the nearest neighbor spacing distribution using polynomial unfold, where the polynomial degree is $\eta = 15$. Hence, using the Eq.(2.42) we get the time series $\delta(n)$. In this sense, we define a new ensemble of signals, whose respective spectral densities are obtained from next equation

$$S(k) = |\delta_k|^2, \tag{2.58}$$

where δ_k is the Fourier transform defined as follows

$$\delta_k = \frac{1}{\sqrt{N}} \sum_{n=1}^{N} \delta_n exp\left(\frac{-2\pi ikn}{N}\right). \tag{2.59}$$

The term $\frac{-2\pi k}{N}$ plays a role of a frequency. We can note that the Eq.(2.57) is a version of the Eq.(2.51) taking into account that $\delta(n)$ is analogous to the random process.

In order to avoid statistical fluctuations we characterize the power spectrum as average over entire ensemble considering close of 6% of the values at the beginning and the end of the signal. The result is obtained in the figure 14 given in logarithmic scale.

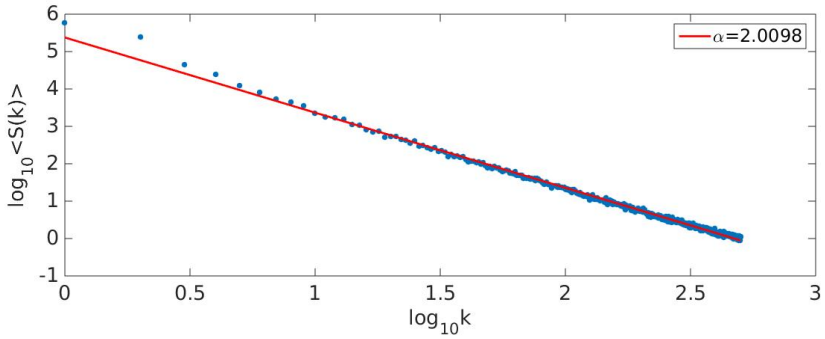

Figure 14 – Average power spectrum of $\delta(n)$ for GDE ensemble. The red line represents the fitting.

As we can see, the behavior of the average spectral density is clearly linear except by frequencies grater than $log_k = 2.7$ since the presence of finite size effects. The fit shows a power $\alpha_{GDE} = 2.01$ with an uncertain close to 1.2%.

The nature of the GDE ensemble is based on the matrix construction because they are diagonal and every element takes place in a Gaussian distribution. For this reason, we have the Poisson condition over this ensemble, whose unfold energies reveal an uncorrelated spacing. We also note that, the diagonal elements are random independent variables and, therefore $\delta(n)$ is made by a sum of N-1 independent random spacings. Consequently, the signals obtained from GDE ensemble are described by a power spectral behavior $1/k^2$ showing very well a convergence point with the previous result in the figure 12 proving the Poisson nature for α_{GDE}.

Due to results obtained for GDE ensemble, we must highlight the independence of the unfolding parameter used for describing the spectral density form of GDE since the unfolding procedure is a method whose parameter makes it an arbitrary technique giving misleading information. However, when we increase the polynomial degree the α_{GDE} values reveals a closeness to the theoretical exponent value $\alpha_{GDE} = 2$. In the case of the GOE ensemble, the figure 15 shows the behavior of the average power spectral density.

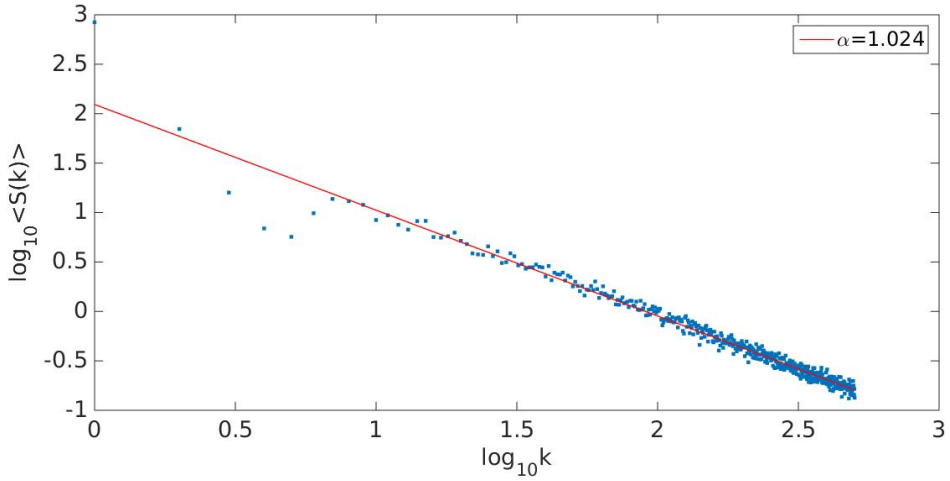

Figure 15 – Average power spectrum of $\delta(n)$ for GOE ensemble. The red line represent the fitting.

On the other hand, the calculus of the spectral density for GOE ensemble reveals a strong dependence on the unfolding polynomial degree η, hence the figure 17 displays the behavior obtained when we unfold the GOE ensemble using different η. In this sense, the unfolding method may produce spurious long range correlations which can be responsible for misleading signature of quantum chaos in the system.

Therefore, in(MORALES et al., 2011) it provides the implementation of a method for reducing the unfolding dependence in the analysis: The *empirical mode decomposition* or EMD. This is based on time series analysis and the steps to be following are:

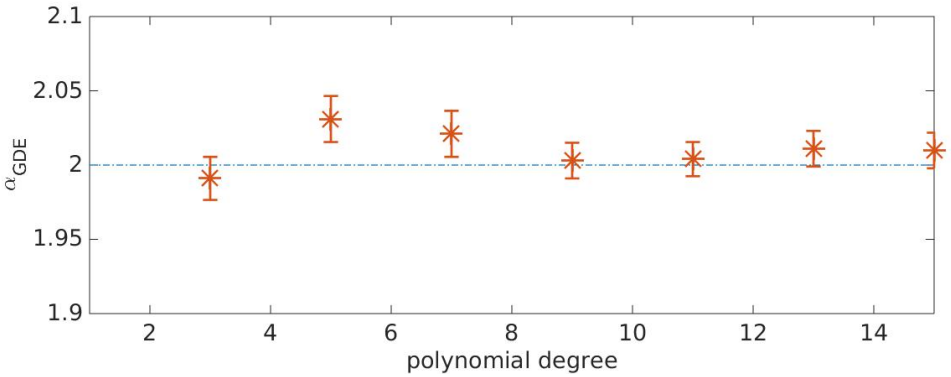

Figure 16 – Value of the α exponent of the power law behavior in the average power spectrum for GDE ensemble. The dashed line represents the theoretical value for GDE. The error bars are the confident intervals of 95%.

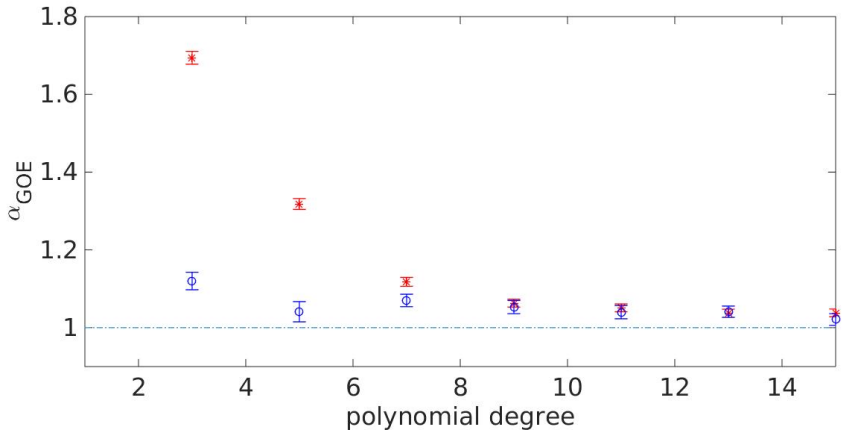

Figure 17 – Value of the α exponent of the power law behavior in the average power spectrum for GOE ensemble. The dashed line represents the theoretical value for GOE. The error bars are the confident intervals of 95%. The red points correspond to α obtained without using EMD. The blue points correspond to α using EMD.

1. Localize the total local maxima and minima of the time series. Separately, connect every set by a cubic spline, which defines the upper and lower envelopes.

2. Calculate the value of upper and lower envelopes $m(1)$, as well as the difference with the time series

$$\delta_i - m_i^{(1)} = h_i^{(1)} \tag{2.60}$$

Due to the envelopes include all extrema, $h^(1)$ reveals oscillations between δ_i and $m_i^{(1)}$. Hence, the function should be an *intrinsec mode function* or IMF, although the process generates new extrema and it is necessary to produce more iterations in order to extract one correct IMF. Every new iteration is used as a new data set.

3. Repeat the steps 1 and 2 using the last new component as a new data set, this is defined as follows

$$\delta_i^{(1,i-1)} - m_i^{(1,k)} = h_i^{(1,k)}, \tag{2.61}$$

The process must stop when the last component is an IMF. That occurs when the local maxima are positive and all local minima are negative, and the mean of envelopes is locally zero. That ensures symmetry in IMF. If it is obtained after k iterations the function $h^{(1.k)}$ is defined as IMF.

$$c^{(1)} = h^{(1,k)} \tag{2.62}$$

4. Subtract the obtained IMF from the original data

$$\delta_i - c_i^{(1)} = r_i^{(1)}. \tag{2.63}$$

The residue $r^{(1)}$ is the new data version. The finest oscillation has been removed, However, this quantity still contains information for longer period components. Then, we have to remove additional components.

5. Repeat the steps 1-4 to extract all IMF of the original data. Using as a new version of the data the residue obtained in the previous iteration.

$$r^{(1)} - c^{(2)} = r^{(2)}, \ldots, r^{(m-1)} - c^{(m)} \tag{2.64}$$

where m is the of IMF's in the data. This process can be stopped either for specific convergence criteria or when the mth-residue is a monotonic function and there is no possibility to extract more IMF's. The last residue is called the trend of the data. It is important to say that every residue constitutes a partial trend for the previous extracted oscillation.

For details of procedure and convergence criteria see (MORALES et al., 2011; HUANG et al., 1998; HUANG, 2014).

After this procedure, the original signal can be described through a superposition of $c^{(i)}$ and $r^{(m)}$

$$\delta_i = \sum_{j=1}^{m} c^{(j)} + r^{(m)}. \tag{2.65}$$

The trend must be a constant for $\delta(n)$. Therefore the figure 18 shows a signal obtained from a real symmetric matrix, which belongs to GOE, of size $N = 2000$ and its equivalent signal after removing the trend r. Due to the border conditions in $\delta(n)$ we must drop a quantity of eigenvalues of a signal (almost 5% at the edges) since they affect spuriously the fit done by the splines in the computational algorithm. Taking this results in mind, we will find out the power spectral measure for chaos. Hence, we will find how the behavior of the power spectral density for GOE is. We write the time series obtained from EMD method, which is showed in the figure 18 as $\delta(n)' = \delta(n) - r$ we construct one GOE ensemble with the same parameters explained before for GDE ensemble. The signals are obtained from Eq.(2.59). The main idea is to compare the increasing polynomial degree with the behavior of the spectral density exponent implicit in the power law mentioned before. As we can see, the EMD makes the exponent closer to the theoretical value found in(NO et al., 2002). We have to note that the power law behavior is an approximation since the higher frequencies are not taken into account.

The figure 17 shows that $\alpha = 1$ for spectral density average revealing correlations in many scales. On the other hand, a low polynomial degree is a signature of the existence of spurious long-range correlations and the lower frequencies of the power spectrum are enhanced generating power exponents larger than theoretical value. For this reason we use the EMD procedure to take out the trend of every signal in the ensemble time series made by $\delta(n)$ and obtaining α values closer to 1. It is important to say that higher polynomial degrees destroy the correlations in the models producing α too higher or too smaller than 1. The figure 15 shows the linear form when it is taken the logarithm of <S(k)> and the exponent for average power spectral density which is $\alpha_{GOE} = 1.024$ close to the theoretical value obtained by the theory.

Consequently, the ensembles GDE and GOE are characterized by $1/k^{\alpha}$ noise having $\alpha = 2$ for GDE ensemble and $\alpha = 1$ for GOE. The last one is strongly associated with the unfolding procedure, for that reason we use the EMD to take out the spurious correlations and reducing the

unfolding dependence in the analysis. We must note that the $1/k^{\alpha}$ noise is a law found in diverse areas, e.g, biology, physics, mathematics etc.

For example, electric devices like amplifiers have presented evidences of $1/f$ noise(HARTMANN, 1921). Indeed, J.B. Johnson measured flicker noise and white noise through model, which explains these effects based on electron transport in vacuum tube. After explaining this model the flicker noise, whose spectral density is quite variable, was found in other electronic devices behaving like $1/k^{\alpha}$, where α is a range of 0.5 to 1.5.

Another example which presents signature of $1/f$ noise is found in biophysics since the electrical dipole moment of lysozome enzyme presents fluctuations. These phenomena are very interesting because it provides information about the water structure interacting with biological molecules(PEYRARD, 2001; CARERI; CONSOLINI, 2000) have been studying these topics and also have found the signature $1/f^{\alpha}$ noise in the biological systems. Another important fact is the scaling invariance of $1/f$ noise since it looks equal for any choice of frequency. For this reason it has been considered a clearly manifestation of fractal phenomena in the nature. This property is related to self-organized criticality due to the results found by Bak, Tang and Wiesenfeld in 1987. They created a model which describes a non-linear process that had fractal characteristics, besides the spectral density that has $1/f$ behavior.

The presence of $1/f$ noise in the phenomena mentioned before reveals how an important statistical property is implicit in diverse systems.

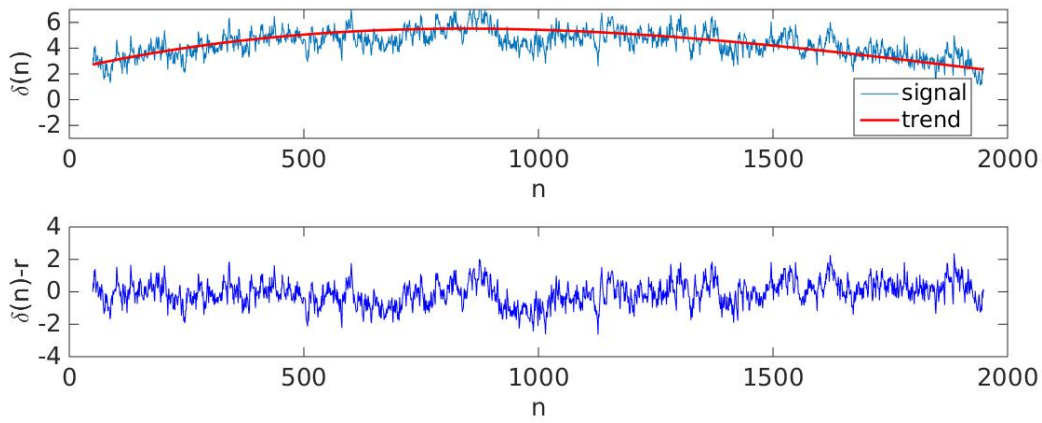

Figure 18 – Time series of matrix GOE. The red line shows the trend signal. Note that the signal without trend is fluctuating with zero media.

3 Random Matrix Theory in Random Networks

The complex networks theory provides elements that describe the behavior of diverse systems in many knowledge areas. The models consist in topological graph whose connections are not completely random since there are intrinsic properties in the network. For instance, the random networks are associated to RMT and, therefore with the time series analysis. Hence, in this chapter we discuss the connection between random networks with RMT and we will study the relation between noise and the spacing properties related to this kind of networks(WATTS; STROGATZ, 1998; BARABÁSI; ALBERT, 1999; YE; LI; MA, 2010; RANDOM. . . , ; JALAN; BANDYOPADHYAY, 2007).

3.1 Eigenvalues and Spacing Distribution Analysis

The recent years have had diverse advances in the complex systems theory. More precisely, the complex networks since these kinds of models are presented in technological, biological, physical and social topics of knowledge. There are some models whose features determine the kind of network. Furthermore they share properties like scale free and hierarchy.

One of the most common models was created by Watts and Strogatz(WATTS; STROGATZ, 1998), it is usually called small-world network, whose main features are the high clustering and small diameter. The simplest example of a small-world network consists in N nodes, Each node is connected with $2k$ neighbors until forming a ring. The additional connections are generated by a probability value P_c'; if P_c' is equal to zero there is no connection. However if P_c' is different from zero one connection. Hence, it becomes to introduce disorder in the network. Another principal feature in network models was found by Barabasi and Albert(BARABÁSI; ALBERT, 1999) proving that many real world networks have a power law behavior. This implies the connection between nodes is not regular since there are some nodes that are much more connected than others. This model is known as *scale free network*.

In this way, Barabasi-Albert and Watts-Strogatz contributed to understand real systems through the network models showing that real world networks have coexistence of randomness and

regularity(BARABÁSI; ALBERT, 1999). Moreover, the initial model, whose results allowed the arising of the last two theories mentioned before, is based on the random graph construction. This is called in the literature *Erdos Reny algorithm* or *R model* and is useful to create the simplest network model: the random network. Suppose that we have N nodes and random connections between them following the probability p_c.e.g. If a probability variable that determines the connection is less than p_c, one connection is done. We also define the average degree of the network as $K = p_c(N-1) \simeq p_c N$(YE; LI; MA, 2010) which measures in a global way how much the network is connected itself. To understand more precisely how the random network works, we interpreted it through adjacent matrix. Then, a adjacent matrix G is defined qualitative as follows:

1. One node i is connected with another node j. This connection is represented in the matrix with the number 1. That is $G_{ij} = 1$.

2. If two any nodes i and j are not connected it will be represented by one 0 in the matrix. Then, the non-connected nodes are given by $G_{ij} = 0$.

We can conclude that the matrix G is symmetric because a node i connected with j is the same as j connected with i and the diagonal elements are zero since one node can not connect itself.

Hence, we defining the connection probability p_c. Therefore we construct one ensemble of 10 adjacent matrices following the next algorithm:

1. Generated a matrix A with random numbers between 0 and 1. Simultaneously replace the elements that are less than p_c by 1. Elements grater than p_c are changed by 0.

2. the step 1 generates a matrix A whose elements are 0's and 1's. Take the upper triangular form of A which is called A_t.

3. Symmetrize A_t adding its transpose, that is $G = A_t + A_t^T$. Therefore, G is our Adjacent matrix.

For computational details of this process see(RANDOM...,). One example of random network is showed in the figure 19. As we can see there are too many nodes and the connections for every node represent high numbers

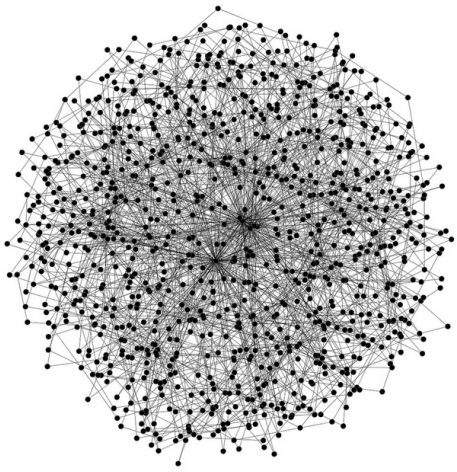

Figure 19 – Random network diagram, the node connections are represented by lines. Taken from(RANDOMNETWORKS,).

On the other hand the figure 20 shows numerical results for 10 realizations of adjacent matrices whose dimensions are $N = 1000$. As we can see, the histogram obtained has a semicircular shape and the eigenvalues of adjacent matrices are in the range of -6 to 6.

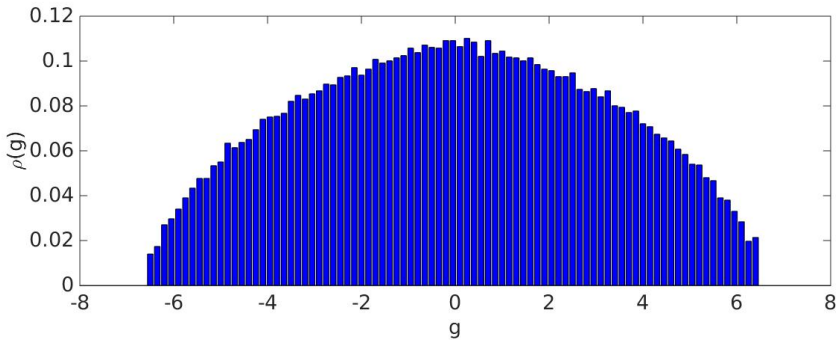

Figure 20 – Eigenvalues Histogram for one ensemble of 10 random networks of adjacent matrices of size $N = 1000$.

The spectral fluctuations presented in random networks can be studied from the eigenvalues distribution since it reveals interesting properties of the system. If we desire to understand those properties we must eliminate the non-universal features. Hence, we make a transformation of adjacent matrix eigenvalues $g_i, i = 1,...,N$ to another set $\varepsilon_i, i = 1,...,N$ using the unfolding procedure. Thus, the eigenvalues of every adjacent matrix that represents a random network is unfolded through the polynomial unfolding, we choose a suitable polynomial degree $\eta = 15$ to

obtain the nearest neighbor spacing distribution. The results in figure 21 reveal the Wigner-Dyson behavior over this adjacent matrix ensemble.

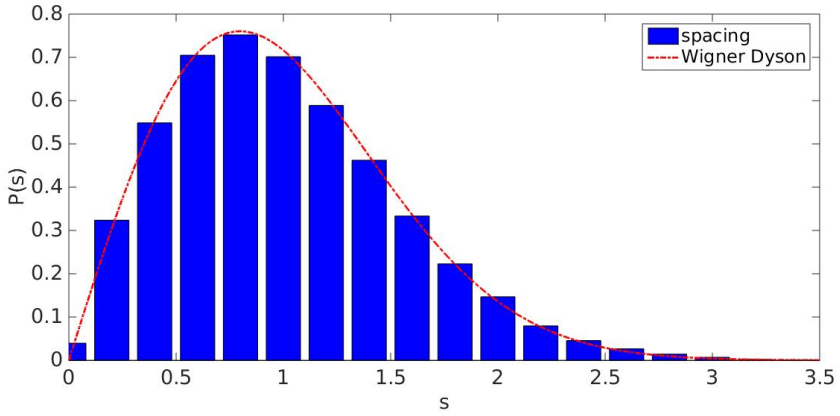

Figure 21 – Spacing distribution for network ensemble of $n = 10$ realizations. The red line corresponds to Wigner-Dyson distribution.

3.2 Time Series Analysis and Spectral Density for a Random Networks

In order to understand the spectral fluctuations present in random networks we follow the previous analysis used for the random matrix theory since it provides theoretical elements in order to find out if some systems have relation to the chaotic behavior. Then we use the Eq.(2.40), making one accumulative sum over spacing distribution associated with adjacent matrix. Such sum can be defined as follows

$$\delta(n) = \sum_{i=1}^{N} (s_i - < s >). \tag{3.1}$$

It represents the fluctuating behavior for every spacing respect to the mean spacing value. The importance of this quantity is due to $\delta(n)$ describes the time series. Therefore, we calculate such quantity for one random network dropping 5% of adjacent matrix eigenvalues, the initial value of matrix size is $N = 1000$.

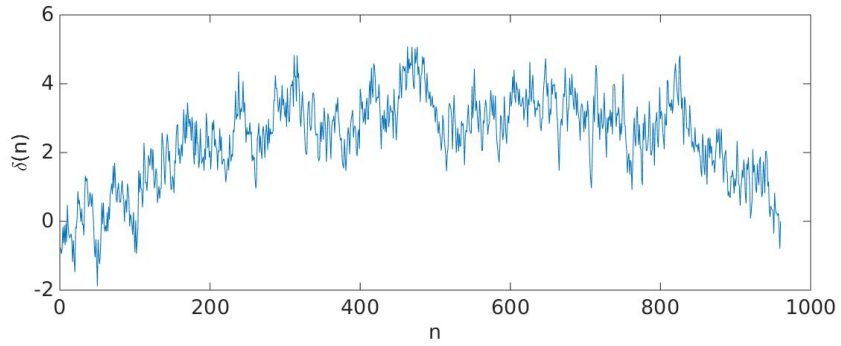

Figure 22 – Time series for random network using the $\delta(n)$ statistics, Eq.(2.40)

To characterize properties of the networks and checking whether they have relation to additional properties, which describe chaotic or integrable systems, we calculate the mean power spectral density $< S(k) >$ over the ensemble using Metha-Dyson statistics Eq.(2.40). Initially, the power spectral density is obtained from Eq.(2.58). However, due to the implications of using polynomial unfolding the quantities, whose goals is to determine if the chaos arises, can be affected by this statistical method, The spurious correlations are introduced in our analysis allowing the arising of misleading conclusions of the system properties. For this reason, we use the EMD to eliminate the trends of signals in our random network ensemble before obtaining the mean power spectrum. Thus, one comparison is done between a mean power spectrum usually obtained from Eq.(2.40) and another where the signals, defined by $\delta(n)$, are treated without their trends:$\delta'(n) = \delta(n) - r$. Our results are obtained in figure 23

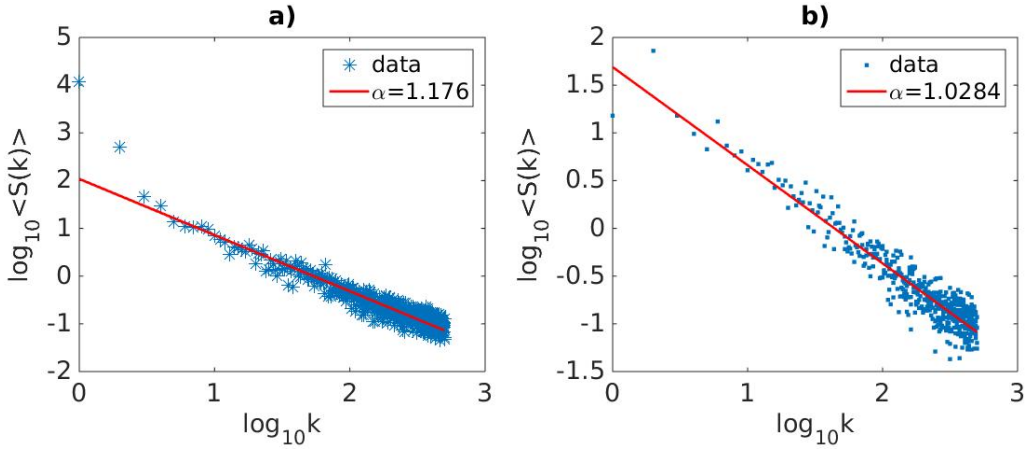

Figure 23 – Power spectrum of Adjacent matrix ensemble using $\delta(n)$ statistics. a) represents the power spectrum for one ensemble of 10 adjacent matrices without using EMD. The signals are obtained of $\delta(n)$. b) represents the power spectrum for one ensemble of 10 adjacent matrices using EMD $\delta'(n) = \delta(n) - r$, r is the trend of $\delta(n)$. Note the $1/k^{\alpha}$ behavior.

As we can see the figure 23 reveals a power law behavior $1/k^{\alpha}$ in the random network ensemble for two different ways of obtaining $< S(k) >$. We also see that the exponents change considerably since $\alpha = 1.1760$ to 1.0284, Indeed, the correction produced by EMD implementation gives information very well if the random networks can be related to $1/k^{\alpha}$ noise. Consequently the random networks present one behavior $1/k^{\alpha}$ noise with $\alpha \backsimeq 1$ as it is obtained in (YE; LI; MA, 2010),for this reason they provide information of intrinsic characterization that GOE and random networks share. However the origin of this power law behavior is not clear. There are other quantities that have been found in chaotic systems as number variance and Δ_3 statistics. In fact, in(JALAN; BANDYOPADHYAY, 2007) they studied the relation of three different model networks and spectral rigidity proving the long range correlations existence.

4 Transition to Chaos in Spin Systems

The Heisenberg spin model is characterized by integrability properties. However, such properties can be broken by diverse kinds of interactions that yields the system to chaotic domain. This integrability breaking is associated with interactions like external magnetic fields or next nearest neighbor interaction. If these parameters increases the system undergoes a transition from integrable to chaotic domain being observed through diverse quantities.

Therefore, in this chapter we will describe how the transition to chaos occurs for the Heisenberg spin model with three different interactions, which break the integrability: External magnetic field placed in the middle of the spin chain, random magnetic field in each spin of the chain and next nearest neighbor interaction in z direction. The transition is observed in function of the constant couplings and the quantities which describe the transition are the exponent average power spectral density, the *Kullback–Leibler divergence* and the burstiness coefficient. We explore universal crossover functions obtained from these quantities, which describes the transition in the spin chains systems.

4.1 Heisenberg Chain Model

The two body interaction systems have been studied in order to understand the phase transitions in statistical mechanics. One of the most common model is the $1D\ Ising\ model$. It consists in one dimensional chain where the spins interact each other in the z direction. However, this model can be generalized considering interaction terms in any direction, the result is known as $The\ Heisenberg\ spin\ model$. In one dimension the Ising model has a chain shape which depending on their boundary conditions it could be open or close. Therefore, if we consider one spin ensemble whose interactions are given in z direction.

However, before explaining the Heisenberg model we will consider the previous concepts in order to a better understanding of this physical system. Therefore, suppose that we have a system composed by spins-1/2. The possible spin measures over one single spin-1/2 in x, y or z are given by set operators $\hat{S}^{x,y,z} = \hat{\sigma}^{x,y,z}/2$. where $\hat{\sigma}^{x,y,z}$ are the Pauli matrices defined as follows

$$\hat{\sigma}^x = \begin{bmatrix} 0 & 1 \\ 1 & 0 \end{bmatrix}, \hat{\sigma}^y = \begin{bmatrix} 0 & -i \\ i & 0 \end{bmatrix}, \hat{\sigma}^z = \begin{bmatrix} 1 & 0 \\ 0 & -1 \end{bmatrix}$$

where $\hbar = 1$. The eigenvalue equations for the z spin operator are

$$\hat{S}^z |\uparrow\rangle = +\frac{1}{2} |\uparrow\rangle \qquad \hat{S}^z |\downarrow\rangle = -\frac{1}{2} |\downarrow\rangle \tag{4.1}$$

The first corresponds to the excitation, thus we associated the ket $|\uparrow\rangle$ to the 1/2- eigenvalue and $|\downarrow\rangle$ to -1/2 eigenvalue. If we have more than one spin they might interact each other. Therefore, suppose that we have L spins-1/2 forming a chain, the interaction is done in pairs where the Hamiltonian that describes the model is

$$\hat{H} = \sum_{n,m} J^z_{n,m} \hat{S}^z_n \hat{S}^z_m + h \sum_i \hat{S}^z_n. \tag{4.2}$$

Here the spin operator $\hat{S}_{n(m)}$ acts on the spin placed in n(m) $J^z_{n,m}$ is the strength interaction in the spin n(m). This is the $1D$ *Ising model*. The interaction is given for any pair spins in the chain. The h term corresponds to a external magnetic field action on each spin. We can consider that $m = n+1$, then we will have nearest neighbor interaction. Therefore, if we only consider the first part of the Hamiltonian we get

$$\hat{H}_{zz} = \lambda J \sum_{n=1}^{T} \hat{S}^z_n \hat{S}^z_{n+1} \tag{4.3}$$

Where T is related to the boundary conditions. Due to the interaction in pairs, we have the next equations

$$\lambda J \hat{S}^z_n \hat{S}^z_{n+1} |\uparrow,\uparrow\rangle = \frac{\lambda J}{4} |\uparrow,\uparrow\rangle \qquad \lambda J \hat{S}^z_n \hat{S}^z_{n+1} |\downarrow,\uparrow\rangle = -\frac{\lambda J}{4} |\downarrow,\uparrow\rangle . \tag{4.4}$$

Such equations provide information of how the energy is associated with the adjacent spin interaction. Moreover, the term $J\lambda$ and Eq.(4.3) establishing what kind of phase has the chain

- $J\lambda > 0$: The chain is antiferromagnetic with antiparallel neighboring spin.
- $J\lambda < 0$: The chain is ferromagnetic and the spins are aligned in the same direction.

On the other hand, we have two kinds of boundary conditions that change the Hamiltonian form. Hence, if the chain is open $\hat{H} = \hat{H}^{open}_{zz}$ we have $T = L - 1$ since the first spin can only

interact with the second spin and the last spin can only interact with the spin placed in the site L-1. If the chain is closed $\hat{H} = \hat{H}_{zz}^{close}$ we have $T = L$. A spin placed in the first site can interact with a spin on the second site and also with the last one, which interacts with the first one and the L-1 spin too. This kind of boundary condition makes us to interpret the chain as a ring.

The last model only has taken into account z-spin interaction, for this reason we can consider additional interactions in x and y.

$$\hat{H}_{xxz} = \sum_{n=1}^{L-1} \left(J[\hat{S}_n^x \hat{S}_{n+1}^x + \hat{S}_n^y \hat{S}_{n+1}^y] + J\lambda \hat{S}_n^z \hat{S}_{n+1}^z \right). \tag{4.5}$$

We have used open boundary conditions. The term λ is the ratio between Ising interaction and the strength of the term $\hat{S}_n^x \hat{S}_{n+1}^x + \hat{S}_n^y \hat{S}_{n+1}^y$. The λ term has an important relevance since if $\lambda = 1$ the system is isotropic, whose name in the literature is H_{xxx} model, if $\lambda \neq 1$ the model is anisotropic and it is called H_{xxz} model. The first term in Eq.(4.5) is known as flip-flop term. It can be mapped onto a non-interacting spinless fermion model(SANTOS,).

It is important to say that we are working in the z base, for this reason the operators $\hat{S}^x$ and $\hat{S}^y$ can be written in terms of ladder operators. Hence, $\hat{S}^x$ and $\hat{S}^y$ are defined as follows

$$\hat{S}^x = \frac{\hat{S}^+ + \hat{S}^-}{2} \qquad \hat{S}^y = \frac{i(\hat{S}^- - \hat{S}^+)}{2}. \tag{4.6}$$

Then we have two alternatives to express the flip-flop term: either using $\hat{S}^y$ and $\hat{S}^x$

$$J(\hat{S}_n^x \hat{S}_{n+1}^x + \hat{S}_n^y \hat{S}_{n+1}^y) \left|\uparrow_n \downarrow_{n+1}\right\rangle = \frac{J}{2} \left|\downarrow_n \uparrow_{n+1}\right\rangle \tag{4.7}$$

or ladder operators

$$\frac{J}{2}(\hat{S}_n^+ \hat{S}_{n+1}^- + \hat{S}_{n+1}^+ \hat{S}_n^-) \left|\uparrow_n \downarrow_{n+1}\right\rangle = \frac{J}{2} \left|\downarrow_n \uparrow_{n+1}\right\rangle. \tag{4.8}$$

Notice that

$$(\hat{S}_n^x \hat{S}_{n+1}^x + \hat{S}_n^y \hat{S}_{n+1}^y) \left|\uparrow_n \uparrow_{n+1}\right\rangle = \left|\uparrow_n \uparrow_{n+1}\right\rangle = 0 \tag{4.9}$$

andFIgure

$$(\hat{S}_n^x \hat{S}_{n+1}^x + \hat{S}_n^y \hat{S}_{n+1}^y)\,|{\downarrow_n}{\downarrow_{n+1}}\rangle = |{\downarrow_n}{\downarrow_{n+1}}\rangle = 0. \tag{4.10}$$

Since the spins only have two possible values and the orientation of the two adjacent spins can be coupled by the term $\hat{S}_n^x \hat{S}_{n+1}^x + \hat{S}_n^y \hat{S}_{n+1}^y$. This term only acts in nearest neighbor spins that differ in their orientations. Therefore, the last models do not create spin states only change the spin orientation along the chain.

On the other hand, the Hamiltonians of Eq.(4.2) and Eq.(4.5) can be associated with symmetries whose representations are made by operators. Hence, one symmetry is related to one operator $\hat{O}$ that commutes with the Hamiltonian being a constant of motion and, therefore a conserved quantity. That is easy to see using the Ehrenfest equation

$$\frac{d<\hat{O}>}{dt} = [\hat{H}\hat{O} - \hat{O}\hat{H}] = 0. \tag{4.11}$$

The expected value does not change in the time. In the case of H_{xxz} the total spin is conserved. For this reason we have $[\sum_i^L \hat{S}_n^z, \hat{H}] = 0$. Thus, the number of spins is constant for each eigenstates and the system is invariant under rotations around z. The Hamiltonian is also invariant under reflection. That implies H_{xxz} commutes with a parity operator

$$\hat{\Pi} = \begin{cases} \hat{P}_{1,L}\hat{P}_{2,L-1}\cdots\hat{P}_{\frac{L}{2},\frac{L+2}{2}} & for \qquad L = even \\ \\ \hat{P}_{1,L}\hat{P}_{2,L-1}\cdots\hat{P}_{\frac{L-1}{2},\frac{L+3}{2}} & for \qquad L = odd \end{cases} \tag{4.12}$$

Where $\hat{P}_{nm}$ is the *permutation operator*, it permutes n-th with m-th in the vector space. This invariance may be understood as a mirror figure at the edges of the chain. If the parity is conserved the participation of each basis vector in the eigenstate is equal to its reflection(SANTOS,).

4.2 Chaos in Heisenberg Chain with Impurity

One of the properties of H_{xxz}^{open} model is the integrability. This means that, the nearest neighbor spacing distribution, obtained from the energy spectrum, has a Poisson form. However, we may introduce in this model two terms associated with one specific chain site, which is

equivalent to apply one external magnetic field in z direction over the spin placed in this chain position. It produces a Zeeman splitting defect being different from the rest sites. Therefore, the defect plays a role of *impurity* in the Heisenberg XXZ model and the Hamiltonian will be

$$\hat{H}^{imp}_{xxz} = J\lambda' S^z_1 + J\lambda S^z_{L/2} + \sum_{n=1}^{L-1} \left(J_{xy}[\hat{S}^x_n \hat{S}^x_{n+1} + \hat{S}^y_n \hat{S}^y_{n+1}] + J_z \hat{S}^z_n \hat{S}^z_{n+1} \right). \tag{4.13}$$

J,J_z and J_{xy} are parameters which measure how much the coupling strength is in their respective spin direction. Hence, a large J_z value means a strong interaction between two spins in z direction. $J\lambda' S^z_1$ and $J\lambda S^z_{L/2}$ are the introduced defects. The first one affects only the first spin in the chain breaking reflection symmetries (parity) and total spin conservation. The second defect has λ value, which plays a fundamental role for the integrability conservation since if λ increases the system begins to enter in chaotic domain. It is also a strength parameter over associated with external field applied in the spin placed in the middle of the chain. Usually, in the literature the chaotic behavior is studied through the ration of J_z and λ(ALCARAZ et al., 1987; SANTOS, 2004). However, we can study how the chain changes its properties through increasing the λ value from 0 to 0.25 in order to understand how the Transition of integrable to chaotic domain occurs.

Therefore, we have anisotropic chain of size $L = 17$ with 6 up spins $N_{up} = 6$, $J = 1$, $J_z = \frac{1}{4}$ and $J_{xy} = 1/2$. The defect size is placed in the middle of the chain $S^z_{n=8}$, the eigenvalues energy distribution for a Heisenberg model described by Eq.(4.13) are given in the figure 24

λ	σ^2	μ
0.0	2.146	0.058
0.1	2.147	0.058
0.175	2.161	0.059
0.25	2.212	0.059

Table 3 – Statistical parameters of the energy eigenvalues distribution for $\hat{H}^{imp}_{xxz}$ model. σ^2 and μ are the variance and mean respectively.

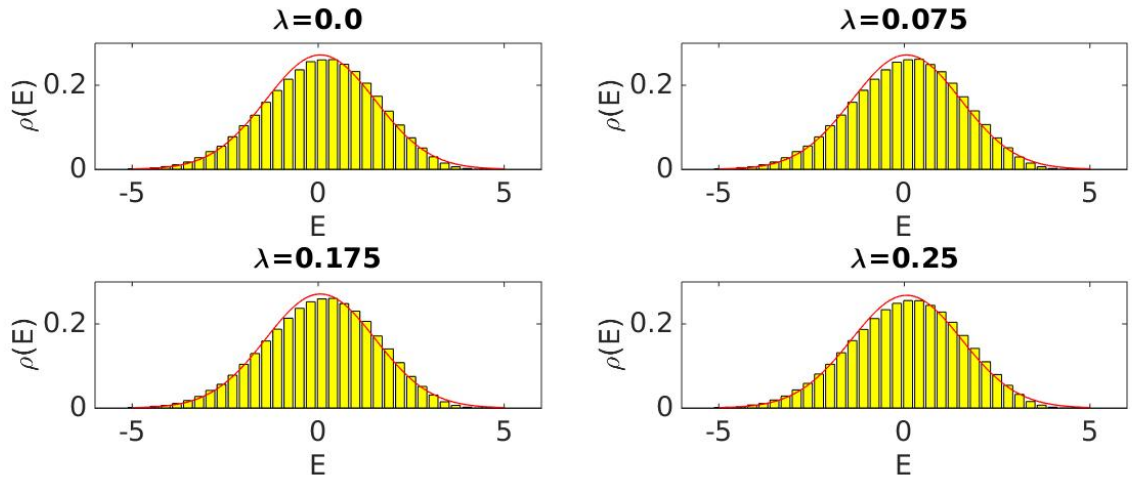

Figure 24 – Eigenvalues histograms of impurity model for $\lambda = 0.00$,$\lambda = 0.075$,$\lambda = 0.175$ and $\lambda = 0.250$ with $L = 17$, $N_{up} = 6$. The eigenvalues number for every histogram is $E_{imp} = 12376$. The values σ^2 and μ are the variance and mean . The red line is the theoretical fit obtained from σ^2 and μ.

As we can see, the energy distribution for $\hat{H}^{imp}_{xxz}$ model has a Gaussian form. Hence the parameters like mean and variance are found in the Table 3. The site basis number or dimension is given by $D = L!/(N_{up}!N_{down}!)$

We can infer from figure 24 that the distribution are not symmetric since the fits (red lines) differ from the statistical distribution. The variance tends to increase with λ different from the mean behavior which does not change. We also, note that the number of spins in one direction determines that the system enters in chaotic domain. Hence, for $1/3$ of the spins in one direction we have optimal results.

On the other hand, due to the integrability breaking for $\hat{H}_{xxz}^{imp}$ model, it is possible to analyze the transition when the λ parameter begins to be larger. Hence, the eigenvalues distribution obtained in the figure 24 are unfolded using the polynomial unfold method with the polynomial degree $\eta = 15$ and dropping close to 2% eigenvalues. Therefore the spacing distribution are given in figure 25.

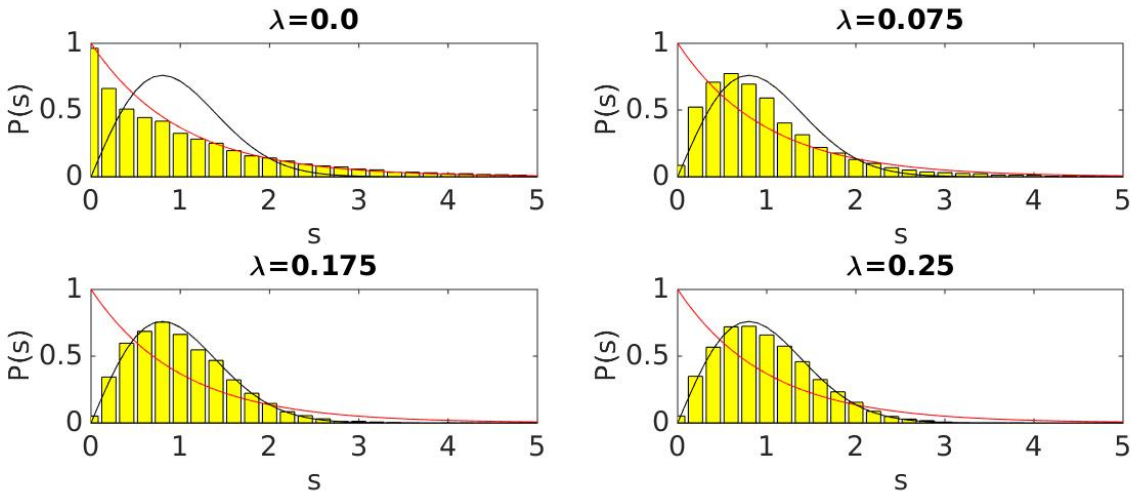

Figure 25 – Spacing distributions for $\hat{H}_{xxz}^{imp}$ model with $\lambda = 0.00$,$\lambda = 0.075$,$\lambda = 0.175$ and $\lambda = 0.250$ with $L = 17$. The red and black lines represent the Poisson and Wigner-Dyson distributions respectively.

figure 25 reveals a transition from integrable to chaotic in $\hat{H}_{xxz}^{imp}$ when the λ value increases. It is important to note that if the defect value becomes too large it will split the system in two independent and integrable chains,i.e This system becomes equivalent to two smaller and uncoupled ideal chains, and the integrability is therefore recovered(SANTOS, 2004). The chaos in this model arises due to the interaction between J and λ, for this reason we changes the λ on a range of 0 to 0.25. Values more larger than $\lambda = 0.25$ yields to system in integrable domain.

On the other hand, we can use the $\delta(n)$ statistics in order to find others characteristics, which make the system $\hat{H}_{xxz}^{imp}$ go to integrable domain to chaotic domain. Hence, using the Eq.(2.40) for different λ values, we construct time series for $\lambda = 0.00$,$\lambda = 0.075$,$\lambda = 0.175$ and $\lambda = 0.250$,

we also drop close to 9% of the data in $\delta(n)$ due to emergent fluctuations. These time series provide interesting information about the transition done by the system. However, we have seen that the unfolding procedure affects the $\delta(n)$ statistics giving results that might be misleading. For this reason, we use again the EMD to obtain the time series trend r. Hence, the figure 26 shows the resulting signals after eliminating the trend of each time series.

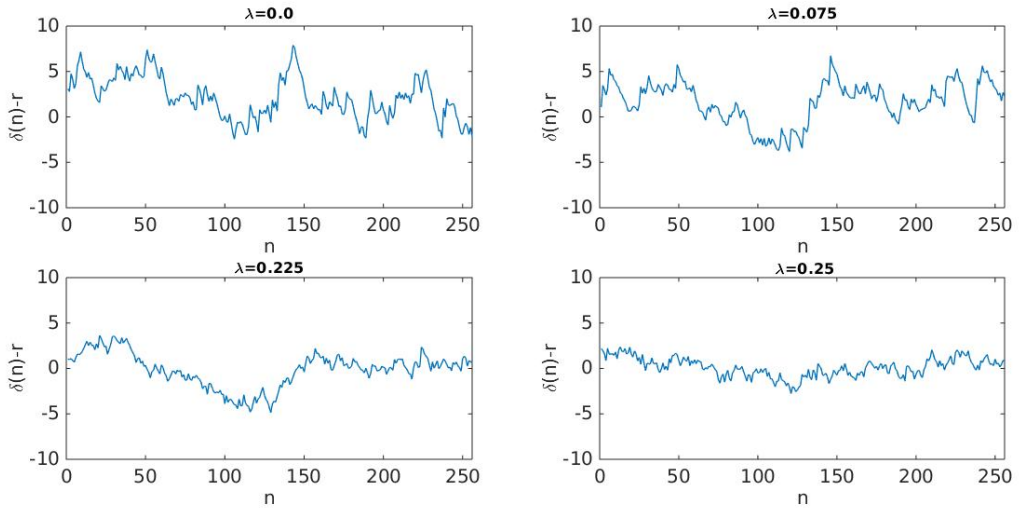

Figure 26 – Time series $\delta(n) - r$ for different λ values of 256 consecutive energy levels.

Note that the signals in figure 26 are made taking 256 consecutive energy values. That is, we calculate the total time series $\delta(n) - r$. The signals are obtained in figure 26 using only 256 consecutive values. The behavior of these signals shows that for $\lambda = 0$ the levels are uncorrelated, as λ increases the energy levels of the systems begin to show repulsion themselves. We note the spacing of consecutively eigenvalues does not differ much from the mean spacing. This property is called *antipersistence* and it is present in systems whose time series are associated with $1/k^{\alpha}$ noise, where $1 < \alpha < 2$. For this reason, we may calculate the power spectrum for different values of λ and finding out if there is a relation between the time series behavior and the spectral density.

Therefore, in order to avoid statistical fluctuations we calculated the average power spectrum for the same λ values. We fragment each time series $\delta(n) - r$ in 42 sets of 256 energy levels ε_n (note that the Eq.(2.42) which relates $\delta(n)$ to ε_n). The result is given in the figure 27.

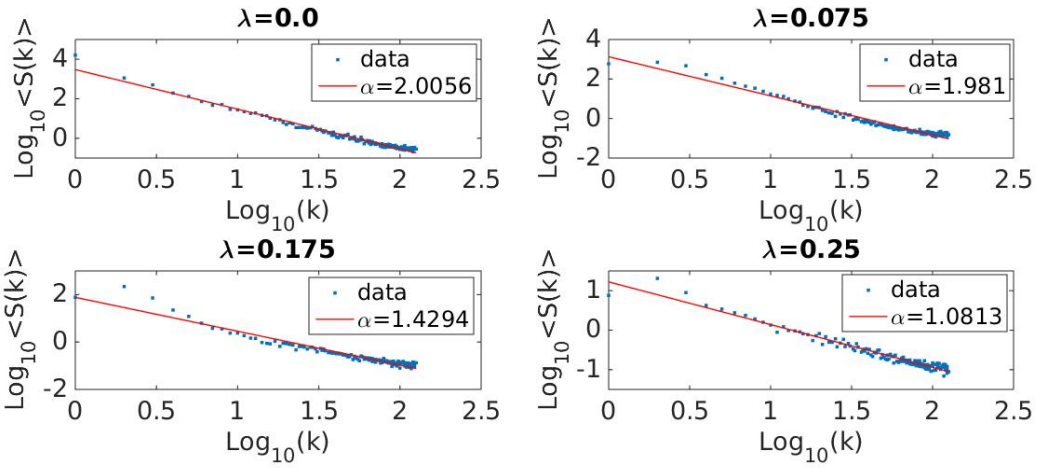

Figure 27 – Average power spectrum $< S(k) >$ of $\delta(n) - r$ for different values of λ. The red lines represent the linear best fit and α is the respective exponent. Note the power law behavior $1/k^{\alpha}$ is obtained.

Hence, the relation between the times series and power spectrum is found. The antipersistence property increases when the system becomes more chaotic. Other main fact is that the system follows the law

$$< S(k) > \propto \frac{1}{k^{\alpha}}. \tag{4.14}$$

This relation is approximated since we work with frequencies less than $Log(k) < 2.1$. For larger frequencies this relation does not have enough accuracy. We can conclude that the power exponent is a well measure of chaos in the system since it follows the predictions of random matrix theory: $1 < \alpha < 2$ where $\alpha = 2$ for integrable systems and $\alpha = 1$ for chaotic systems. In this way, the α exponent provides excellent information if the systems present a transition of integrable to chaotic domain. Then we can characterize this transition that depends on the λ values. It is found in the figure 28 following the procedure explained before.

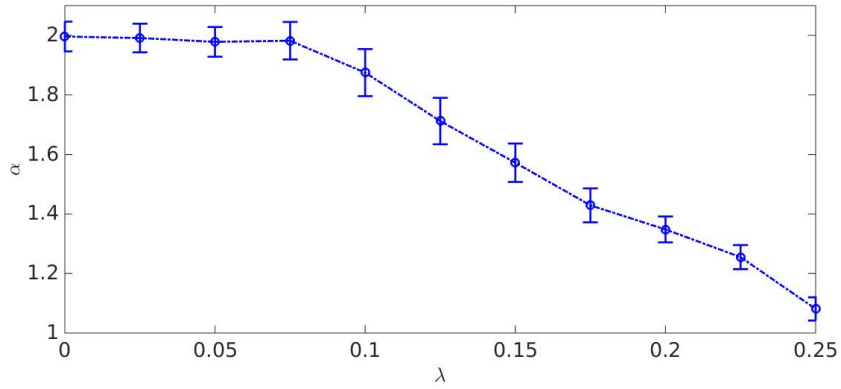

Figure 28 – Behavior of the power spectrum α in function of λ parameter. The error bars are the confident intervals of 95%.

The α exponent evolves with λ showing a smooth transition. We note that the $\lambda < 0.1$ values preserve part of integrability, However, for $\lambda > 0.1$ the system presents a coexistence between integrable and chaotic behavior. That is, it presents an intermediate phase. The last values show entering in chaotic domain. In conclusion, α characterizes the chaoticity in the system. Moreover, the origin of the power law behavior $< S(k) > \propto \frac{1}{k^{\alpha}}$ is demonstrated in the integrable case for $\alpha = 2$ and $\alpha = 1$ in the chaotic case.

On the other hand, the transition to chaos in spins systems is not only characterized by the spacing distribution and mean spectral density behavior. Hence we may consider a measure over the spacing distributions which provides more accuracy information of how the system changes as λ increases. Therefore, the *Kullback–Leibler divergence* is a good measure to understand the chaos following the objectives exposed before. This function is defined as follows

$$D_{kl}(P(x)|Q(x)) = \sum_i P(x_i) Log\left(\frac{P(x_i)}{Q(x_i)}\right) \tag{4.15}$$

where $P(x)$ and $Q(x)$ are probability distributions. $D_{kl}(P(x)|Q(x))$ measures how much two distribution differ from each other. Usually, it is used to compare empirical distribution obtained from experiments with theoretical distributions. Hence, P(x) represents the distribution associated with theoretical statistic model and Q(x) is the distribution obtained from observation or realization of one experiment. It has some important properties

- $D_{KL}(P|Q) \geq 0$ and 0 when $P = Q$

- $D_{KL}(P|Q) \neq D_{KL}(Q|P)$ (Asymmetry)
- $D_{KL}(P|Q) = D_{KL}(P_1|Q_1) + D_{KL}(P_2|Q_2)$ with $P(x,y) = P_2(x)P_2(y)$ and $Q(x,y) = Q_1(x)Q_2(y)$

Therefore, we compare every spacing distribution of the $\hat{H}^{imp}_{xxz}$ associated with each λ value in a range of $[0, 0.25]$ with the theoretical Wigner-Dyson distribution Eq.(2.21) in order to find out how D_{LK} changes increasing λ parameter. We normalize the D_{LK} divergence for a better understanding of a possible quantum chaos transition defining

$$\eta_{lk} = \frac{D_{LK}(P_{W-D}|P_{data})}{D_{LK}(P_{W-D}|P_{\lambda=0})}. \tag{4.16}$$

Where P_{W-D} is the Wigner-Dyson distribution, P_{data} is the data distribution obtained for every λ used in the figure 28 and $P_{\lambda=0}$ corresponds to empirical distribution obtained for $\lambda = 0$. The figure 29 shows the behavior of the η_{lk} with λ.

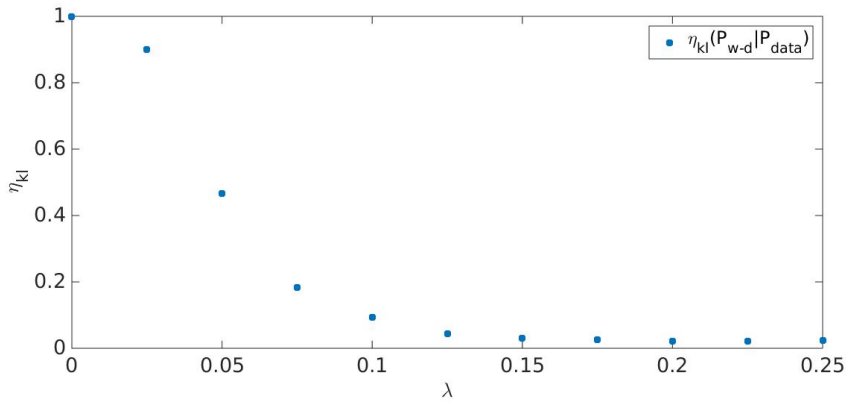

Figure 29 – Behavior of the normalized *Kullback–Leibler divergence* D_{lk} using Eq.(4.16) as a function of parameter λ.

We note that figure 29 characterizes a transition between integrable and chaotic regime. The values of η_{lk} trend to zero in asymptotically way since the last values of λ represent approximations of nearest neighbor spacing distribution, which is in our case the Wigner-Dyson distribution.

Therefore, the quantities α and η_{lk} provide information that how the chaotic transition arises. Although, in context of human activities it has been assumed that for long periods of times the human activities are uniform in time, thus they are modeled using a Poisson process.

Recently, the last years the scientist have had access to large-scale data base, where the researches could extract information. The human activities have demonstrated to be heterogeneous in time and, moreover exhibit *Burstiness*. The burstiness has become in a quantity widely studied in complex systems since the macroscopic, as well as microscopic complex systems can be better understood through the use of this quantity instead of Poisson function. Hence, the measures of inhomogeneity in complex systems can be divided in two categories, one that measures distribution of waiting times i.e intervals between two consecutive events in an activity sequence, and the other related to the correlations presented in the time series(HOLME, 2014). It is important to note that these sequences are explained in the literature either Poisson distribution $P_{poisson}(\tau) = (1/\tau_0)exp(-\tau/\tau_0)$(GOH; BARABáSI, 2008) or power law $P(\tau) \propto 1/\tau^{\alpha}$, which depends on the time interval between events τ. Hence, the first of these measures proposed before represents in some way how $P(\tau)$ is deviated from Poisson signal. It is defined as a coefficient that depends on mean m_τ and variance σ_τ: the *burstiness parameter* B,written as follows

$$B = \frac{(\sigma_\tau/m_\tau - 1)}{(\sigma_\tau/m_\tau + 1)} = \frac{\sigma_\tau - m_\tau}{\sigma_\tau + m_\tau}. \tag{4.17}$$

The last equation is applicable if the mean exists. The case of infinite mean has to be treated with care. B also is defined in a boundary range $(-1,1)$. If $B = 1$ the signal is most bursty, $B = 0$ represents a neutral signal and $B = -1$ corresponds to periodic and regular signal.

Therefore, the burstiness coefficient can be calculated for every spacing distribution in the $\hat{H}^{imp}_{xxz}$ model. The behavior of B as λ increases is showed in the figure 30

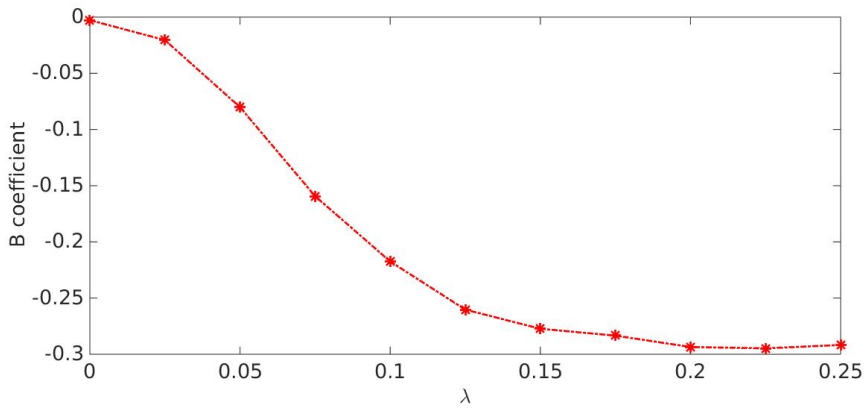

Figure 30 – B coefficient function of parameter λ.

The figure 30 displays the behavior for every λ value of a system. The first point is close to zero in figure 30 due to the B coefficient gives information that how long the data distribution is to Poisson distribution. If the B value is close to zero the equation reveals that the mean and variance of the data distribution is approximately Poisson type. Hence, the 1 term in that equation can be interpreted as $m_{Poisson}/\sigma_{Poisson}$ which is 1. The B values are $B < 1$ for distributions in chaotic domain since the spacings tend to be close to zero. That implies the spacing interpreted as a signal is regular in this context producing one anti-bursty effect.

Consequently, the chaos arising in $\hat{H}^{imp}_{xxz}$ model is due to impurity in the middle of the chain is one of the many examples of how the integrability can be broken. Thus, there are other causes that produce the system entering in chaotic domain as we shall later see.

4.3 Chaos in Heisenberg Model with Random Interaction

The impurity introduced in the model explained before is one of the way that makes the chaos arise in the Heisenberg spin model. Such impurity increases breaking the integrability of the system. However, it is possible to introduce more than one defect in the model turning it in a disorder system. Those defects must satisfy some specific properties related to the strength of external magnetic interaction. Therefore, the Hamiltonian can be defined as follows

$$\hat{H}^{r}_{xxz} = \sum_{i=1}^{L} \delta_n S^z_n + \sum_{n=1}^{L-1} \left(\frac{J}{4} [\hat{S}^x_n \hat{S}^x_{n+1} + \hat{S}^y_n \hat{S}^y_{n+1}] + \frac{J_z}{2} \hat{S}^z_n \hat{S}^z_{n+1} \right). \tag{4.18}$$

where δ_n is a coupling strength for the site n in the chain that we will explain later. As we can see this Hamiltonian is characterized by the presence of one defect in z direction over each spin in the chain with energy splitting δ_n. One defect corresponds to an energy value for specific site which differ from others. Moreover, the Hamiltonian of Eq.(4.18) describes an anisotropic model, whose boundary conditions are open, that is the chain is non-periodic since a closed chain is characterized by a large number of degenerated states.

On the other hand, an open chain with defects only on the edges is also integrable(ZANGARA et al., 2013). Then, it could be solved analytically using the Bethe Ansatz(BETHE, 1931). However, the integrability can be broken by the introduction of a defect in each site. It is described in

the Hamiltonian $\hat{H}^{r}_{xxz}$. In each site the defect plays the role of magnetic field whose strength is given by δ_n. Such δ_n can be defined by $\delta_n = \lambda^2 b_n$, where b_n are a random Gaussian numbers which have $< b_n >= 0$ and $< b_n b_m >= b^2 \delta_{nm}$. If $b_n = 0$ the system is integrable described by the Poisson distribution. As b increases the system begins to lose integrability.

The level density of eigenvalues can be described constructing a random ensemble as b parameter increases. Therefore, we construct one ensemble of 50 Hamiltonian matrices from Eq.(4.18) for an open chain of size $L = 15$ with $N_{up} = 5$ spin up and $N_{down} = 10$ spin down. The eigenvalues set for every matrix is 3003. Hence, the figure 31 displays the changes of level density of energy values as λ increases

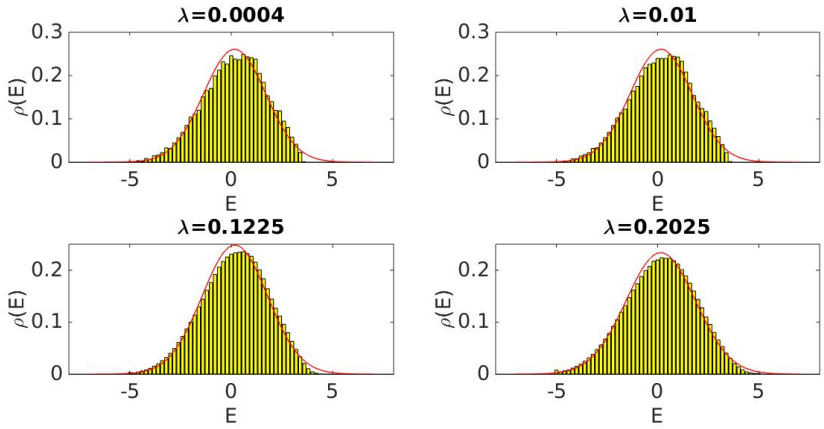

Figure 31 – Level density histograms of Heisenberg model with random field interaction for $\lambda = 0.0004$,$\lambda = 0.01$,$\lambda = 0.1225$ and $\lambda = 0.2025$ with $L = 15$, $N_{up} = 5$. The eigenvalues number for every histogram is $E = 3003$. The red line is the theoretical fit obtained from σ^2 and μ.

The behavior of the extreme values of the histograms show some kind of cut in the level density. That is, the histograms closer to the integrable domain do not have the extreme values in the Gaussian form, such values represent energies with low frequency in the total spectrum. This anomalous effect could be related to the finite size effects since the matrix dimensions for each Hamiltonian is $N = 3003$, which is a small value due to the results predicted by the random matrix theory i.e. when $N \longrightarrow \infty$ the level density is the result obtained analytically. However, the distributions whose correspondence is the chaotic domain, are closer to a Gaussian. The

λ	σ^2	μ
0.0004	2.341	0.166
0.01	2.342	0.166
0.1225	2.581	0.176
0.2025	2.917	0.152

Table 4 – Statistical parameters of the energy eigenvalues distribution for $\hat{H}^r_{xxz}$ model. σ^2 and μ are the variance and mean respectively.

red lines in figure 31 are the theoretical Gaussian distributions obtained from the mean μ and variance σ^2. The table 4 has the values for λ values mentioned before.

The level distributions have increasing behavior of the variance in the system, although the mean value does not change considerably.

The fit obtained for each histogram in figure 31 is not accurate, indeed the red lines do not describe correctly the Gaussian behavior of the level density. Therefore, the chaotic signature must be studied using the assumption that the Gaussian shape of these densities is unknown. Hence we use the unfolding polynomial, whose polynomial degree is $\eta = 15$, fitting the accumulative density to describe a transition present in $\hat{H}^r_{xxz}$ model. The figure 32 shows the level spacing distribution for this random model.

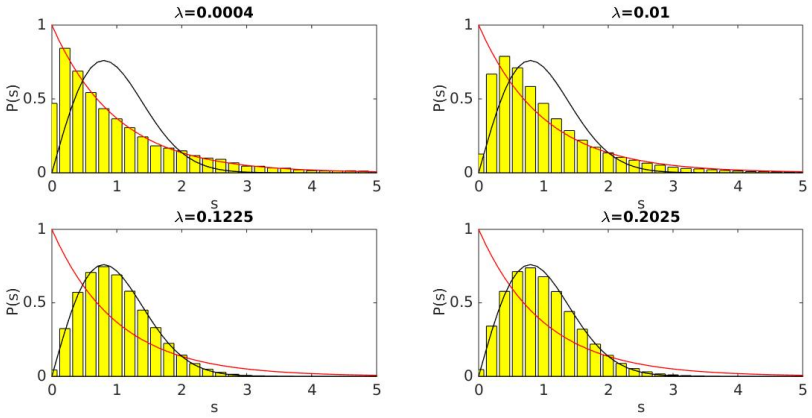

Figure 32 – Nearest neighbor spacing distribution for $\lambda = 0.0004$,$\lambda = 0.01$,$\lambda = 0.1225$ and $\lambda = 0.2025$ values. The red line represents the Poisson distribution and the black line is the Wigner distribution.

The histograms in figure 32 reveal the robust of the spacing distribution function due to the

number of realization. The transition behavior occurs similar to the impurity model and the smallest λ value is chosen due to the approximation with the integrable regime. If $\lambda = 0$ the system is completely integrable, although the matrix size is small for a good approximation i.e the result will not be accurate to the Poisson theoretical distribution. Moreover, the integrable case in this model does not allow one statistical ensemble construction since the first term in Eq.(4.18) will vanish. It yields to a standard Heisenberg spin model.

In order to characterize the transition of a Heisenberg spin model with random external field in z direction we use the time series analysis used for the impurity model. The signals are obtained from Eq.(2.40). They also are constructed taking only 256 unfolded energy levels ε_i according to this equation. Therefore the figure 33 shows the landscape for every signal, whose respective values are $\lambda = 0.0004$,$\lambda = 0.01$,$\lambda = 0.1225$ and $\lambda = 0.2025$.

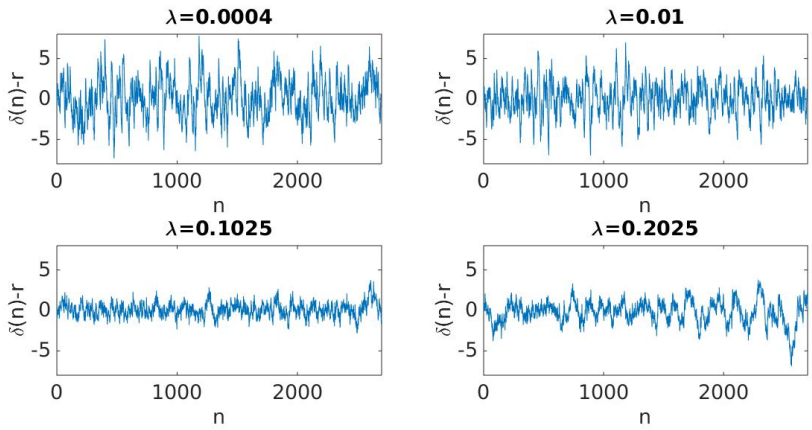

Figure 33 – Time series for Heisenberg spin model with random external field. The signals correspond to random matrices that belong to the model of Eq.(4.18) using the λ parameters mentioned before.

Each signal in figure 33 corresponds to a Hamiltonian matrix that has associated one of these λ strength coupling. These signals were taken to show the global behavior of the series as the parameter, which produces the transition, increases. This description is a qualitatively way to understand how the chaos arises in this Heisenberg spin model. Although, a better way to describe the chaotic transition is based on the power spectral density, as we have seen in the case of impurity model. Therefore, we construct the power spectrum through averaging over a set of

500 series made with 256 energy data. The power spectrum is showed in the figure 34.

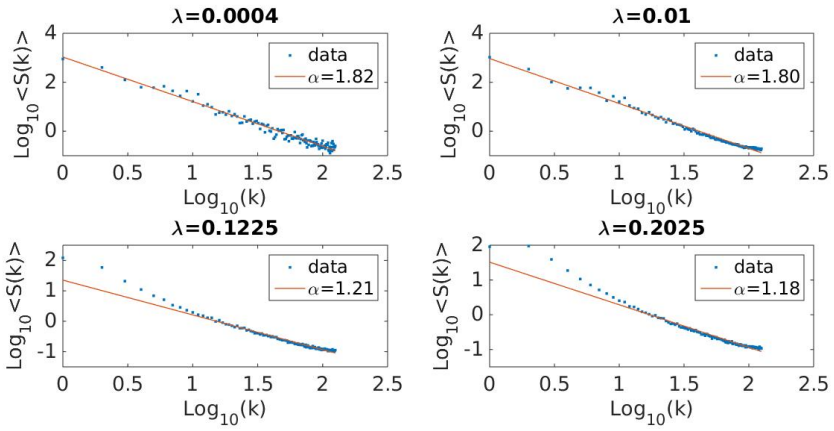

Figure 34 – Mean power spectral density for $\lambda = 0.0004$, $\lambda = 0.01$, $\lambda = 0.1225$ and $\lambda = 0.2025$ values. The graphics are associated with random matrices corresponding to the model $\hat{H}^r_{xxz}$. The red line is the better fit using last square and α is the power spectrum. Note the behavior $1/k^\alpha$ noise.

The figure 34 allows us to infer that α exponent is a quantity which describes the transition to chaotic domain in the Heisenberg spin mode with random external field. The results are analogous to impurity model. However the $\lambda = 0$ value is not considered due to small value of a Hamiltonian matrix. We note that in absence of external random field this model coincides with the impurity model when the defects introduced are zero.

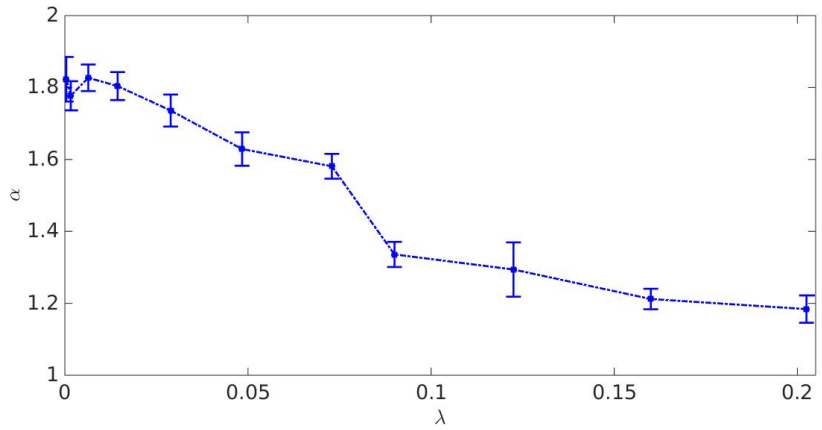

Figure 35 – Behavior of the power spectrum exponent α in function of λ parameter for Heisenberg spin model with random magnetic field. The error bars are the confident intervals of 95%.

The error bars are close to 6%. The RMT predictions say that the integrable regime corresponds to $\alpha = 2$ and the chaotic domain is given by $\alpha = 1$. Although, the results of the model described in figure 34 are approaches of those predictions due to the matrix size. However, figure 34 displays an evident transition between those regimes: integrable chaotic. Moreover, it reveals correctly the integrability breaking due to random defects.

On the other hand, the α exponent is a parameter directly related to the noise of the time series associated with unfolded energy levels and the histograms are associated to the statistical eigenvalues of spacing distribution. There are quantities that are related to the spacing distributions whose results provide interesting information. For instance, in(SANTOS, 2004) they proposed one coefficient, whose dependence implies the Poisson and Wigner-Dyson distributions, that measures in a continuous way one kind of distance between those distributions. It goes from 1 to 0 when the system is chaotic. However, following the analysis used for impurity model the *Kullback–Leibler divergence* D_{lk} is a useful measure of how far two distribution are from each other. Since the system experiments one chaotic transition displayed by the histogram in figure 32 the divergence D_{lk} will give us information about the transition integrable-chaotic. Therefore in figure 35 we have the transition for Heisenberg spin model with random external field

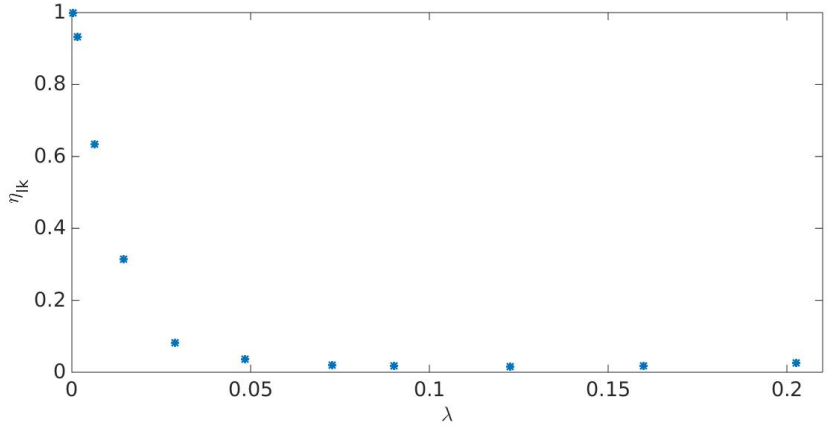

Figure 36 – Behavior of the normalized *Kullback–Leibler divergence* D_{lk} using Eq.(4.16) as a function of parameter λ for $\hat{H}^r_{xxz}$. Each point in the figure is obtained from one ensemble over 50 energy spectra sets. The realization number is $n = 50$.

The divergence D_{lk} is a discrete statistical measure obtained from spacing distribution. In(SANTOS; RIGOL, 2010) they consider one α value, which is a discrete measure, that takes into account the distance between an arbitrary $P(s)$ distribution with the Wigner-Dyson distribution. It is normalized and reveals the same conclusion obtained from divergence D_{lk}.

Another quantity which changes as λ increases is the burstiness parameter. We have already seen in the case of impurity model that almost all B coefficients are negatives then figure 37 displays a similar behavior.

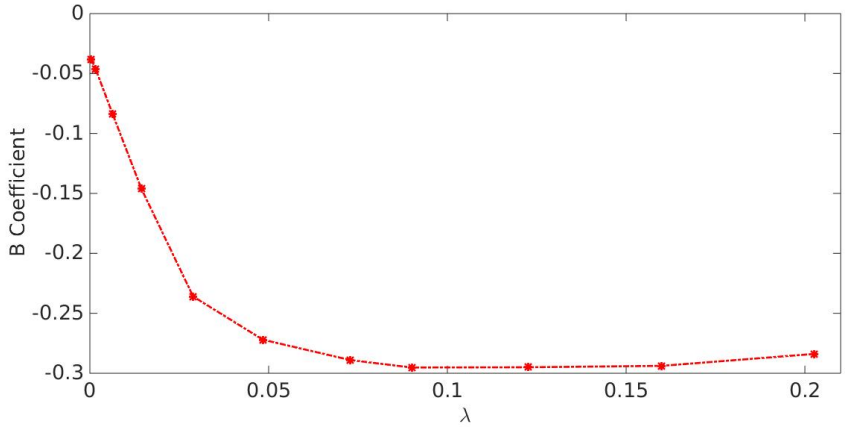

Figure 37 – Burstiness coefficient for Heisenberg $\hat{H}^{r}_{xxz}$ model. B is calculated over the total ensemble for each λ parameter.

In this case, figure 37 reveals the chaotic behavior which produces a burstiness more regular in the sense of the spacing distribution is interpreted as time differences distribution of events set. In other words the unfolded energies are interpreted as events which have associated a time occurrence.

On the other hand, the last point in the graphics shows a possible transition to integrability of the system, since the transition is only observed in a range of λ. If this parameter is larger enough the system returns to integrable state.

4.4 Chaos in Heisenberg Model with Next Nearest Neighbor Interaction

It is well known the chaos arising occurs by the introduction of external parameter that breaks the integrability and symmetries in the system. When λ' and λ are different from zero in Eq.(4.13) the system begins to lose integrability producing that it enters in chaotic domain. However, if only one defect is considered in the first site of the chain the system does not experiment one transition to chaos regime and, therefore it will be analytically solvable by the Bethe Ansatz(BETHE, 1931). Hence, if we desire that the system experiments a transition to chaos we must add additional couplings. For this reason, we may introduce a term in the H_{xxz}

model considering coupling not only with the nearest neighbor but with next nearest neighbor for each spin in the chain. Thus the Heisenberg spin chain Hamiltonian with nearest neighbor couping for open boundary conditions is given by

$$\hat{H}_{NN} = \sum_{i=1}^{L-1} [J_{xy}(\hat{S}_i^x \hat{S}_{i+1}^x + \hat{S}_i^y \hat{S}_{i+1}^y) + J_z \hat{S}_i^z \hat{S}_{i+1}^z], \tag{4.19}$$

where J_{xy} and J_z measure the strength coupling in their respective directions. The additional coupling is known in the literature as *Next Nearest Neighbor couping* (SANTOS; MITRA, 2011).

$$\hat{H}_{NNN} = \sum_{i=1}^{L-2} [J'_{xy}(\hat{S}_i^x \hat{S}_{i+2}^x + \hat{S}_i^y \hat{S}_{i+2}^y) + J'_z \hat{S}_i^z \hat{S}_{i+2}^z]. \tag{4.20}$$

J_{xy} and J'_z play analogous roles as J_{xy} and J_z. The total Hamiltonian is written as follows

$$\hat{H}_\lambda = \hat{H}_{NN} + \lambda \hat{H}_{NNN}. \tag{4.21}$$

λ represents the strength of the $\hat{H}_{NNN}$ term. That is, it is a parameter which provides information of how much intense is the NNN coupling in any direction. Therefore the chaos can arise in various scenarious(GUBIN; SANTOS, 2012) derived from this model.

1. Absence of Ising interactions, $J_z = J'_z = 0$
2. Absence of the flip-flop term between next nearest neighbors, $J'_{xy} = 0$
3. absence of Ising interaction between next nearest neighbors, $J'_z = 0$
4. presence of all four terms

Taking into account these possibles circumstances that arise in chaotic domain over the system, we are going to considerate the absence of J'_{xy} term, $J_{xy} = 1$ and $J_z = J'_z = 1/2$. Then The NNN coupling will be given only in z direction. Another important fact is the relation between chaos and symmetries of the system. Indeed, the Hamiltonian eigenvalues must be separated according to specific symmetries since eigenvalues of different symmetries are uncorrelated and independent, they do not tend to repel each other. Thus, the Hamiltonian symmetries in this model are: reflection, transition and spin rotation around z axis, whose quantum numbers are momenta, total spin in z direction and parity. The last one is useful to desymmetrize the

Hamiltonian obtaining a good behavior about the chaos arising. Therefore, we consider an anisotropic chain of $L = 18$ with $N_{down} = 12$ and $N_{up} = 6$ then the Hamiltonian dimension will be $D = L!/(N_{up}!N_{down}!) = 18564$. The parity separation divides the $\hat{H}_\lambda$ spectrum in two sets: $E_{even} = 9324$ and $E_{odd} = 9240$. The level density histograms are showed in figure 31 and figure 32 for even and odd parities for different values of NNN strength coupling λ: $\lambda = 0$,$\lambda = 0.2$,$\lambda = 0.7$ and $\lambda = 1$.

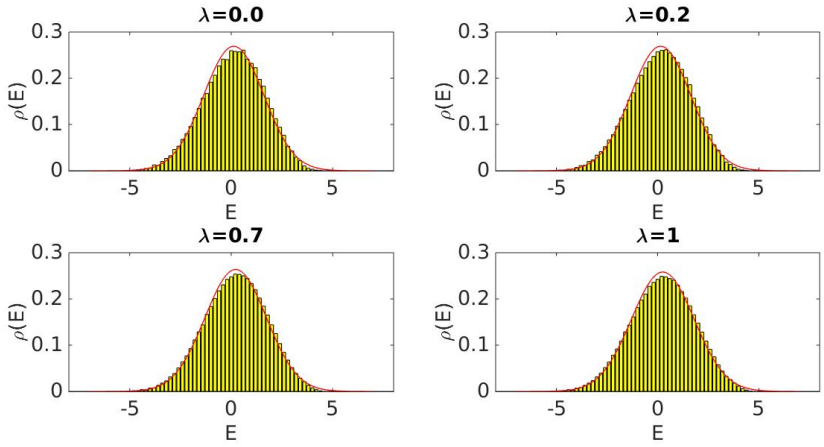

Figure 38 – Level density histograms of NNN model for $\lambda = 0.0$,$\lambda = 0.2$,$\lambda = 0.7$ and $\lambda = 1$ with $L = 18$, $N_{up} = 6$. The eigenvalues number for every histogram is approximately $E_{even} = 9324$ due to the degeneracy. The red line is the theoretical fit obtained from σ^2 and μ.

λ	σ^2_{odd}	μ_{odd}	σ^2_{even}	μ_{even}
0.0	2.196	0.125	2.215	0.125
0.2	2.195	0.148	2.214	0.148
0.7	2.286	0.219	2.307	0.218
1	2.385	0.255	2.406	0.253

Table 5 – Statistical parameters of the energy eigenvalues distribution for NNN model. σ^2 and μ are the variance and mean respectively. The subindex *odd* and *even* represent the parity.

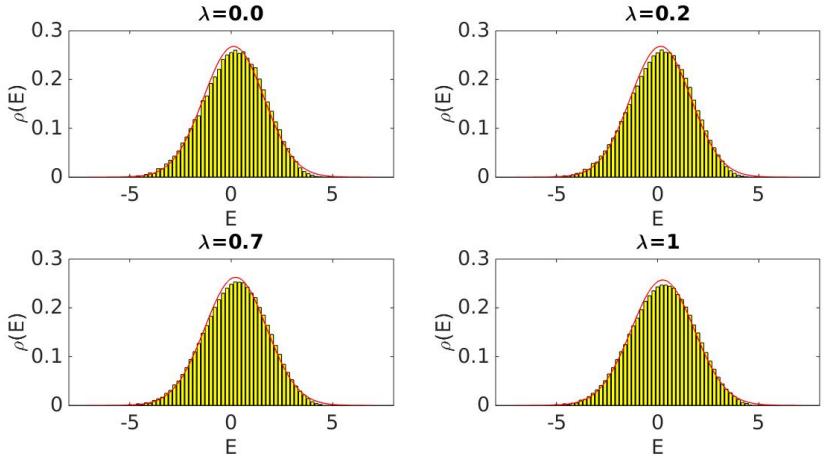

Figure 39 – Level density histograms of NNN model for $\lambda = 0.0$,$\lambda = 0.2$,$\lambda = 0.7$ and $\lambda = 1$ with $L = 18$, $N_{up} = 6$. The eigenvalues number for every histogram is approximately $E_{odd} = 9240$ due to the degeneracy. The red line is the theoretical fit obtained from σ^2 and μ.

The figure 38 and figure 39 display the Gaussian density of levels. Due to the fits it is possible to infer the asymmetric behavior of these distributions. Moreover, the mean and variance are found in the table 5

Taking into account the eigenvalues for even and odd parity, we analyze the chaotic behavior through the spacing distribution. Hence, the energy levels are transformed in another set using polynomial unfolding, where the polynomial degree is $\eta = 15$. The results are displayed in figure 40 and figure 41

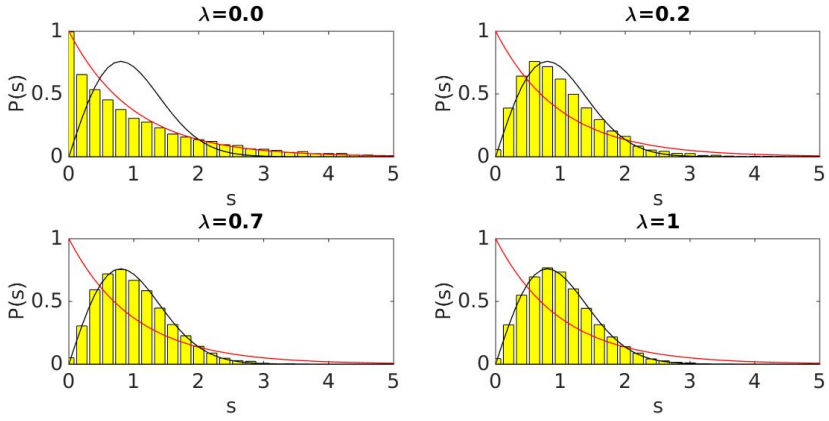

Figure 40 – Spacing distribution for four different λ values. The energy sets correspond to eigenvalues associated with states with odd parity. The red and black lines are the Poisson and Wigner- Dyson distributions.

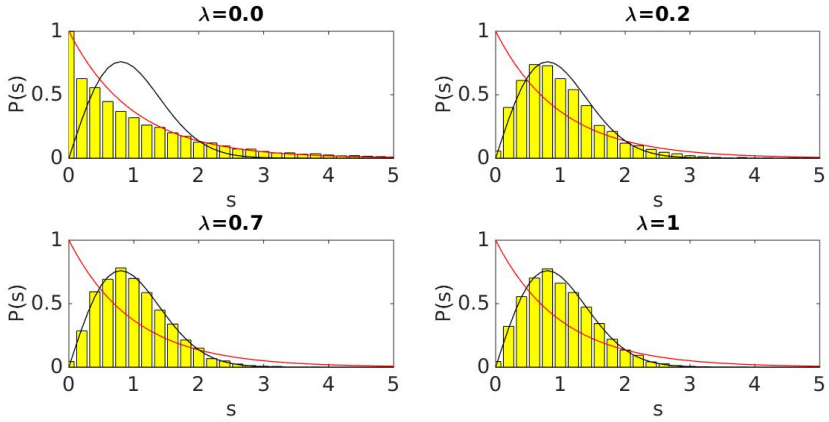

Figure 41 – Spacing distribution for four different λ values. The energy sets correspond to eigenvalues associated with states with even parity. The red and black lines are the Poisson and Wigner-Dyson distributions.

The figure 40 and figure 41 show transitions for both eigenvalues sets, whose characteristics are similar. If the coupling strength λ is between 0 and 0.2 the system remains in intermediated phase,i.e the system is neither integrable nor chaotic. Therefore, the transition behavior is related with the coupling strength due to the integrability breaking depends on how much the strong coupling is of the next nearest neighbor coupling and its relation to other coupling strengths J'_{xy},J_{xy},J_z and J'_z. In fact, anomalous behavior of spacing distribution has been found(KUDO;

DEGUCHI, 2005) when the total spin in z direction is equal to zero, even when the system is not integrable. For this reason, the choosing of the fixed number spin position in one direction, whose value is $1/3$ of the spin number does not take into account the possibility of having $N_{up} = N_{down}$ in the chain since the same spin number in one direction implies the conservation of total spin in z.

On the other hand, the approaches made in the model are related to the chain size and the strength coupling terms, thus the model involves finite size effects. If we consider some specific values for J'_{xy}, J_{xy}, J_z, J'_z and λ we obtain that for $\lambda \approx 0$ the behavior of the distributions becomes closer to Poisson. Another possibility is obtaining integrability due to the symmetry enhancement(KUDO; DEGUCHI, 2005).

According to the last results using the time series analysis Eq.(2.42) we obtain the signals associated with the same λ parameters of figure 40 and figure 41.

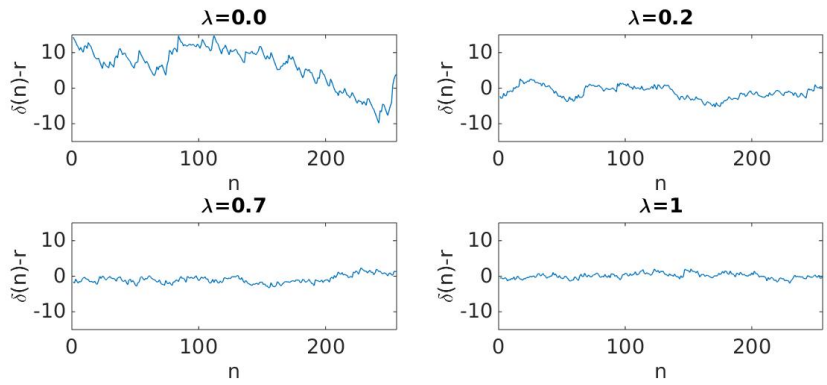

Figure 42 – Time series for NNN model of parameters $\lambda = 0.0$,$\lambda = 0.2$,$\lambda = 0.7$ and $\lambda = 1$ with $L = 18$, $N_{up} = 6$. The signals correspond to a set energy with parity odd. Each signals is composed of 256 unfolded energy ε_n values.

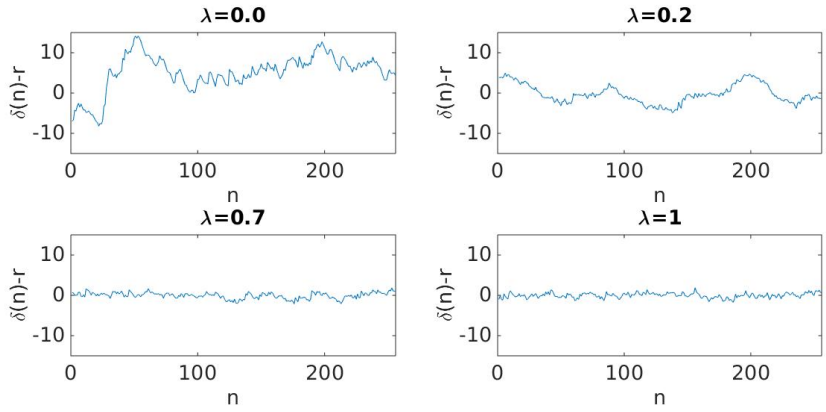

Figure 43 – Time series for NNN model of parameters $\lambda = 0.0$,$\lambda = 0.2$,$\lambda = 0.7$ and $\lambda = 1$ with $L = 18$, $N_{up} = 6$. The signals correspond to a set energy with parity even. Each signals is composed of 256 unfolded energy ε_n values.

The figure 42 and figure 43 display the behavior already found in the impurity model. However, signals for both parity sets reveal characteristics that are very close to the time series of impurity model for $\lambda > 0.2$, whose results correspond to chaotic domain, That is signals associated to $\lambda > 0.2$ approximately reveal chaotic behavior. To see those characteristics we calculate the power spectral density for both sets of different parities using the same parameter already mentioned. The results are showed in figure 44 and figure 45. They are obtained from 34 sets of 256 consecutive energies.

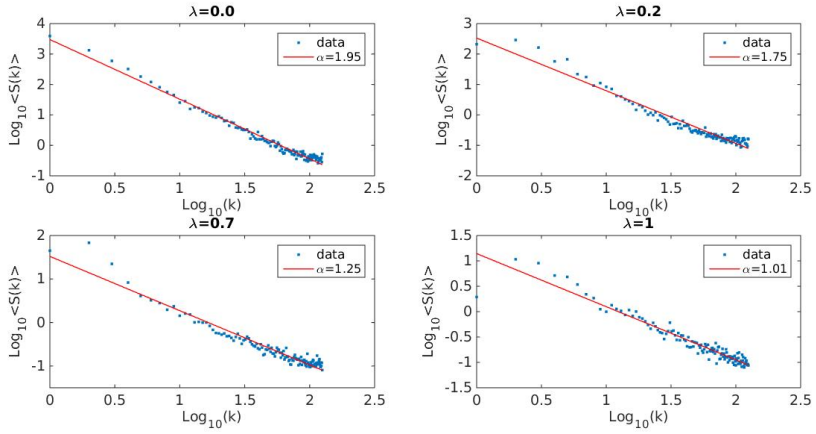

Figure 44 – Average power spectrum $< S(k) >$ for odd energy ε_i levels. The red lines represent the linear best fit and α is the respective exponent. Note the power law behavior $1/k^{\alpha}$ is obtained.

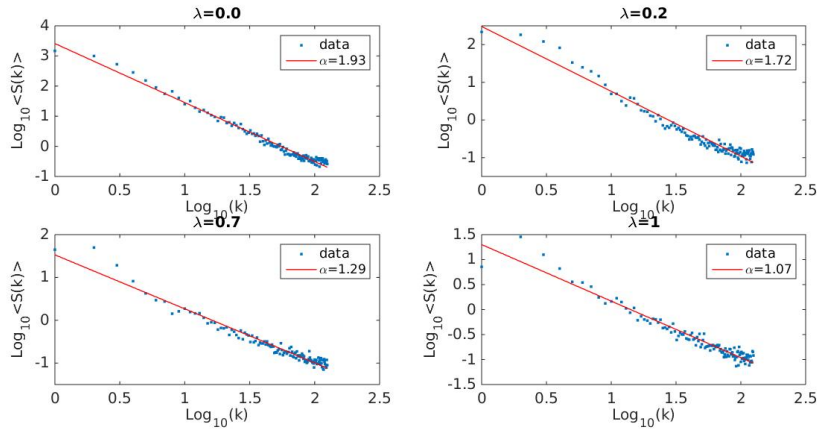

Figure 45 – Average power spectrum $< S(k) >$ for even energy ε_i levels. The red lines represent the linear best fit and α is the respective exponent. Note the power law behavior $1/k^{\alpha}$ is obtained.

The figure 44 and figure 45 provide general information of how the transition to chaotic regime occurs, moreover we can see that the mean power spectral density has the same behavior found for the impurity model: both figures follow the rule $1/k^{\alpha}$. The error is close to 5%. Although, this transition can be described in a better way taking into account each exponent α for a specific λ. Therefore the figure 46 reveals the transition to chaotic domain for both kinds of parity sets

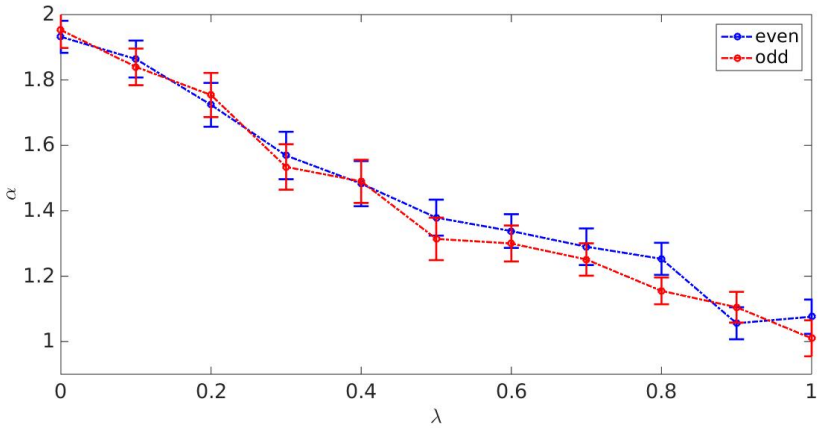

Figure 46 – Power exponent transition for both energy sets in function of λ. The error bars are the confident intervals of 95%.

As we can see the system goes from integrable regime to chaotic domain when λ increases i.e when the NNN interaction begins to be stronger. That implies the chaos is produced by the

interaction between second nearest neighbors. Moreover, the level spacing distributions and α are not the unique quantities that change when the chaotic system suffer a transition. In the case of impurity model we used to analyze such transition through *burstiness* and *Kullback–Leibler divergence*. Therefore the figures 47 and 48 display the behavior of these quantities.

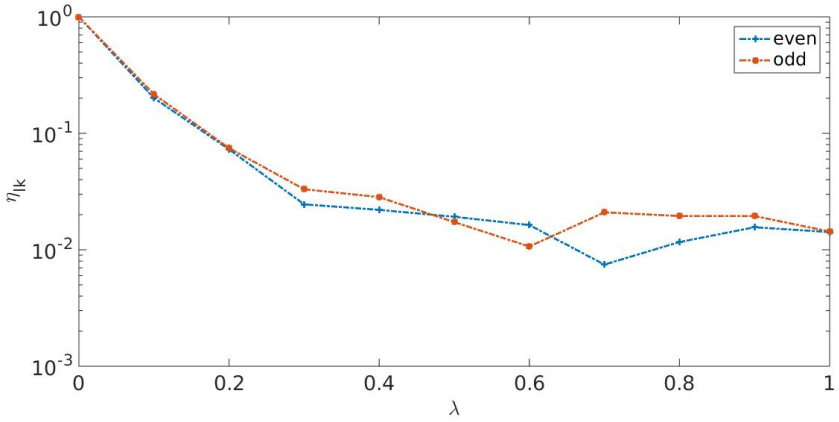

Figure 47 – Transition of divergence η_{lk} For both parity energy sets. η_{lk} is the result of normalizing for the largest D_{lk} value in both parity sets.

The η_{lk} coefficient shows how the transition occurs giving additional information about the spacing distributions since the Kullback–Leibler divergence provides information of how much these distribution differ from the theoretical value. η_{lk} is showed in figure 48 in logarithmic scale due to the closeness between the even and odd data. Each parity set is normalized by its largest value, that is for the D_{lk} associated to even parity every η_{lk} is obtained by $\eta_{lk}^{even} = D_{lk}(P(s)_{wd}|P(s)_{data}^{even})/D_{lk}(P(s)_{wd}|P(s)_{poisson-data}^{even})$, where $D_{lk}(P(s)_{wd}|P(s)_{poisson-data}^{even})$ corresponds to l-k divergence for $\lambda = 0$. The same procedure is used for odd data too.

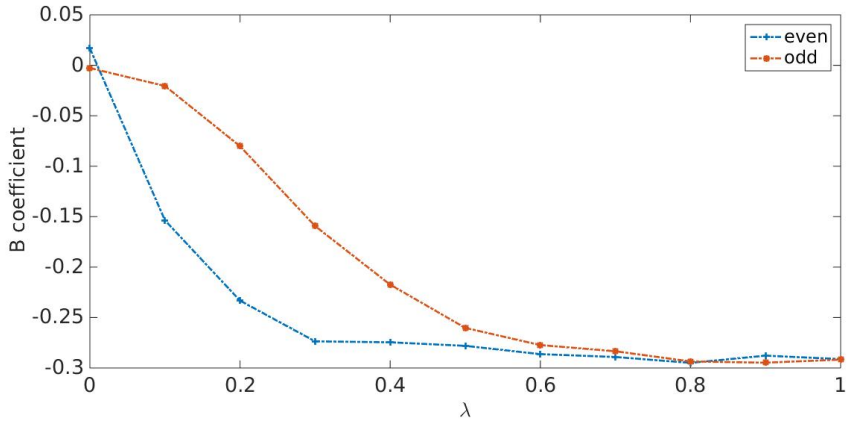

Figure 48 – B coefficient behavior in function of λ parameter for Heisenberg NNN model for both parity sets.

On the other hand, the burstiness in figure 48 reveals a transition of this quantity as the NNN coupling strength increases. If we realize the last point in this figure are closely to value $B = -0.3$. In fact, the transition of B coefficient reveals the fact that the chaotic B value for large next nearest neighbor coupling tends to be 0.3. It can be proved analytically as follows: The mean spacing for the spacing distribution is $< s >= 1$ and the $< s^2 >$ is obtained from the integral

$$< s^2 >= \int_0^\infty \frac{\pi s^3}{2} e^{-\frac{\pi}{4}s^2} ds = \frac{4}{\pi}. \tag{4.22}$$

Taking into account the spacing distribution as a probability distribution, the variance will be

$$\sigma_s = \sqrt{< s^2 > - < s >^2} = \sqrt{< s^2 > -1} \approx 0.52. \tag{4.23}$$

Using the Eq.(4.17) we get

$$B = \frac{(\sigma_s/m_s - 1)}{(\sigma_s/m_s + 1)} = \frac{\sigma_s - m_s}{\sigma_s + m_s} = -0.313. \tag{4.24}$$

Therefore, we have the transition for NNN system going from a *neutral* value(GOH; BARABáSI, 2008) for B coefficient to regular B values, whose analytical value is obtained in Eq.(4.23).

The general behavior of burstiness for three systems shows that the transition is, generally speaking, the same due to each system experiments a transition to chaotic domain, whose distribution is the same. For this reason, the figures 30, 37 and 47 are differentiated in their

initial points since these points represent the spacing distribution associated to Poisson type. The interpretation of the burstiness in these kinds of systems is as follows: The unfolded energy levels are events and the distribution which relates the spacing between events is the associated distribution i.e the nearest neighbor spacing distribution. The burstiness B measures how much separated are those events in a general way. As we saw before, a distribution, whose events are randomly separated, will be represented by a larger B coefficient close to one, meanwhile a distribution, whose events are equally separated, the burstiness will be negative close to -1. The $B = 0$ is an intermediated case between both states. For this reason, distributions with events or energies with constant separation are approximately are Dirac delta functions. The opposite case i.e randomly separation between events are described by arbitrary distributions. They models of these distributions are displayed in the literature with power law behavior.

4.5 Crossover Functions

As we can observe there are three quantities that describe a transition as the λ parameter increases: spectrum exponent α, D_{lk} divergence and burstiness $B.\lambda$ may be a strength coupling, which is the case of NNN model or might be a parameter associated with external field acting in one spin site or in each spin site of the system.

The λ parameter belongs to a family parameters which are responsible for integrability breaking. In other words, these parameters produce the transition integrable-chaotic. They are involved in the Hamiltonian of the system usually being interaction strength terms. It is important to note that the transitions in specific systems are described by functions that follow fundamental properties. They are known as *Crossover functions*. These kinds of functions follow interesting properties. For example, in(MODAK; MUKERJEE; RAMASWAMY, 2014) it is exposed two models; The spineless fermion Hamiltonian and the Hubbard model. Both models describe crossover functions, whose fundamental parameters are the hopping term t for the Hubbard model and the interaction neighbor term for spineless fermion model τ. The crossover consists in functions whose dependence is ruled by these parameters and have the same functional form for different system size L. The quantities which change as τ and t increase are the variance distribution and the Drude weight. They also prove that for every fixed parameter τ and t there is one spacing distribution associated. Therefore, they found a general dependence of L with τ and

t which yields in a power law form.

There are other examples of crossover functions, whose fundamental parameter is the strength coupling, indeed the peak position of spacing distribution and the tail parameter depend on this strength coupling. Hence, these functions involve a hyperbolic tangent form for the model found in(RABSON; NAROZHNY; MILLIS, 2004). However, we propose two functional relations that differ from this analysis since we will relate two of three quantities mentioned before vanishing the λ dependence.

Therefore, we can consider the next change of variable for η_{lk} and burstiness B values obtained for three Heisenberg chain models

$$\psi = \frac{\eta_{lk}}{1-\eta_{lk}} \qquad and \qquad \phi = \frac{1-|B'|}{|B'|} \tag{4.25}$$

where $B' = B/B_{wg}$ thus B is normalized by the burstiness of Wigner-Dyson distribution. Therefore, the crossover function for ψ in function of $\alpha - 1$ is given in figure 49

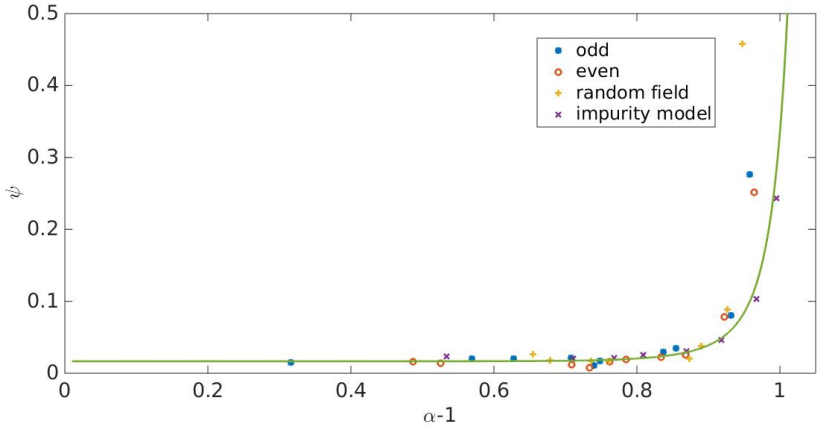

Figure 49 – Crossover function between the power spectrum exponent α and ψ. The green line represents the best fit.

The function, which represents the best fit in figure 49, is defined as follows

$$f(\alpha-1) = ae^{b(\alpha-1)^{\frac{3}{c}}}, \tag{4.26}$$

where the parameters are: $a = \frac{1}{60}$, $b = 3$ and $c = \frac{1}{4}$. This function represents a good approximation in the chaotic domain for the three systems. It is important to note that the parameter, which produces the transition in each system, is vanished. Thus we obtain one universal relation between

two quantities which changes when the integrability is breaking. This fact displays the crossover as transition parametric function where the implicit parameter is λ. In the case of the burstiness it is possible to obtain a crossover function displayed in the figure 50

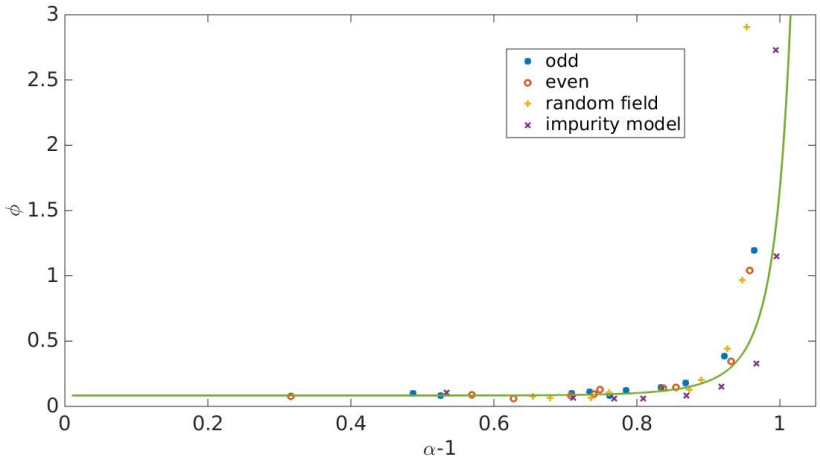

Figure 50 – Crossover function between the power spectrum exponent α and ϕ. The green line represents the best fit.

The crossover in this case can be described by a function which is similar to the Eq.(4.26). Indeed it can be written as follows

$$g(\alpha-1) = a' e^{b'(\alpha-1)^{\frac{3}{c'}}}. \tag{4.27}$$

The parameters are: $a = \frac{1}{12}$, $b = 3$ and $c = \frac{1}{4}$. Both function reveal the same exponential form and each system is characterized by the same exponential crossover function. These phenomena are analogous to the Van Der Waals gas since the universal curve relates the density with the temperature. On the other hand, we may construct a third function vanishing the dependence of α in the variables ϕ and ψ. Therefore, points close to the chaotic domain tend to behave in a linear form. It is showed in the figure 51

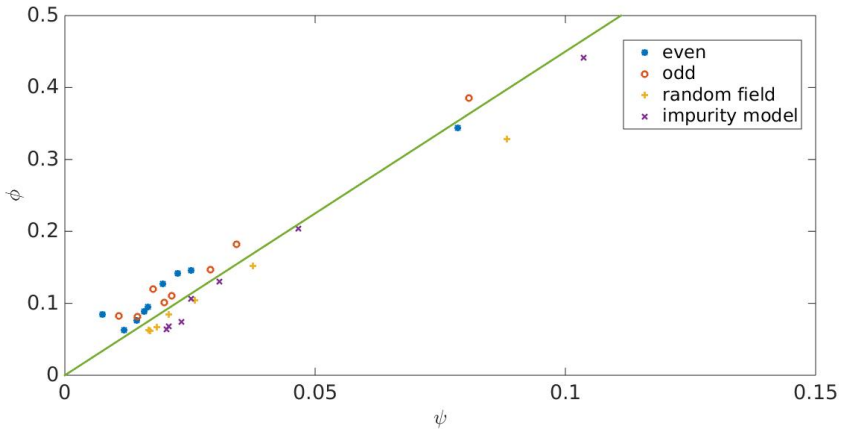

Figure 51 – Crossover linear function for ϕ in function of ψ.

This linear form in given by $\phi = \frac{9}{2}\psi + d$ where d is an arbitrary constant. The importance of this function is similar to the crossover displayed before: the figure 51 reveals a state law for the burstiness and the Kullback-Lieber divergence. However, we found that the linear dependence reveals a trivial relation between the burstiness and the l-k divergence since the behavior of both variables is the same after making the relation between them. In other words, B coefficient and η_{lk} are the same if they are written in terms of ψ and ϕ, the unique difference is a factor which plays the role of slope.

These relations display a general behavior which is the same for each spin system. The fundamental difference of these functions with the crossovers found in the literature (RABSON; NAROZHNY; MILLIS, 2004; SANTOS; RIGOL, 2010; SAKHR; NIEMINEN, 2005; MODAK; MUKERJEE; RAMASWAMY, 2014) is that those functions are represented in terms of the parameter which produces the transition to chaos. In our case, this parameter is vanished producing a state law which is universal for spin systems.

5 Conclusion and outlook

The random matrix theory provides the fundamental description for many body systems such as nucleus, billiards, spin chains,ETC. The description of this theory is based on the Hamiltonian system structure, whose symmetries determine a matrix form and, therefore the ensemble features. If the Hamiltonian system is invariant under orthogonal transformation it will preserve the time reversal and rotational symmetries. This is called *Gaussian Orthogonal Ensemble* (*GOE*). There are other two ensembles:*Gaussian Unitary Ensemble* (*GUE*) and *Gaussian symplectic Ensemble* (*GSE*). The first describe Hamiltonian systems which do not preserve time reversal symmetry. The second one is useful to describe a system with rotational symmetry broken. The eigenvalues of each matrix ensemble provides fundamental information through the *level spacing distribution*. However, such eigenvalues must be unfolded in order to obtain universal properties of the system. Therefore, the spacing distribution associated to GOE ensemble is known as *Wigner-Distribution* and it is present in any chaotic system. In the case of integrable systems the spacing associated distribution is *Poisson* type and the ensemble related to this system is called *Gaussia Diagonal Ensemble* (*GDE*).

The consequences of the random matrix theory are also found in the complex systems. Such as the case of complex networks i.e the small world, the free scale and the random networks have eigenvalue sequence which after being unfolded describe the Wigner-Dyson distribution(YE; LI; MA, 2010). In our case we have also seen how the random networks have associated a spectral density whose behavior obeys a power law.

For this reason, we showed that the spacing distribution is not the only one chaotic feature. In fact, the spacing distribution has an intrinsic relation to the time series analysis. This relation allowed us to conclude that chaotic and integrable systems are also described by a power spectral density. In other words: the chaotic and integrable systems behave as $S(k) \propto 1/k^{\alpha}$ noise, where $\alpha = 1$ to chaotic domain and $\alpha = 2$ to integrable case.

The power spectral behavior is not only associated with chaotic systems. Hence, we found that the complex networks can be described by this statistical quantity. For instance, in random network the spacing distribution reveals a Wigner Distribution and the power spectrum associated is close to the chaotic case predicted by the time series analysis over the random matrix theory.

Due to the universal role behavior $1/k^{\alpha}$ noise in integrable and chaotic systems we may wonder if there are evidences of a transition to integrable-chaotic. For this reason, we studied three kinds of Heisenberg spin model whose integrability could be broken through different ways. We developed computational analysis which proved that these systems described a transition from integrable to chaotic domain through three different quantities: Spacing distribution shape, Kullback–Leibler divergence, burstiness and power spectrum exponent. The last one goes from $\alpha = 2$, which corresponds to integrable case, to $\alpha = 1$ as the parameter associated with transition increasing. It allows us to infer another signature of chaos. Other two quantities display a trend to specific values. For instance, the Kullback–Leibler divergence goes to zero when the system is in chaotic domain due to the comparison made between the theoretical Wigner-Dyson distribution and the data distributions obtained from λ increasing parameter. In the case of the burstiness the chaotic domain is characterized by $B = (\pi/4-1)/(\pi+1) \approx -0.3$ revealing the regular structure of the spacing distribution if they are interpreted as an event sequence.

On the other hand, the crossover functions presented here show how the transition to chaos can be described through quantities, which change when this process begins without taking into account the physical parameter that makes the chaos to take place in the systems. In other words, the transition to chaos, described by crossover functions is given only in terms of quantities that change when the integrability is broken. In our case the Kullback–Leibler divergence and burstiness coefficient have functional dependence on average power spectral exponent α. Therefore, we can see that these functional forms are universal since they are the same for every spin system.

This approach is more general than the crossovers found in the literature(RABSON; NAROZHNY; MILLIS, 2004; SANTOS; RIGOL, 2010; MODAK; MUKERJEE; RAMASWAMY, 2014) since they describe the transition to chaos in terms of the parameter that breaks the integrability, whose result does not provide the possibility of constructing a states law as Van Der Waals description of gases. Therefore, in our case it is possible of establish the first step to make this universal law in spin systems.

The quantity, which describes the transition to chaos, as well as provides information of short correlations is the power spectral exponent. However, there are other quantities, whose results allow to infer conclusion of long-range correlations. For instance, the Δ_3 statistics(MEHTA, 2004) and the number variance(GUHR; MÜLLER-GROELING; WEIDENMÜLLER, 1998a)

give information about spectral rigidity. The Δ_3 function, which is given in Eq.(2.39), can be associated with Hausdorff measure(SANTHANAM; BANDYOPADHYAY; ANGOM, 2006). Therefore, from this work it is possible to explore one crossover function, whose parameters would be the power spectral density exponent and Hausdorff measure. Thus, this crossover would represent a functional form between one quantity that gives information about short-range correlation and another that is related to long-range correlations.

Another interesting result that would be studied from this work consists in the construction of one stochastic differential equation associated with the time series presented in this thesis. Due to results obtained in (RUSECKAS; KAULAKYS, 2014; KAULAKYS; GONTIS; ALABURDA, 2005; KAULAKYS; RUSECKAS, 2004) there is a relation between the power spectral exponent of $1/f^{\alpha}$ noise and general form of a stochastic differential equation. The power spectral exponent is specific parameter in this equation. Therefore, it would be interesting to obtain a possible equation which describes statistically the spin systems.

Bibliography

ALCARAZ, F. C. et al. Surface exponents of the quantum xxz, ashkin-teller and potts models. *Journal of Physics A: mathematical and general*, IOP Publishing, v. 20, n. 18, p. 6397, 1987. 72

ATAS, Y. et al. Distribution of the ratio of consecutive level spacings in random matrix ensembles. *Physical review letters*, APS, v. 110, n. 8, p. 084101, 2013. 44

BAE, M. et al. Chaos-to-order transition in spherical heavy nuclei. *Physical review letters*, APS, v. 69, n. 16, p. 2349, 1992. 40, 42, 43

BARABÁSI, A.-L.; ALBERT, R. Emergence of scaling in random networks. *science*, American Association for the Advancement of Science, v. 286, n. 5439, p. 509–512, 1999. 62, 63

BAXTER, R. J. *Exactly solved models in statistical mechanics*. [S.l.]: Elsevier, 1982. 27

BENETTIN, G.; GALGANI, L.; STRELCYN, J.-M. Kolmogorov entropy and numerical experiments. *Phys. Rev. A*, American Physical Society, v. 14, p. 2338–2345, Dec 1976. Disponível em: <https://link.aps.org/doi/10.1103/PhysRevA.14.2338>. 16

BERRY, M. V. Quantizing a classically ergodic system: Sinai's billiard and the kkr method. *Annals of Physics*, Elsevier, v. 131, n. 1, p. 163–216, 1981. 24

BERRY, M. V.; TABOR, M. Level clustering in the regular spectrum. In: THE ROYAL SOCIETY. *Proceedings of the Royal Society of London A: Mathematical, Physical and Engineering Sciences*. [S.l.], 1977. v. 356, n. 1686, p. 375–394. 46

BETHE, H. Zur theorie der metalle. *Zeitschrift für Physik*, Springer, v. 71, n. 3-4, p. 205–226, 1931. 80, 87

BOHIGAS, O.; GIANNONI, M.; SCHMIT, C. Lecture notes in physics. *Vol. 209Springer, Berlin*, p. 1–99, 1984. 24, 40

BOHIGAS, O.; GIANNONI, M. J.; SCHMIT, C. Characterization of chaotic quantum spectra and universality of level fluctuation laws. *Phys. Rev. Lett.*, American Physical Society, v. 52, p. 1–4, Jan 1984. Disponível em: <https://link.aps.org/doi/10.1103/PhysRevLett.52.1>. 46, 47

BOHR, N. Neutron capture and nuclear constitution. *Nature*, v. 137, n. 3461, p. 344–348, 1936. 7, 33, 34

BRODY, T. A. et al. Random-matrix physics: spectrum and strength fluctuations. *Rev. Mod. Phys.*, American Physical Society, v. 53, p. 385–479, Jul 1981. Disponível em: <https://link.aps.org/doi/10.1103/RevModPhys.53.385>. 30

BRUUS, H.; D'AURIAC, J.-C. A. Energy level statistics of the two-dimensional hubbard model at low filling. *Phys. Rev. B*, American Physical Society, v. 55, p. 9142–9159, Apr 1997. Disponível em: <https://link.aps.org/doi/10.1103/PhysRevB.55.9142>. 40, 43

BUNIMOVICH, L. A. On ergodic properties of certain billiards. *Functional Analysis and Its Applications*, Springer, v. 8, n. 3, p. 254–255, 1974. 17

CARERI, G.; CONSOLINI, G. Dielectric 1/f noise of proton glass on a hydrated protein surface. *Physical Review E*, APS, v. 62, n. 3, p. 4454, 2000. 61

CASATI, G.; CHIRIKOV, B.; GUARNERI, I. Energy-level statistics of integrable quantum systems. *Physical review letters*, APS, v. 54, n. 13, p. 1350, 1985. 46

CHATTERJEE, A.; CHAKRABARTI, B. K. *Econophysics of stock and other markets: proceedings of the Econophys-Kolkata II*. [S.l.]: Springer Science & Business Media, 2007. 32

DYSON, F. J. A brownian-motion model for the eigenvalues of a random matrix. *Journal of Mathematical Physics*, AIP, v. 3, n. 6, p. 1191–1198, 1962. 40, 42

EDELMAN, A.; SUTTON, B. D.; WANG, Y. Random matrix theory, numerical computation and applications. *Modern Aspects of Random Matrix Theory*, American Mathematical Society, v. 72, p. 53, 2014. 37, 44

FLORES, J. et al. Spectral statistics of the two-body random ensemble revisited. *Physical Review E*, APS, v. 63, n. 2, p. 026204, 2001. 45

FRENCH, J.; WONG, S. Some random-matrix level and spacing distributions for fixed-particle-rank interactions. *Physics Letters B*, Elsevier, v. 35, n. 1, p. 5–7, 1971. 40, 42, 43

GOH, K.-I.; BARABáSI, A.-L. Burstiness and memory in complex systems. *EPL (Europhysics Letters)*, v. 81, n. 4, p. 48002, 2008. Disponível em: <http://stacks.iop.org/0295-5075/81/i=4/a=48002>. 79, 96

GÓMEZ, J. M. G. et al. $1/f^{\alpha}$. *Phys. Rev. Lett.*, American Physical Society, v. 94, p. 084101, Mar 2005. Disponível em: <https://link.aps.org/doi/10.1103/PhysRevLett.94.084101>. 31, 40, 42, 43

GREIS, N.; GREENSIDE, H. Implication of a power-law power-spectrum for self-affinity. *Physical Review A*, APS, v. 44, n. 4, p. 2324, 1991. 52

GUBIN, A.; SANTOS, L. F. Quantum chaos: An introduction via chains of interacting spins 1/2. *American Journal of Physics*, AAPT, v. 80, n. 3, p. 246–251, 2012. 88

GUHR, T.; MÜLLER-GROELING, A.; WEIDENMÜLLER, H. A. Random-matrix theories in quantum physics: common concepts. *Physics Reports*, Elsevier, v. 299, n. 4, p. 189–425, 1998. 7, 22, 23, 40, 42, 102

GUHR, T.; MÜLLER-GROELING, A.; WEIDENMÜLLER, H. A. Random-matrix theories in quantum physics: common concepts. *Physics Reports*, Elsevier, v. 299, n. 4, p. 189–425, 1998. 30

GUNSON, J. Proof of a conjecture by dyson in the statistical theory of energy levels. *Journal of Mathematical Physics*, AIP, v. 3, n. 4, p. 752–753, 1962. 42

HAAKE, F. *Quantum signatures of chaos*. [S.l.]: Springer Science & Business Media, 2013. v. 54. 36, 37, 40, 43

HARTMANN, C. A. Über die bestimmung des elektrischen elementarquantums aus dem schroteffekt. *Annalen der Physik*, Wiley Online Library, v. 370, n. 9, p. 51–78, 1921. 61

HOLME, P. *Temporal networks*. [S.l.]: Springer, 2014. 79

HSU, T. C.; D'AURIAC, J. C. A. Level repulsion in integrable and almost-integrable quantum spin models. *Phys. Rev. B*, American Physical Society, v. 47, p. 14291–14296, Jun 1993. Disponível em: <https://link.aps.org/doi/10.1103/PhysRevB.47.14291>. 29

HUANG, N. E. *Hilbert-Huang transform and its applications*. [S.l.]: World Scientific, 2014. v. 16. 60

HUANG, N. E. et al. The empirical mode decomposition and the hilbert spectrum for nonlinear and non-stationary time series analysis. In: THE ROYAL SOCIETY. *Proceedings of the Royal Society of London A: Mathematical, Physical and Engineering Sciences*. [S.l.], 1998. v. 454, n. 1971, p. 903–995. 60

JALAN, S.; BANDYOPADHYAY, J. N. Random matrix analysis of complex networks. *Physical Review E*, APS, v. 76, n. 4, p. 046107, 2007. 62, 67

KAC, M. Can one hear the shape of a drum? *The american mathematical monthly*, JSTOR, v. 73, n. 4, p. 1–23, 1966. 23

KAULAKYS, B.; GONTIS, V.; ALABURDA, M. Point process model of 1/ f noise vs a sum of lorentzians. *Physical Review E*, APS, v. 71, n. 5, p. 051105, 2005. 103

KAULAKYS, B.; RUSECKAS, J. Stochastic nonlinear differential equation generating 1/ f noise. *Physical Review E*, APS, v. 70, n. 2, p. 020101, 2004. 103

KUDO, K.; DEGUCHI, T. Level statistics of xxz spin chains with discrete symmetries: Analysis through finite-size effects. *Journal of the Physical Society of Japan*, The Physical Society of Japan, v. 74, n. 7, p. 1992–2000, 2005. 92

LUUKKO, P. Spectral analysis and quantum chaos in two-dimensional nanostructures. University of Jyväskylä, 2015. 40, 41

MCDONALD, S. W.; KAUFMAN, A. N. Spectrum and eigenfunctions for a hamiltonian with stochastic trajectories. *Phys. Rev. Lett.*, American Physical Society, v. 42, p. 1189–1191, Apr 1979. Disponível em: <https://link.aps.org/doi/10.1103/PhysRevLett.42.1189>. 23

MEHTA, M. L. *Random matrices*. [S.l.]: Academic press, 2004. v. 142. 21, 34, 39, 48, 102

MODAK, R.; MUKERJEE, S.; RAMASWAMY, S. Universal power law in crossover from integrability to quantum chaos. *Physical Review B*, APS, v. 90, n. 7, p. 075152, 2014. 97, 100, 102

MORALES, I. O. et al. Improved unfolding by detrending of statistical fluctuations in quantum spectra. *Physical Review E*, APS, v. 84, n. 1, p. 016203, 2011. 44, 57, 60

MOURA, F. A. de; LYRA, M. L. Delocalization in the 1d anderson model with long-range correlated disorder. *Physical Review Letters*, APS, v. 81, n. 17, p. 3735, 1998. 53

MÜLLER, G. Nature of quantum chaos in spin systems. *Phys. Rev. A*, American Physical Society, v. 34, p. 3345–3355, Oct 1986. Disponível em: <https://link.aps.org/doi/10.1103/PhysRevA.34.3345>. 25, 26, 27

NO, A. R. et al. Quantum chaos and $1/f$ noise. *Phys. Rev. Lett.*, American Physical Society, v. 89, p. 244102, Nov 2002. Disponível em: <https://link.aps.org/doi/10.1103/PhysRevLett.89.244102>. 32, 55, 60

OGANESYAN, V.; HUSE, D. A. Localization of interacting fermions at high temperature. *Physical Review B*, APS, v. 75, n. 15, p. 155111, 2007. 44

PAAR, V. et al. Broken isospin symmetry in the shell model and chaotic behavior. *Physics Letters B*, Elsevier, v. 271, n. 1-2, p. 1–6, 1991. 40, 42, 43

PEYRARD, M. Glass transition in protein hydration water. *Physical Review E*, APS, v. 64, n. 1, p. 011109, 2001. 61

PORTER, C. E. *Statistical Theories of Spectra: Fluctuations: A Collection of Reprints and Original Papers*. [S.l.]: Acad. Press, 1965. 36

RABSON, D. A.; NAROZHNY, B. N.; MILLIS, A. J. Crossover from poisson to wigner-dyson level statistics in spin chains with integrability breaking. *Phys. Rev. B*, American Physical Society, v. 69, p. 054403, Feb 2004. Disponível em: <https://link.aps.org/doi/10.1103/PhysRevB.69.054403>. 30, 98, 100, 102

RANDOM Graphs with Matlab. Disponível em: <https://www.cs.purdue.edu/homes/dgleich/demos/erdos_renyi/generate.html>. 62, 63

RANDOMNETWORKS. Disponível em: <http://apps.cytoscape.org/apps/randomnetworks>. 8, 64

REICHEL, L. The transition to chaos. In: *Conservative Classical System: Quantum Manifestations*. [S.l.]: Springer Berlin, 1992. 14, 36, 37

RISKEN, H.; EBERLY, J. The fokker-planck equation, methods of solution and applications. *Journal of the Optical Society of America B Optical Physics*, v. 2, p. 508, 1985. 51

ROBNIK, M. Classical dynamics of a family of billiards with analytic boundaries. *Journal of Physics A: Mathematical and General*, IOP Publishing, v. 16, n. 17, p. 3971, 1983. 31

RUSECKAS, J.; KAULAKYS, B. Scaling properties of signals as origin of 1/f noise. *Journal of Statistical Mechanics: Theory and Experiment*, IOP Publishing, v. 2014, n. 6, p. P06005, 2014. 103

SAKHR, J.; NIEMINEN, J. M. Poisson-to-wigner crossover transition in the nearest-neighbor statistics of random points on fractals. *Phys. Rev. E*, American Physical Society, v. 72, p. 045204, Oct 2005. Disponível em: <https://link.aps.org/doi/10.1103/PhysRevE.72.045204>. 31, 100

SANTHANAM, M.; BANDYOPADHYAY, J. N.; ANGOM, D. Quantum spectrum as a time series: Fluctuation measures. *Physical Review E*, APS, v. 73, n. 1, p. 015201, 2006. 103

SANTOS, L. Integrability of a disordered heisenberg spin-1/2 chain. *Journal of Physics A: Mathematical and General*, IOP Publishing, v. 37, n. 17, p. 4723, 2004. 72, 74, 85

SANTOS, L. F. Introduction to the computational analysis of static properties and dynamics of one-dimensional spin-1/2 systems. *Yeshiva University*, Department of Physics, Yeshiva University. Disponível em: <https://www.yu.edu/sites/default/files/legacy//uploadedFiles/Faculty/Lea_Ferreira_dos_Santos/Computer_Codes/Izmir2014_04(2).pdf>. 70, 71

SANTOS, L. F. Integrability of a disordered heisenberg spin-1/2 chain. *Journal of Physics A: Mathematical and General*, v. 37, n. 17, p. 4723, 2004. Disponível em: <http://stacks.iop.org/0305-4470/37/i=17/a=004>. 30

SANTOS, L. F.; MITRA, A. Domain wall dynamics in integrable and chaotic spin-1/2 chains. *Physical Review E*, APS, v. 84, n. 1, p. 016206, 2011. 88

SANTOS, L. F.; RIGOL, M. Onset of quantum chaos in one-dimensional bosonic and fermionic systems and its relation to thermalization. *Phys. Rev. E*, American Physical Society, v. 81, p. 036206, Mar 2010. Disponível em: <https://link.aps.org/doi/10.1103/PhysRevE.81.036206>. 30, 86, 100, 102

SRIDHAR, S. Experimental observation of scarred eigenfunctions of chaotic microwave cavities. *Phys. Rev. Lett.*, American Physical Society, v. 67, p. 785–788, Aug 1991. Disponível em: <https://link.aps.org/doi/10.1103/PhysRevLett.67.785>. 24

SRIDHAR, S.; HELLER, E. J. Physical and numerical experiments on the wave mechanics of classically chaotic systems. *Phys. Rev. A*, American Physical Society, v. 46, p. R1728–R1731, Aug 1992. Disponível em: <https://link.aps.org/doi/10.1103/PhysRevA.46.R1728>. 24

STÖCKMANN, H.-J. *Quantum chaos: an introduction*. [S.l.]: AAPT, 2000. 19, 36, 37

STOFFREGEN, U. et al. Microwave billiards with broken time reversal symmetry. *Physical review letters*, APS, v. 74, n. 14, p. 2666, 1995. 24

WATTS, D. J.; STROGATZ, S. H. Collective dynamics of 'small-world'networks. *nature*, Nature Publishing Group, v. 393, n. 6684, p. 440–442, 1998. 62

WEYL, H. Das asymptotische verteilungsgesetz der eigenwerte linearer partieller differentialgleichungen (mit einer anwendung auf die theorie der hohlraumstrahlung). *Mathematische Annalen*, Springer, v. 71, n. 4, p. 441–479, 1912. 23, 42

YA.G. Burstiness and memory in complex systems. *Math. Dokl*, v. 17, n. 4, p. 17 196, 1976. 16

YE, B.; LI, H.-j.; MA, X.-p. 1/fα noise in spectral fluctuations of complex networks. *Physica A: Statistical Mechanics and its Applications*, Elsevier, v. 389, n. 22, p. 5328–5331, 2010. 62, 63, 67, 101

ZANGARA, P. R. et al. Time fluctuations in isolated quantum systems of interacting particles. *Physical Review E*, APS, v. 88, n. 3, p. 032913, 2013. 80